ADAPTIVE OPTICS FOR FAST OPTICAL COMMUNICATION:

SPATIAL SOLUTIONS FOR SPECTRAL ISSUES

Thesis submitted for the degree of
"Doctor of Philosophy"

By

DAVID SINEFELD

Submitted to the Senate of the Hebrew University of Jerusalem
October/ 2013

This work was carried out under the supervision of:

Prof. Dan M. Marom

This work is dedicated to my beloved wife and my wonderful children.

Without your encouragement it couldn't have happened...

Abstract

In recent decades, the use of fast optical signals has become increasingly dominant, both in scientific research and in engineering applications. High speed photonics serves as the core of modern worldwide communication networks, as well as in many optical signal processing applications. Such applications rely on the ability to control, filter and manipulate large bandwidth signals. Traditionally, such control can be realized using fast electronics. However, continuous growth in data rates makes this option impractical, since the signals become too fast to control even for cutting edge electric circuit technology. The alternative is to use an all-optical system, where signal control is done in the frequency (spectral) domain. Such a system must be capable of manipulating large bandwidth signals with high spectral resolution. Such optical systems are essential in optical communication networks, for performing signal conditioning, impairment mitigation and WDM channel power equalization.

In this work I explore a family of optical sub-systems combining guided-wave and free-space optics for spectrally resolving optical signals at unprecedented resolution, and actively manipulating the spectral components with spatial light modulator (SLM) technology. The ability to combine the employed cutting edge technologies, including a high resolution planar lightwave circuit (PLC) arrayed waveguide grating (AWG), together with the state-of-the-art phase SLM, which was adapted from the light projection industry, enables the design and demonstration of high resolution photonic spectral processors (PSP). This system is capable of applying arbitrary spectral phase and amplitude at high spectral resolution to an optical signal and of controlling its properties in the time domain. A PSP can be configured for addressing the entire conventional optical communication band, at a price of poor resolution due to the finite space-bandwidth trade-off. Alternatively, the PSP can be designed as a colorless adaptive device, operating with a free spectral range (FSR) matching the channel plan, e.g. with a 100-GHz FSR, for in-band high-resolution wavelength division multiplexing (WDM) filtering applications. By using two-dimensional free-space optics achieved by crossing the PLC AWG with a bulk grating, a new broadband processor was introduced. This PSP is capable of controlling independent WDM channels on the 100 GHz grid at the high resolution of the colourless solution, thereby shattering the space-bandwidth limitation.

Based on these concepts, a family of novel systems and implementations were developed and investigated. In this thesis I introduce six papers which demonstrate the design and implementation of three PSP systems, based on hybrid waveguide/free space optics arrangements. The papers are divided into two groups: in the first group, three papers present the evolution of the spectral processing device, from the simplest version of colorless PSP up to two dimensional PSP arrangement with full spectral, control along the c-band. The second group contains three papers describing several implementations of these technologies, including amplitude filtering applications (Nyquist-WDM generation), phase filtering applications (tunable chromatic dispersion compensation and group delay stairs generation) and a demonstration of a new fiber laser which was built using the PSP platform. These high spectral resolution devices and systems can serve as an important element in controlling dispersion, enhancing signal quality and optimally filtering a distorted signal, and their development is essential for the progress in the optical fiber communication world.

Acknowledgments

First and foremost, I would like to express my gratitude to my supervisor, Professor Dan M. Marom for his continuous support, encouragement and guidance during my graduate studies. His leadership, experience and knowledge always had guided me towards better understanding of the world of optics. His constant pursuit for perfection has always inspired me, showing me the path to become an experienced researcher.

As the first and senior Phd student who graduates in his group, I always felt a special relation between us that was more than just a professor-student relationship. Spending seven years in his lab revealed me an honest and kind man with clear and open mind. His trust in me, which expressed in his willing to give me a free hand and responsibility in many projects, is the main reason for my progress. It was a privilege to work with him, a prevelige which I am grateful for.

I would like to thank my fellow students in the lab along the years:
Dror, Ami, Yaron, Yoram, Asael, Yoni, Amitay, Yiska, Moran, Yedidya, Miri, Noam, Ori, Leonid Roy and Rene.
It was an honor to be a part of this fine group. I learned a lot from our collaborated work, and I hope we will have the opportunity to work together again someday.

Last and most importantly, I would like to thank my parents, my supporting wife and my wonderful children for their unconditional support, encouragement and patient through these years. This thesis is devoted to them.

Contents

List of Publications

Journal papers

[1] D. Sinefeld, and D.M. Marom, “Hybrid Guided-Wave/Free-Space Optics Photonic Spectral Processor Based on LCoS Phase Only Modulator," IEEE Photon. Technol. Lett. 7, 510-512 (2010)

[2] D. Sinefeld, and D.M. Marom, “Insertion Loss and Crosstalk Analysis of a Fiber Switch Based on a Pixelized Phase Modulator,” IEEE J. Lightwave Technol. 29, 69-77 (2011).

[3] D. Sinefeld, S. Ben-Ezra, C. R. Doerr, and D. M. Marom, "All-channel tunable optical dispersion compensator based on linear translation of a waveguide grating router," Opt. Lett. 36, 1410-1412 (2011).

[4] D. Sinefeld, C. R. Doerr, and D. M. Marom, "A photonic spectral processor employing two-dimensional WDM channel separation and a phase LCoS modulator," Opt. Express 19, 14532-14541 (2011).

[5] D. Sinefeld and D. M. Marom, "Tunable fiber ring laser with an intracavity high resolution filter employing two-dimensional dispersion and LCoS modulator," Opt. Lett. 37, 1-3 (2012).

[6] D. Sinefeld, Y. Fattal, and D. M. Marom, "Generation of WDM adaptive-rate pulse bursts by cascading narrow/wideband tunable optical dispersion compensators," Opt. Lett. 37, 4290-4292 (2012).

[7] D. Sinefeld, S. Ben-Ezra, and D. M. Marom, "Nyquist-WDM filter shaping with a high-resolution colorless photonic spectral processor," Opt. Lett. 38, 3268-3271 (2013).

List of Figures

Abbreviations

ADC	**A**nalog to **D**igital **C**onversion
AWG	**A**rrayed **W**aveguide **G**rating
CD	**C**hromatic **D**ispersion
CW	**C**ontinues **W**ave
DPSK	**D**ifferential **P**hase **S**hift **K**eying
EDFA	**E**rbium **D**oped **F**iber **A**mplifier
FSR	**F**ree **S**pectral **R**ange
FWHM	**F**ull **W**idth **H**alf **M**ax
GD	**G**roup **D**elay
IL	**I**nsertion **L**oss
LC	**L**iquid **C**rystals
LCoS	**L**iquid **C**rystal **o**n **S**ilicon
MEMS	**M**icro **E**lectro **M**echanical **S**ystems
MLL	**M**ode **L**ocked **L**aser
MPS	**M**odulation **P**hase **S**hift
N-WDM	**N**yquist **W**avelength **D**ivision **M**ultiplexing
OSA	**O**ptical **S**pectrum **A**nalyzer
OVA	**O**ptical **V**ector **A**nalyzer
PLC	**P**lanar **L**ightwave **C**ircuit
PSP	**P**hotonic **S**pectral **P**rocessors
SLM	**S**patial **L**ight **M**odulator
SMSR	**S**ide **M**ode **S**uppression **R**atio
TLS	**T**uneable **L**aser **S**ource
TODC	**T**uneable **O**ptical **D**ispersion **C**ompensator
VIPA	**V**irtually **I**maged **P**hased **A**rray
WDM	**W**avelength **D**ivision **M**ultiplexing
WGR	**W**aveguide **G**rating **R**outer

Chapter 1. Introduction

1.1 Photonic signal generation and processing: Spectral vs. Temporal domain

In recent decades, the use of fast and ultrafast optical signals had become more and more dominant, not just in the scientific world, but also in many engineering applications. High rate optics serves as the core of the lightwave communication industry, as well as in modern Analog to digital conversion (ADC) systems which are based on photonically assisted sampling schemes. Ultrashort optics attracts considerable scientific attraction with a wide range of applications, since it allows research of many nonlinear phenomena due to increasing peak powers as the pulse duration decreases.

Modern science has two major techniques for generation, manipulation and characterization of such ultra short pulses and high speed signals. The first, which is most common in the lightwave communication industry, uses a continues wave (CW) laser as a source, an electro-optical modulator for signal generation and a fast detector connected to a fast oscilloscope for signal detection and analysis (Fig. 1.1a).

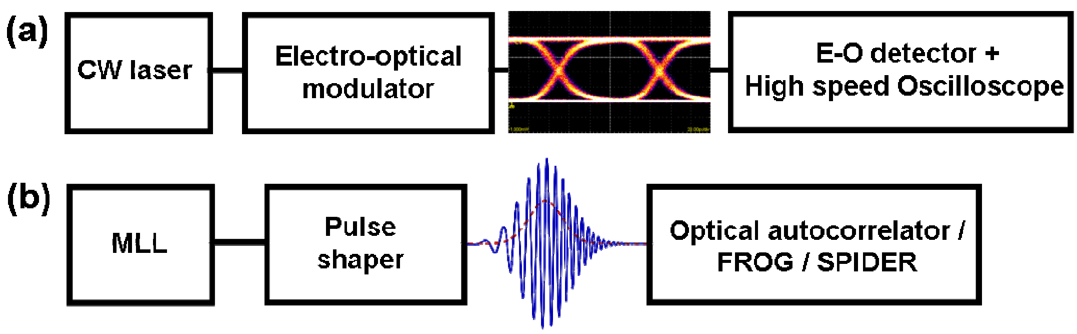

Figure 1.1- Two main approaches toward fast optical signals generation, manipulation and characterization (a) Time domain approach: using a CW laser as a source, electro optical modulator for temporal signal shaping and fast detector and oscilloscope for time domain diagnostics (b) Spectral domain approach: mode locked lasers serve as a femto second laser source, pulse shaping methods are used to control the signal spectrally and various interferometeric methods are used to detect the pulse shape.

This conservative, but effective "text-book" method, which works almost entirely in the temporal domain, enabled the evolution of fast optical communication over the last four decades, reaching up to rates of tens of GHz with temporal pulse width of less than 10 ps [1].

A different approach is needed when ultrashort pulses are to be manipulated and measured. Such short pulses are usually generated using a mode locked laser (MLL) with typical pulse width of tens to hundreds of femtoseconds and a very large spectral bandwidth (~40 nm). Signal control is done usually with a pulse shaper [2] which works by spatial filtering of the spectral domain (Fig 1.1b). Several methods were invented in order to detect and characterizes ultra-short pulses. Among them are the traditional intensity autocorrelation [3], and more sophisticated methods as the frequency-resolved optical gating (FROG) [4] and the spectral phase interferometry for direct electric field reconstruction (SPIDER) [5]. These methods use complicated free space optical arrangements and different slow detection schemes in order to reconstruct the temporal pulse shape with additional signal processing. Between these two distinct areas of research, there is a "middle zone" which becomes more and more important. In this "zone", signals are too fast for electronics, but are slow enough to have an important fine spectral structure which cannot be resolved with standard pulse shaping methods. A good example for such need can be found in the challenging world of modern optical communication. Lightwave communication systems have evolved considerably since the earliest commercial deployment to today's ultra long-haul, ~100 channel count wavelength division multiplexed (WDM) systems. Such optical systems employ channel rates of 40 Gb/s with increasing demand for even larger bandwidths. Current state-of-the-art systems which are designed for commercial deployment are designed with transmission capacity of 100 Gb/s per channel. Higher channel rates with 400 Gb/s and even 1 Tb/s were already demonstrated in lab experiments [6-10], and are considered to be the next generation to be implemented in field systems during the coming years.

With increasing channel transmission rates, the broad signal spectrum becomes more susceptible to filtering and dispersion, resulting in a degraded signal reaching the receiver. Such systems rely on the ability to control large bandwidth signals with high spectral resolution. Although temporal methods are still more common in high speed optical systems as in the case of optical fiber communication systems, when signal rates increases with the growing demands, they become too fast to control even for the cutting edge electric circuit technology. One way to deal with those high rates is to use optical inter connects and maintain the temporal domain approach [11]. This approach has its own difficulties, since it requires new manufacturing processes which are extremely challenging.

In this work we suggest a different approach which is suitable for high rates signal manipulations in the spectral domain with slow rate control. Such optical devices can be found in optical communication performing signal conditioning and controlling WDM traffic. Those devices are important for maximizing the performance of optical communication systems. Channel power equalizers are required for maintaining the same OSNR across all amplified channels in a long-haul system, and dispersion compensators are essential in communication systems employing direct or differential detection, and can reduce the digital processing overhead in coherent reception systems. The significance of all these "middle zone" processing elements does not rely on their fast response but rather on their ability to control the temporal shape and phase of the pulses inside the transmission sequence. An elegant way to realize such temporal manipulation is by using the optical concepts which are common in ultrashort pulse science. Those methods which are generally referred as "pulse shaping" are applied in the spectral domain and can control even ultrafast signals. However, those methods suffer from a few disadvantages which make them unsuitable for actual engineering systems as in the case of optical communication. First, ultra short pulses techniques use large scale optics which limits the possibility of field implementation in real systems. Second, conventional pulse shapers use a diffractive grating as a dispersive element, where grating dispersion limits the spectral resolution of conventional pulse shapers. This limitation which can be ignored when dealing with ultra short pulses which have relatively slow rate, become crucial in high speed optical communication system which need also full scale temporal control. This demand can be translated to a need for a fine resolution control in the spectral domain. Such control (<10 GHz) cannot be achieved with common pulse shaping methods.

1.2 Photonic spectral processing: modifying the classical pulse shaper

As was mentioned in the previous paragraph, in order to control fast signals one can control the phase and amplitude in the spectral domain instead of manipulations in the time domain. Using this approach, it is possible to filter out undesired spectral features, reshape phase and amplitude, retime pulses and compensate for channel amplitude impairments by spectral carving and phase impairment by dispersion compensation.

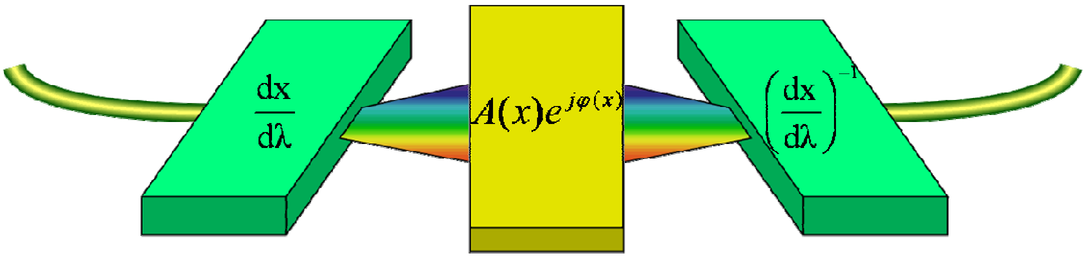

Figure 1.2 - Photonic Spectral Processor concept: a dispersion element forms a spectral spread on a real plane. Placing a spatial light modulator in this plane enables phase and amplitude modulation for each spectral component. The output coupled light carries these spectral manipulations on the signal.

Achieving all of the above with one device can be done within a system we call a photonic spectral processor (PSP). This system is based on the concept of using spatial dispersion to separate the light's frequency components that radiate out from a fiber port, together with a spatial light modulator (SLM) which is placed in the spectral plane (Fig. 1.2). With the SLM one can apply any desired phase and amplitude on the spectrally resolved signal. The light which is then coupled back to the output fiber port carries the spectral information which determines its new temporal properties by the predefined spectral manipulations.

This concept which was originally developed for ultrashort pulse shaping can be used for our purposes as well, as long as the spectral manipulation abilities will match the needs. A classical grating based pulse shaper is shown in Fig 1.3[12-14]. A 4-f arrangement is used to project the spectral components on the Fourier plane. Phase or amplitude manipulations can be applied on the spectral plane by a phase / amplitude SLM. Although very useful in ultrashort pulse shaping, such concept fail to perform sharp spectral filtering since its limited resolution which is determined by its dispersive grating.

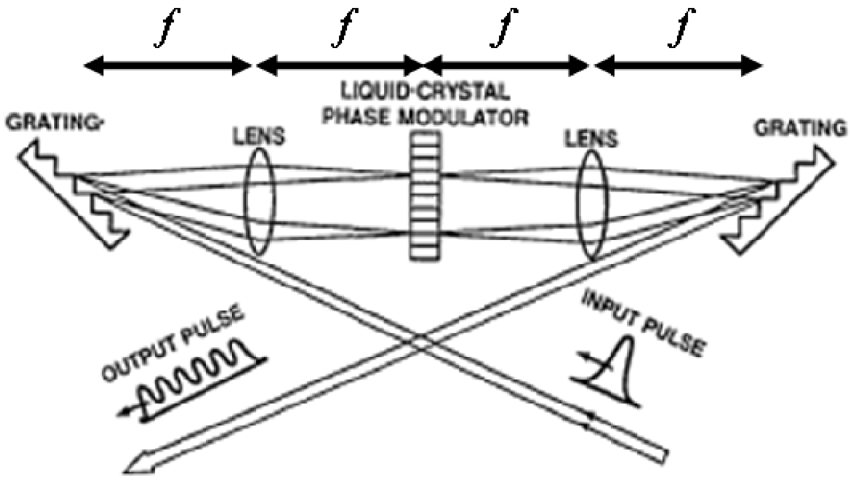

Figure 1.3 Standard pulse shaper optical scheme: A short pulse is dispersed using a despesive grating. The light is projected using a Fourier lens on a spatial SLM (in the drawing the SLM that had been used works in transmission. However, in most pulse shapers a reflecting SLM is being used, resulting in a folded optical arrangement). The spectrally manipulated light is than projected through a second Fourier lens, forming the shaped pulse which carries the spectral manipulations in its new temporal shape.

In order to manifest a PSP with the ability to apply adaptive filtering functions which are relevant to the high rate optical communication signals [15-18], a high spectral resolution dispersive element must be used. The optical performance of such spectral processing devices depends on the spectral resolution which are determined by the dispersing optics solution and on the spectral addressability, which is a function of the SLM technology. Both issues will be discussed briefly in the following sections.

1.3 Choosing the dispersive element: spectral resolution vs. free spectral range

1.3.1 Dispersion element alternatives and properties

The dispersion element which controls the distribution along the spectral plane should be optimized in order to enable both high resolution and large bandwidth. The common free-space diffraction grating is in most cases unsuitable for this mission since its dispersion is limited by the periodic structure and its feature size which limits the amount of the spectral dispersion. Instead, an element with high dispersion is needed. Such an element with channel-matched free spectral range (FSR) dispersion is usually based on virtually imaged phased array (VIPA) [19], or on arrayed waveguide grating (AWG) (sometimes called waveguide-grating-router (WGR)) [20-24]. VIPA dispersion is based on multiple reflections from a thin plate with its back side coated with 100% reflection coating and the front side coated with a less than 100% reflection coating (Fig 1.4). The multiple outputs interfere resulting in spectral dispersion, where the width of the plate determines the FSR and the reflection of the surface determines its spectral resolution. VIPA technology is commonly used in pulse shaping applications, having many advantages due to its simplicity and high resolution. However, for optical communication applications this solution is not preferable, as the multiple virtual sources do not lie on the same plane (Fig. 2b), resulting in an unbalanced interference between them, which reduces the coupling efficiency when the light is coupled to a single mode fiber (SMF). Another disadvantage of the VIPA is the difficulty to integrate it in a small scale system, especially as a part of on-chip systems.

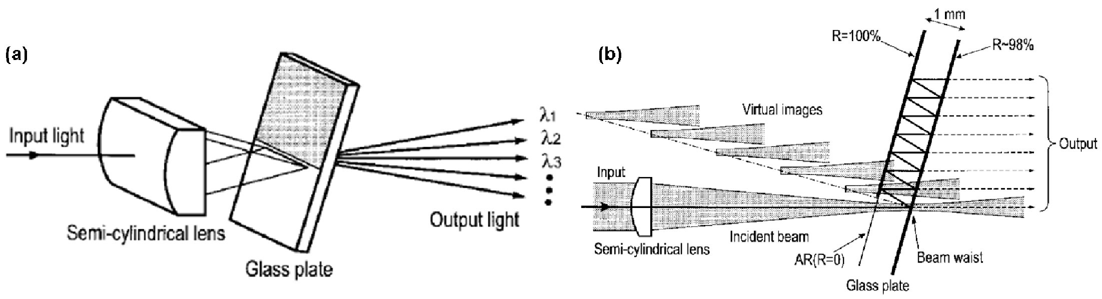

Figure 1.4 - (a) View of the VIPA [19]. The input light is line-focused into the VIPA plate and then collimated light is emitted from the reverse facet with large angular-dispersion. (b) Details of the VIPA. Multiple reflections of the input light virtually create a phased array of light.

In our PSP we use an AWG as the dispersive element. This device is a planar lightwave circuit (PLC) version of an optical phased array, containing a series of waveguides each longer than the other in a constant length. The multiple outputs interfere together resulting in angular dispersion. This option is preferred due to the versatile design possibilities of using a compact PLC element. The use of an AWG as a dispersive element in optical communication system is quite common, since most WDM multiplexers and demultiplexers are based on such a device (Fig 1.5a) [25-27]. Nevertheless, we use an unconventional AWG: instead of employing a second slab-lens region that demultiplexes to output waveguides as in WGR based demultiplexer systems, the grating arms terminate at the PLC edge and the light radiates to free-space (Fig 1.5b). This makes this PLC device the equivalent to a free space grating but with much more versatility in its design options and capabilities.

By controlling the parameters of the AWG it is possible to determine its dispersive properties. The ability to engineer such device to have a desired (large) dispersion, and the fact that this technology is well established in the telecom industry, makes this option the preferred one compared to the alternatives that were introduced before.

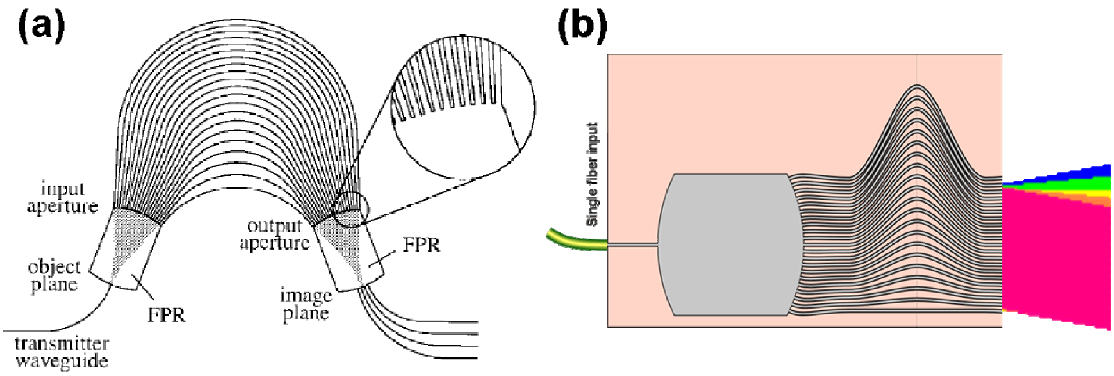

Figure 1.5 - Schematic drawings of an AWG PLC. (a) Classical AWG used as a deultiplexer [25]: Light enters a PLC containing a series of waveguides with a constant length difference ΔL. The PLC is normally fabricated in silica-on-silicon technology. The first slab lens (or free propagation region – FPR) is used to project the incoming light on the waveguides and the second lens collects the light from the waveguides to the output waveguides. In this case the waveguides are arranged to receive different WDM channels according to the desired channel plan. The same component can serve as a multiplexer if the output and input port are switched. (b) Our unconventional AWG: After the first slab lens, The AWG grating arms are terminated at the PLC edge so each wavelength radiates in different angle according to the AWG angular dispersion, resulting in a powerful dispersive element.

1.3.2 Using AWG as the dispersion element – advantages and challenges

The controllable parameters of an AWG are the length difference between two adjacent waveguides - ΔL, its total number of waveguides – N, as well as the parameters of each waveguide (e.g. geometrical properties and index of refraction). The first two parameters have direct impact on AWG performance: ΔL determines the FSR according to [27]: $\Delta\nu_{FSR} = \frac{c}{n_g \Delta L}$, where: c-speed of light and n_g -waveguide group refractive index.

The AWG diffraction properties are similar to a diffraction grating with an m-order of diffraction, where m is determined by: $m = n_c \frac{\Delta L}{\lambda_0}$, where λ_0 is the center wavelength, and n_c is the effective refractive index of the array waveguide. The optical resolution of the AWG is determined according to: $\Delta\nu_{\min} = \frac{\Delta\nu_{FSR}}{N} = \frac{c}{n_g N \Delta L}$, which is related to length difference between the longest and shortest waveguides in the array: $N\Delta L$, and the angular dispersion of the AWG is determined by the equation: $\frac{\Delta\theta}{\Delta\lambda} = \frac{n_g \Delta L}{\lambda_0 n_S p}$ where λ is the wavelength, p is the spacing between two adjacent waveguides and n_S is the effective index in the slab region (in our case, n_S=1 since the waveguides radiate to free space). The above equation implies that by controlling the length difference ΔL, and the number of waveguides N, one can design a highly dispersive element in order to implement it into a PSP. One should note that for a fixed FSR, the resolution is determined solely by the number of array waveguides N.

The AWG PLC that we have been using in most of the papers that are listed in this work was designed in silica on silicon technology and contains 34 waveguides (Fig 1.6). It was designed to have a free spectral range of 100 GHz to match WDM channel plan [12]. The index contrast between the core and the cladding in the silca waveguides is 0.8%, with waveguides rectangular size of 6 μm. The length difference between two adjacent waveguides is $\Delta L=2mm$, and the overall length difference between the longest and shortest waveguide is 64 mm. In order to reach a compact device, the waveguides were folded to a "W" shape which was determined by minimal allowable radius of ~3 mm in order to prevent bend losses. Output waveguides were separated with a pitch of 18.6μm, resulting in diffraction angle of ~ 5^o for 100 GHz channels.

In order to collimate the output radiating light in the vertical (undispersed) direction, we attached a cylindrical lens with a focal length of 3 mm to the output facet of the PLC. The theoretical spectral resolution of such design is 100/34~ 3GHz. As will be shown in the following chapters and in the referred articles, such spectral resolution which is remarkable in spectral processing world, was indeed demonstrated with our AWG based PSP.

The design of the AWG was done through collaboration with Dr. Christopher Doerr, formerly a senior researcher in Alcatel-Lucent Bell Labs and was fabricated in their fab. We must note that although we achieve high dispersion resolution with our AWG, it still suffers from relatively high losses when the light is coupled back. We suspect that most of the losses caused by phase errors formed in the fabrication process [28]. Such losses can be compensated by post production UV phase trimming [29-30]. Although this is a promising method for improving AWG performance, we will not expand the discussion on it here because of space limitations.

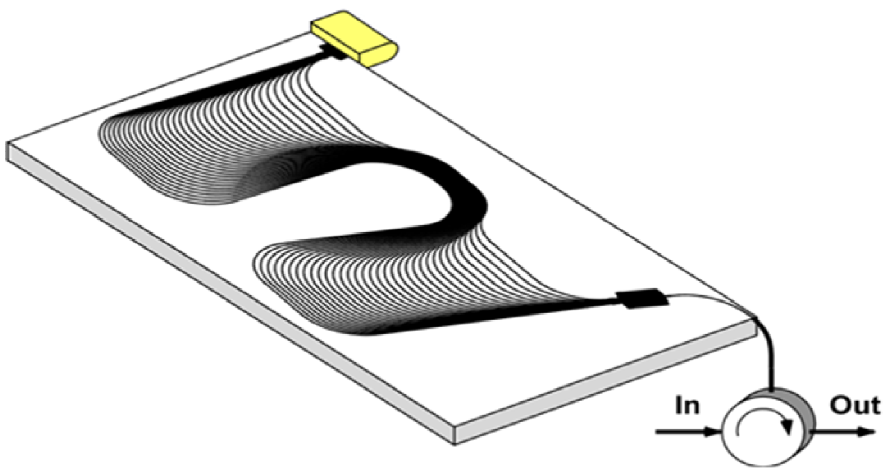

Figure 1.6 – An exact drawing of the AWG PLC that was used in the papers referred in this work. After the first slab lens there are 34 waveguides with ΔL=2mm that radiates out from the far end of the PLC which was manufactured in silica on silicon technology with index contrast of 0.8%. In order to allow a more compact device, a "W" shape was used to fold the waveguides. A cylindrical lens with a focal lens of 3 mm was attached to the radiating facet in order to collimate the light in the vertical direction.

1.4 SLM – controlling the spectral elements

The other core technology which enables the amplitude and phase control for each wavelength component is a spatial light modulator - SLM. As we will discuss in the next section, a phase SLM is capable of doing both phase and amplitude modulations. While such a phase SLM can be implemented in a variety of ways, including micro electro-mechanical systems (MEMS) [16-17,31], and liquid crystal (LC) [32] modulators, in order to address as many as possible WDM channel spectral components with as high as possible spectral resolution, the modulator array must have a large number of modulating elements, more than exists in current state of the art MEMS (Fig 1.7a) and LC modulators.

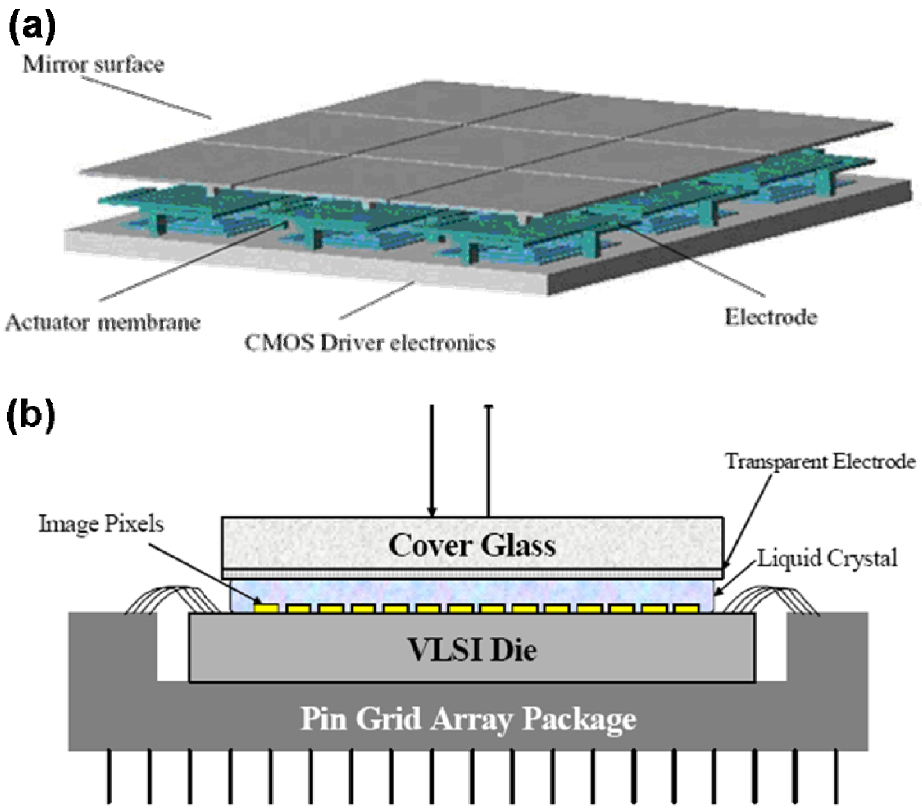

Figure 1.7 – MEMS and LCoS Phase SLM schematic drawings (a) MEMS based phase SLM: by applying voltage with a CMOS electronic driver, an actuator is driven a pixelated mirror up and down up to a $\lambda/2$ travel. Current technology is still limited in the number of pixels in such a device. (b) LCoS based phase SLM: a layer of liquid crystals is placed between a transparent electrode and a VLSI die of two dimensional array of pixels. Different voltage values applied separately on each SLM pixel result in different local index of refraction. This change is equal to a change in the optical path length (OPL) and therefore to a phase delay. In this way one can prescribe a two dimensional phase along the SLM plane with large number of pixels.

Luckily, commercial developments of Liquid Crystal on Silicon (LCoS) modulators (mostly for the display industry) have resulted in the availability of high resolution modulator arrays that can be utilized for WDM spectral manipulations (Fig. 1.7b). The operation method of the LCoS SLM is based on a liquid crystal (LC) layer which lies between a transparent electrode and a VLSI die. When voltage is applied on specific pixel, LC molecules in the pixel area rotates in order to align along the lines of the electrical field (Fig 1.8). The LC molecules angular orientation is dependent on the applied voltage according to [33]: $\theta = \frac{\pi}{2} - 2\arctan(e^{-V})$.

Since LC molecules are elliptic, their rotation effect the index ellipsoid according to [34]: $\frac{1}{n(\theta)^2} = \frac{\cos^2(\theta)}{n_0^2} + \frac{\sin^2(\theta)}{n_e^2}$ where n_o and n_e are the index of refraction of the ordinary and extra-ordinary axis of the LC molecule respectively. The phase that each pixel can apply is therefore given by: $\delta = \frac{2\pi}{\lambda}\left(n(V) - n_0\right)$.

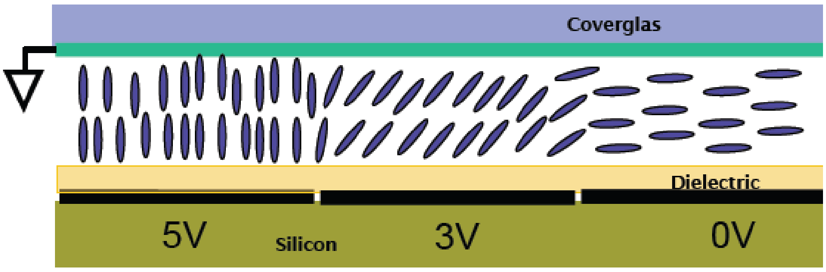

Figure 1.8 – LCoS Phase SLM basic concept of operation: The layer of liquid crystals rotates according the to the applied voltage, resulting in a change in local index of refraction.

In our PSP systems we used two commercially-available LCoS phase modulator arrays. The first was from Boulder Nonlinear Systems (BNS), with 512×512 pixels of 15 μm pitch, and total active size of 7.68×7.68 mm and the second from Holoeye systems with high definition (HD) resolution of 1080×1920 pixels of 8 μm pitch, and total active size of 15.36×8.34 mm. Those phase SLM's were designed especially for working in the NIR spectral region (around 1550 nm) and allows a phase modulation of up to 2π at this wavelength. Two dimensional phase patterns with modulation of more than 2π can be prescribed by applying a modulo 2π phase which is mathematically identical to the original phase. The limitation on the performance of the SLM are due to the number of pixels, the number of controllable gray levels [35] and a fringing field effect caused by the electric field applied on liquid crystals (Fig.

1.9) [36-37]. This fringing field is dependent on the voltage difference between nearby pixels, and limits mostly modulation in high spatial frequencies.

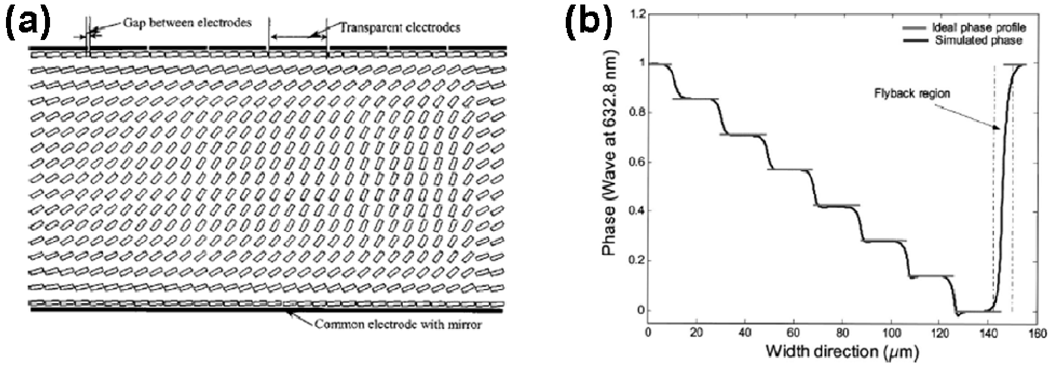

Figure 1.9 – Simulation results of an LCoS flying back effect [36]: (a) Simulated director configuration in one period of an LC blazed (b) Simulated phase profile of an 8 pixel per reset maximum steering grating versus an ideal eight-step stair like blazed grating.

Another limitation that arises when an LC based device is to be used is the operation rate which is limited by the movement mechanism of the LC's and cannot exceed ~100 Hz. This drawback however is not so severe, since most of the application for signal processing do not need real time control. The last issue which is a practical concern for any system with an LCoS SLM is the polarization sensitvity of the device. Since the device work on specific polarization only, a solution for two polarizations must be considered in order allow implementation in real systems. This can be done in two ways: by adding a polarization diversity to the optical setup (usually done by a walk-off prism or a polarization beam splitter (PBS) which duplicate the optical axis of the system) or, if the optical setup is too complicated, by duplicating the whole system, having one system per polarization. These solutions, although not always elegant, are quite common in optical communication systems.

Although those few disadvantages that were discussed here indeed limit the device performance, the fact that LCoS technology was the only commercial phase SLM with large number of pixels that was available for use in 1550 nm, made it the preferred option over the others.

1.5 SLM – PSP operation – a full c-band example

In Fig 1.10, an example of a broadband PSP [38] is shown. The PSP is constructed with those two core technologies using a hybrid free-space and guided-wave optics arrangement. The guiding part accepts an input/output single mode fiber and implements the AWG which imparts angular dispersion that radiates out. The employed AWG consists of 200 grating arms and was designed to match for all the c-band with spectral resolution of ~25 GHz. A cylindrical lens is attached to the PLC in order to collimate the radiating light in the vertical direction (non-information carrying). A Fourier lens converts the angular dispersion to spatial dispersion which is incident on the phase SLM two dimensional array working in reflection. The reflected modulated light traverses back through the optical system to the fiber and is separated by an optical circulator to an output fiber. The Fourier lens projects the beam onto the SLM resulting in an elliptically spot which is significantly larger than the SLM pixel size. Different wavelength components focus at different lateral positions on the SLM plane (e.g. on different columns), and then can be manipulated with the phase SLM (Fig 1.10).

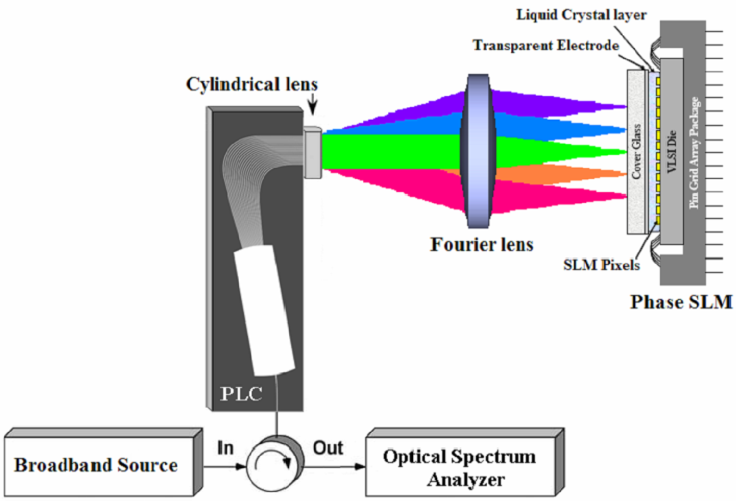

Figure 1.10 – Broadband Spectral Processor based on hybrid guided-wave and free-space optics, combined with a phase SLM [38]. The light comes out from the AWG is being dispersed and broadened by the cylindrical lens, different wavelength components focus on different lateral positions on the SLM plane, and then can be manipulated with the phase SLM.

It is important to note that although we are using a phase only SLM, we can control both phase and amplitude: phase manipulations are done by prescribing an identical phase to all pixels in the column (Figure 1.11a), while amplitude modulation can be achieved in several methods: by setting a phase difference (or "phase step") to the top and bottom halves of the column and by controlling the step position as shown in Figure 1.11b, or by applying phase slope on the specific spectral component, where the applied slope determines the amount of attenuation (Fig 1.11c).

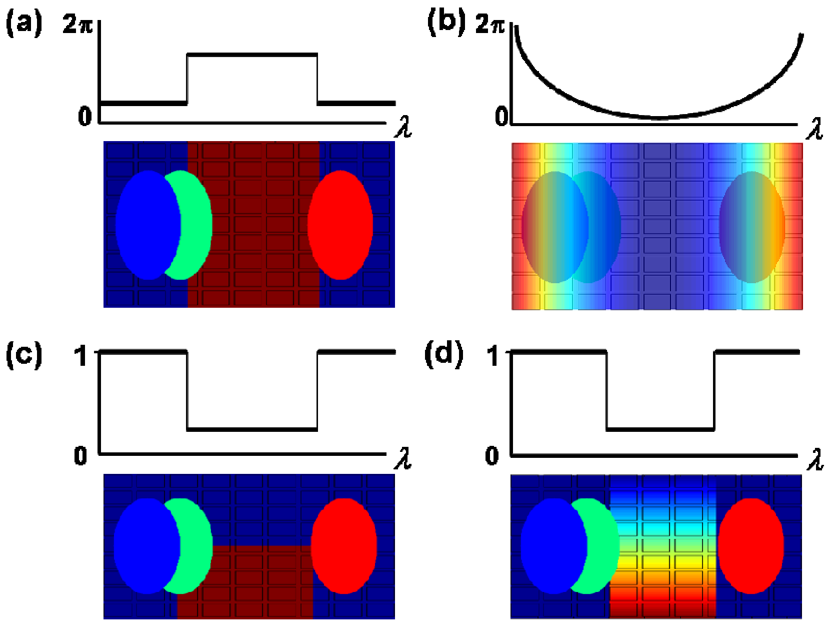

Figure 1.11 - Phase and intensity manipulations using a phase only SLM. The upper part of each drawing shows the desired function of phase/amplitude and the lower part describes the pattern on the SLM: (a) Demonstration of a phase spectral step function with constant phase applied with all the pixels on each column. (b) Demonstration of a phase spectral curved function (c) Amplitude spectral step modulation achieved by applying a π phase jump in the vertical direction (as shown, affecting only the wavelength in the middle). The attenuation can be controlled by moving the vertical position of the phase jump. (d) Amplitude spectral step modulation achieved by applying a phase slope along the specific wavelength components. The attenuation can be controlled by changing slope value.

The combination of phase and amplitude modulation with the lateral dispersion along the SLM axis enables numerous spectral manipulations. However, the performance of such a broadband PSP is limited by the optical resolution of the AWG and the number of columns along the c-band (which is 512 in our BNS SLM). This resolution limitations allow very small manipulations inside each WDM channel since there are less than 20 controllable columns per WDM channel.

The above results imply that such broadband devices which use dispersing elements with a FSR matching or exceeding the whole communication band, have limited performance and applications due to the limited optical resolution of the system [20,38].

1.6 High resolution PSP and its applications

A more interesting family of devices uses the same basic PSP concept, but with a very high spectral resolution which makes this PSP more applicable and relevant. These devices use an engineered dispersing element with an FSR matching the WDM channel spacing [20-24], imparting identical functionality to every channel but with very high resolution. This enables simultaneous multichannel compensation hence called "colorless", and is useful in reducing inventory. Such an arrangement must be based on a high resolution AWG as shown in Fig. 1.12 [39-41]. With the high resolution colorless PSP any phase and amplitude function can be prescribed over a single WDM channel (with replication for all the channels). For example, applying a curved phase along the channel will result in chromatic dispersion (CD) on the signal, which means that the PSP operates as a tuneable optical dispersion compensator (TODC) with wide tuning range. The high resolution of the PSP makes it suitable also for sharp spectral filtering. This could be done with amplitude function for spectral carving [41], a phase slope function for pulse retiming [42-43] or as a special spectral function which is needed for advanced Orthogonal frequency-division multiplexing (OFDM) signal processing [44].

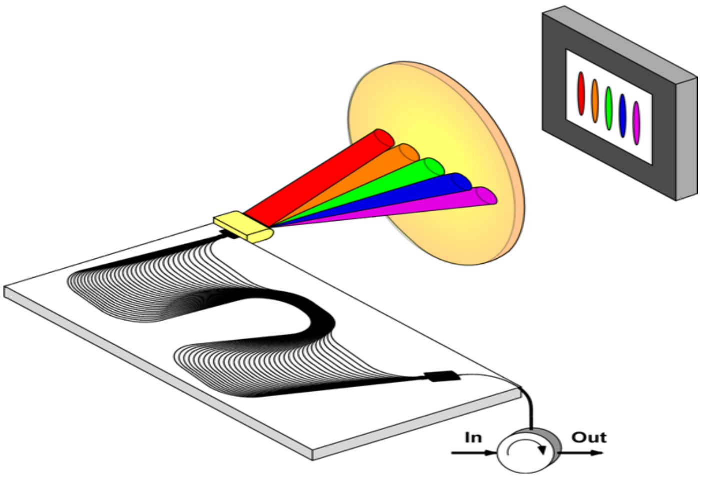

Figure 1.12 - Layout of a colorless PSP. Spectrally dispersed light is projected onto the LCoS SLM with a Fourier lens, generating lateral dispersion along the horizontal axis of the SLM. The SLM reflects the light back to the PLC, carrying the encoded data on the spectrum.

These devices demonstrate that the optical dispersion arrangements of a PSP provide a finite space-bandwidth product that can be allocated to either broad bandwidth at coarse resolution or narrow bandwidth at fine resolution. We therefore are looking for a "super PSP" which can overcome this space-bandwidth limitation and provide the same high resolution as the colorless processor with large working bandwidth as in the broadband one (Fig 1.13).

This space-bandwidth limitation can be overcome by dispersing over two-dimensional space, capitalizing on the additional spatial dimension available with free-space optics. The typical crossed-dispersion optics solution utilizes two gratings where the first has a small FSR with fine resolving capability, and the second crossed grating has a large FSR that separates the diffraction orders of the first grating. This kind of arrangement was introduced before as a solution for a high resolution demultiplexer [45] as well as for pulse shaping [46].

In the next chapter, such two-dimensional, amplitude and phase PSP will be presented. This PSP has the ability to control each WDM channel separately [47-48], with the same high resolution as our earlier colorless PSP [41]. This PSP is based on the combination of two crossed gratings, a high resolution AWG and a free-space bulk grating, together with a LCoS two-dimensional, pixelated phase modulator. Besides from the remarkable performance of our PSP as a tuneable filter as will discussed in detail in the following chapters, its existence brings on variety of new interesting applications. Such an application was already demonstrated when we used our PSP as a part of a high resolution tuneable ring laser [49].

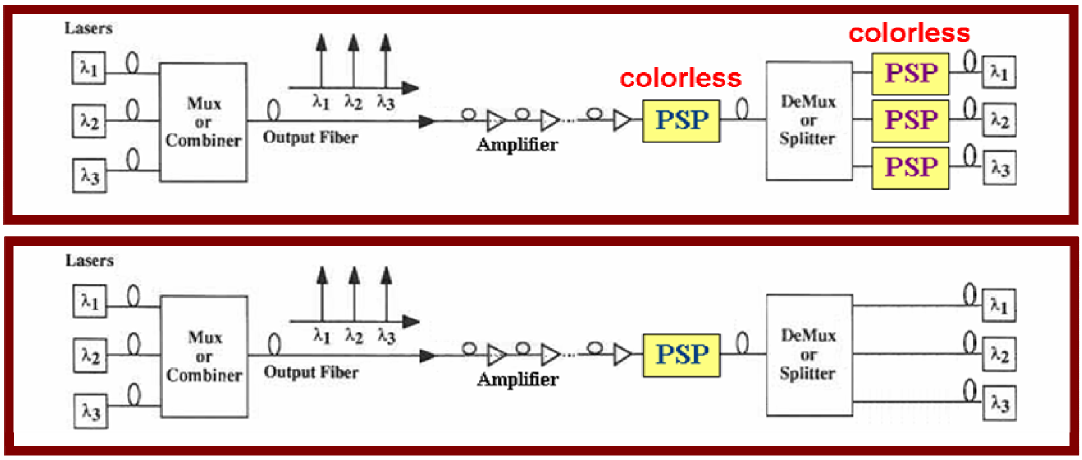

Figure 1.13 - The use of colorless and broadband "super" PSP. UP: a colorless PSP can be used inline where it will share costs but will imply the same filtering for every WDM channels, or as a pre-amplifier with separate filtering for each WDM channel but with many PSP's needed. Down: single "super" PSP which is placed inline but can control each WDM channel separately. This device must have a bandwidth of 30-40 nm with the same high resolution of the colorless PSP.

1.7 Measurement apparatus and methods

Since most of the work that was performed in this research was associated with optical systems and their applications in the spectral and temporal domain, It is significantly important to define the measurement methods that were used in both domains.

1.7.1 Spectral domain measurements: amplitude measurements

In general, one can divide the spectral measurements to amplitude and phase measurements. Amplitude spectral measurements are relatively straight forward and rely mostly on the following options:

- **Optical spectrum analyzer (OSA)**: Probably the most basic measurement technique for optical communication devices. The measurement is done using a broadband (noise) source, where the OSA scan the intensity across the spectrum around 1550 nm.

- **Slow speed detector and a scanning laser**: This method is complementary to the former, where the scanning is done with the laser instead of the OSA detector. This measurement can be done easily using a Luna Optical vector analyzer (OVA) although this is not its main scope.

1.7.2 Spectral domain measurements: phase measurements

Phase measurements on the contrary, are more difficult to perform. Actually we never measure the phase but only the group delay (GD). Two methods were used during the research: a "home made" system working in the modulation phase shift (MPS) method and commercial interferometric measurement using Luna OVA.

- **Modulation phase shift method [50-53]**: In this technique, which was built in our lab [53], the standard MPS measurement method [50] is modified by introducing an additional slow frequency component whose variations are tracked with a lock-in amplifier. The apparatus combines optical frequencies (THz) to be measured, with RF frequencies (MHz-GHz) for differential phase accumulation, and audio frequencies (KHz) for feedback tracking and data extraction with the use of the lock-in amplifier, as shown in Fig 1.14. In this approach the GD is being directly measure as in the standard MPS technique, per a single wavelength. The wavelength dependence of the GD is constructed by laser sweeping over the desired wavelength range. The scanning is relatively slow since for each wavelength an additional scan of the lock-in amplifier is needed in order to determine the GD. However, since in this method the side tones are travelling together along the device under test, there is no limit for the length of the device. This is an important advantage when a long fiber spool need to be measured.

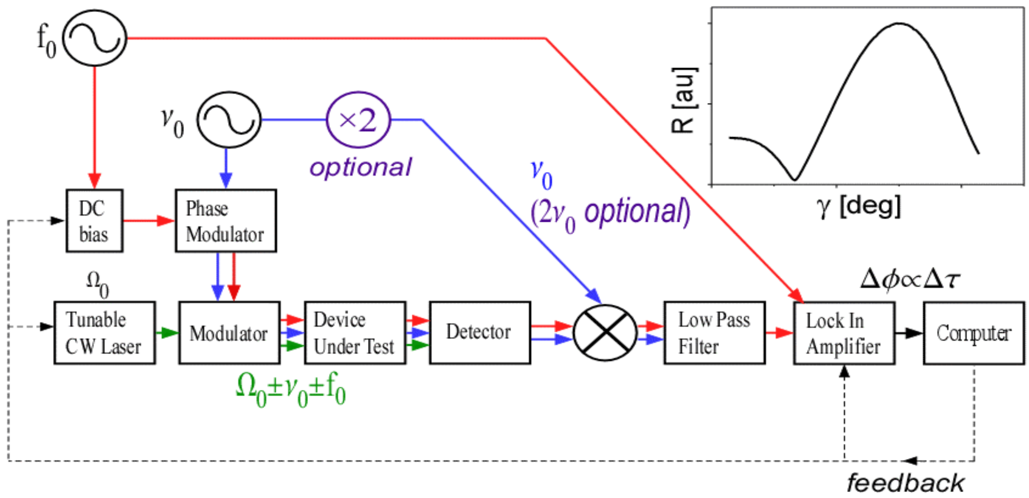

Figure 1.14 - Schematic drawing of revised MPS method, introducing audio dither to the RF drive, RF x2 frequency doubler and Lock In Amplifier. Inset: measured audio signal magnitude as function of DC bias phase.

- **Luna Interferometric optical vector network analyzer (OVA) [54-57]**:

This commercial system, is based on a tuneable laser source (TLS) which is used in combination with concatenated Mach–Zender interferometers, two polarization controllers, a polarization beam splitter, and three photodiodes labeled S, P, and A (Fig 1.15).

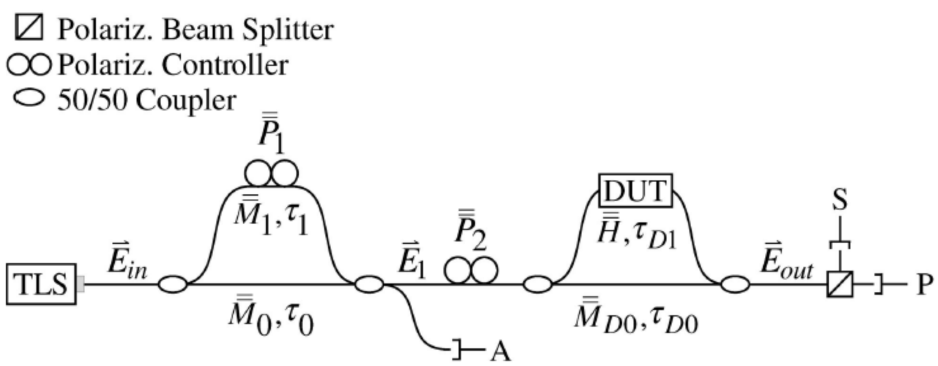

Figure 1.15 - Schematic drawing of Luna optical vector network analyzer system [55]. Tunable laser source is scanning through a Mach-Zender interferometric arrangement and polarizing beam splitters, resulting in interferemotric measurement per polarization and per wavelength.

The system measures the interference of the two polarizations during the laser scan, resulting in a Jones matrix per wavelength. From the parameters of the Jones matrix one can deduce the device insertion loss (IL), group delay (GD), polarization dependent loss (PDL) and polarization mode dispersion (PMD) [58]. Luna OVA measurement is fast, but is limited buy the coherence length of the laser. This limits the length of the device under test which can be measured using this method.

1.7.3 Temporal domain measurements: high rate measurements using real time and sampling scopes

Temporal measurements of high rate signals were performed by a 12 GHz BW detector and a real time scope with 40Gs/sec sampling rate. In addition, some measurements of higher rate signals were executed using a high speed sampling scope with an effective bandwidth sampling rate of 65 GHz.

1.7.4 Spatio-Temporal domain measurements: ultrashort pulse shape measurement

In order to measure ultrashort pulses we used two photon absorption based interferometric intensity autocorrelation measurement (Fig 1.16), with a Si photodetector. In this way we managed to measure the pulse shape and to show that our generated pulse is transform limited [59].

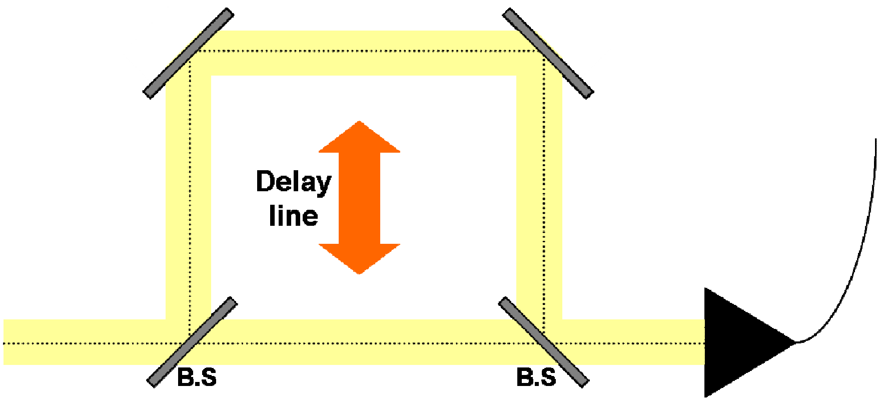

Figure 1.16 - Schematic drawing of interferometric intensity autocorrelation measurement. Optical delay lines serve to change the position between the two pulses, resulting in autocorrelation. a si. detector is used in order to detect the intensity autocorrelation.

1.8 Thesis structure

Six pear-reviewed articles are gathered is this work, all of them were published between 2010-2013 and all of them deal with design or implementation of our PSP. The articles were divided into two separate categories: the first was titled: "The evolution of PSP" and the second: "PSP applications".

The next 2 chapters are therefore arranged according to the following order:

Chapter 2: Contains brief discussion on the evolution of PSP design. This chapter serves as an introduction and summary for the 3 articles that appears on chapters 3-5, all of them deals in different variations and concept of a PSP.

> **Chapter 2A**: D. Sinefeld, and D.M. Marom, “Hybrid Guided-Wave/Free-Space Optics Photonic Spectral Processor Based on LCoS Phase Only Modulator," IEEE Photon. Technol. Lett. 7, 510-512 (2010).
>
> **Chapter 2B**: D. Sinefeld, S. Ben-Ezra, C. R. Doerr, and D. M. Marom, "All-channel tunable optical dispersion compensator based on linear translation of a waveguide grating router," Opt. Lett. 36, 1410-1412 (2011).
>
> **Chapter 2C:** D. Sinefeld, C. R. Doerr, and D. M. Marom, "A photonic spectral processor employing two-dimensional WDM channel separation and a phase LCoS modulator," Opt. Express 19, 14532- 14541 (2011).

Chapter 3: Contains brief discussion on a few implementations of the various PSP's that were introduced before. This chapter serves as an introduction and summary for the 3 articles that appears on chapters 7-9.

> **Chapter 3A**: D. Sinefeld, S. Ben-Ezra, and D. M. Marom, "Nyquist-WDM filter shaping with a high-resolution colorless photonic spectral processor," Opt. Lett. 38, 3268-3271 (2013).
>
> **Chapter 3B**: D. Sinefeld, Y. Fattal, and D. M. Marom, "Generation of WDM adaptive-rate pulse bursts by cascading narrow/wideband tunable optical dispersion compensators," Opt. Lett. 37, 4290-4292 (2012).
>
> **Chapter 3C:** D. Sinefeld and D. M. Marom, "Tunable fiber ring laser with an intracavity high resolution filter employing two-dimensional dispersion and LCoS modulator," Opt. Lett. 37, 1-3 (2012).

Chapter 2.
The evolution of PSP

During my research three different variants of our PSP were developed. The three versions are discussed in the 3 papers appearing in subchapters a-c. The first paper describe the design and performance of a high resolution colorless PSP which was manifested with a special version of an AWG [41]. The second paper describe a compact colorless Tunable optical dispersion compensator (TODC) without the use of SLM in the spectral plane [60]. The third paper describe a two dimensional PSP which cover the whole c-band with high resolution [48].
In the following section we will describe these systems and their results.

2.1 High resolution colorless PSP [41]

In this paper we present our state-of-the-art colorless PSP (that was firstly introduced earlier on section 1.6). We used a high-resolution AWG, with 34 grating arms and an FSR of 100 GHz which was designed to match the 100 GHz WDM grid spacing. An $\boldsymbol{f=3mm}$ cylindrical lens that is affixed at the PLC edge collimates the light in the guided direction. Since the AWG was reused from previous system [22] in which the output waveguides were imaged onto a curved plane, we had to compensate for the curved imaging field. Therefore, we projected the spectrally dispersed curved surface onto a flat plane by using a free-space beam expander using lenses $\boldsymbol{f}_1$ and $\boldsymbol{f}_2$, separated by a distance $\boldsymbol{L}$. The beam expander imparts a magnification of $\boldsymbol{M}=\boldsymbol{f}_2/\boldsymbol{f}_1$ and phase curvature of $1/\boldsymbol{R}=(\boldsymbol{f}_1+\boldsymbol{f}_2-\boldsymbol{L})/\boldsymbol{f}_2^2$. A typical beam expander is set at $\boldsymbol{L}=\boldsymbol{f}_1+\boldsymbol{f}_2$, to prevent residual curvature. However, in our case we wish to compensate for the curved input spectral surface, which is achieved by increasing the distance $\boldsymbol{L}$, as shown in Fig. 2.1, resulting in the spectral components being dispersed along the SLM plane instead of the original curved surface. We use lenses of focal lengths $\boldsymbol{f}_1$=20mm and $\boldsymbol{f}_2$=200mm separated by $\boldsymbol{L}$=420mm, which maps the input 2 mm field curvature onto a flat surface, where the reflecting SLM is placed. The dispersed spectrum of all the WDM channels overlap onto each other, due to the AWG's 100 GHz FSR, resulting in simultaneously same response for all WDM channels.

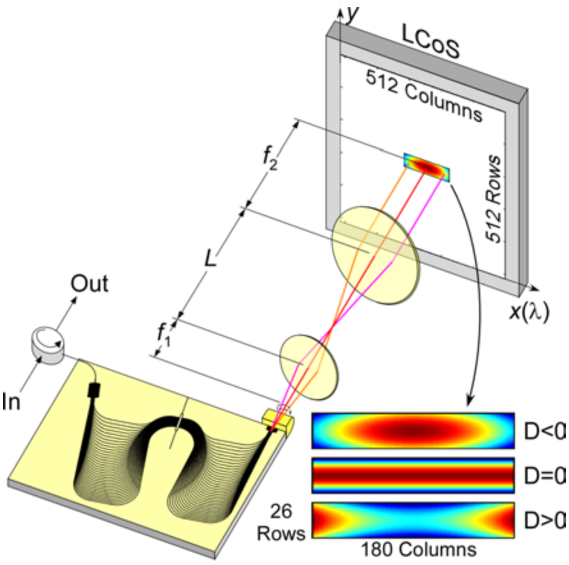

Figure 2.1 – Layout of the PSP. Spectrally dispersed light at the dashed curved surface are projected onto the LCoS SLM at a normal incidence angle. Inset: LCoS phase patterns sent to SLM. Horizontal curvature maps to dispersion; fixed vertical curvature is required for reduced losses. The illuminated area is small in comparison to the SLM.

The optical elements of the colorless PSP, consisting of the AWG PLC, the Fourier lens and the LCoS modulator were assembled on an optical table. A circulator was used to separate the input and output light to the PLC. The usable bandwidth of the PSP was found to be ~75 GHz (see Fig. 2.2 (f)). The insertion loss of the PSP is about 12 dB comprised of 8 dB losses caused by the double-pass in the AWG [21], 2 dB due to the circulator and other fiber connectors, and 2 dB from free-space losses, losses from the SLM and high diffraction orders elimination.

Since the introduction of the LCoS array modulator allows us to prescribe both spectral phase and amplitude modulation, we demonstrate this functionality by imparting attenuation features onto the channel spectrum (Fig. 2.2). This technique can be used to attenuate spectral features and enhance the signal quality in the time domain or optimally filter a signal which has undergone distortion due to multiple spectrally-misaligned channelized components. Any spectral shape, subject to the constraint of the optical resolution, can be prescribed. The dynamic range of the attenuation is greater than 20 dB (Fig. 2.2d), limited mostly by back reflections from the PLC end. However, this result is resolution dependent. When operating a high resolution pattern the dynamic range is lower due to the SLM spatial response.

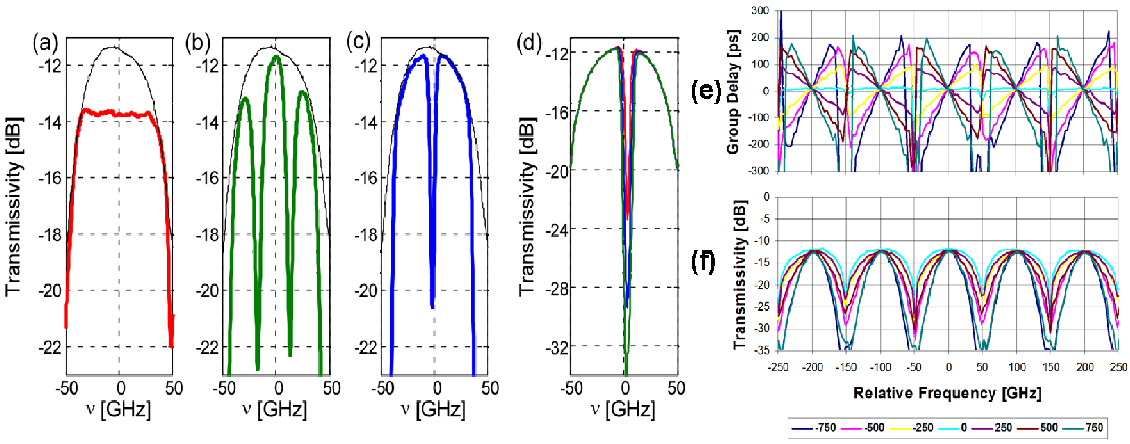

Figure 2.2 - PSP operation as a a spectral shaper and as a TODC. Left: Demonstration of spectral carving across the channel bandwidth, where black line denotes the native spectrum. (a) Spectral flattening, (b) spectrum carved to three sub-bands, (c) spectrum narrowed at edges and a narrow notch inserted, (d) narrow attenuation exhibiting 22dB dynamic range. Right: Quadratic phase (CD compensation) results. (e) Group delay versus frequency. Linear slopes are observed, corresponding to 7 different dispersion values (±750, ±500, ±250 and 0 ps/nm). (f) Transmissivity versus frequency. Spectral narrowing is observed for larger departures from zero dispersion. Passband and dispersion settings are repeated at 100-GHz FSR.

To test the processor as a TODC, quadratic phase functions with varying radii were applied in the dispersion direction. The quadratic phase maps to CD values according to the equation:

$$\boldsymbol{CD} \equiv \frac{2\pi \boldsymbol{c}}{\lambda^2}\frac{\boldsymbol{d}^2\phi(\omega)}{\boldsymbol{d}\omega^2} = \frac{\lambda_0^2}{2\pi \boldsymbol{c}_0}\frac{\boldsymbol{d}^2\phi(\boldsymbol{x})}{\boldsymbol{dx}^2}\left(\frac{\boldsymbol{dx}}{\boldsymbol{d}\lambda}\right)^2 = \frac{\lambda_0}{\boldsymbol{c}_0}\frac{1}{\boldsymbol{R}}\left(\frac{\boldsymbol{dx}}{\boldsymbol{d}\lambda}\right)^2 \tag{2.1}$$

where $\phi(x)=k_0 \cdot x^2/2R$ is the parabolic approximation to a curved phase, λ_0 is the wavelength in vacuum, c_0 is the speed of light, k_0 is the wave vector, $1/R$ is the applied curvature, $dx/d\lambda$ is the spatial dispersion and CD is the chromatic dispersion in units of ps/nm. With our PSP implementation we achieve $\boldsymbol{CD} = 115{,}600 \cdot \boldsymbol{CV}$ [ps/nm] for (where $CV=1/R$ is measured in mm^{-1}). In order to measure the actual CD values that were applied by the PSP, we used a Modulation Phase Shift (MPS) setup [50-53] with a tunable laser. The group delay results for several CD values are shown (Fig 2.2e). Higher CD values result in spectral narrowing (Fig. 2.2f). Bandwidth is reduced down to 30 GHz for CD values of ±750 ps/nm. Note that the passband can be artificially widened by imparting additional loss (Fig. 2.2a).

2.2 colorless compact TODC - passive PSP [60]

In this work we present a compact TODC based on an extremely simple free space arrangement of an AWG, Fourier lens and flat reflecting mirror, with accompanying 42.8 Gb/sec transmission results.

After using a PLC with a curved output, we manufactured a new PLC version which was designed for a flat output. Such PLC does not need the complicated arrangement that was introduced in the last section in order to flatten the curved spectral field. Instead, a simple Fourier lens can be used to project the light on the SLM as was originally shown in Fig 1.11. However, there is an even simpler way to apply a curved phase along the spectral plane. Instead of utilizing spatially controlled quadratic phase elements at the Fourier plane as in our former work, we use a very compact arrangement and simply modify the distance between the AWG and the Fourier lens (as shown in Fig 2.3a).

The longitudinal displacement is equivalent to applying a radial phase at the Fourier plane and results in a curved phase front added to the dispersed spectral components. In this way we can compensate for chromatic dispersion (CD) values up to ±1000 ps/nm. The simplicity of this system makes it effective as a TODC for mitigating dispersion impairments, consuming no power once set and hence will not fail in power outages. The longitudinal displacement of the AWG from the front focal plane (distance $\boldsymbol{f}$ to lens) to an arbitrary distance $\boldsymbol{d}$ (between WGR and lens), results in a quadratic phase added to the beam at Fourier plane with curvature [61]:

$$\frac{1}{\boldsymbol{R}} = \frac{1}{\boldsymbol{f}}\left(1 - \frac{\boldsymbol{d}}{\boldsymbol{f}}\right) = \frac{\Delta \boldsymbol{z}}{\boldsymbol{f}^{2}} \tag{2.2}$$

where $\Delta\boldsymbol{z}=\boldsymbol{f}-\boldsymbol{d}$. Combining this equation together with Eq. 2.1 gives the relation:

$$\boldsymbol{CD} = \frac{2\lambda_0}{\boldsymbol{c}_0}\frac{1}{\boldsymbol{R}}\left(\frac{\boldsymbol{dx}}{\boldsymbol{d}\lambda}\right)^2 = \frac{2\lambda_0}{\boldsymbol{c}_0}\left(\frac{\boldsymbol{dx}}{\boldsymbol{d}\lambda}\right)^2\frac{\Delta \boldsymbol{z}}{\boldsymbol{f}^{2}} = \frac{2\lambda_0}{\boldsymbol{c}_0}\left(\frac{\boldsymbol{d}\theta}{\boldsymbol{d}\lambda}\right)^2 \Delta \boldsymbol{z} \tag{2.3}$$

Hence, CD values have a linear dependence on the displacement $\Delta\boldsymbol{z}$ between the WGR and the Fourier lens. In this way, very simple longitudinal translation of the WGR results in different CD compensation values.

As one can expect from such a system, the quadratic phase imposes not only CD, but also an undesired spectral narrowing, due to the tilt applied to spectral components far from the channel grid.

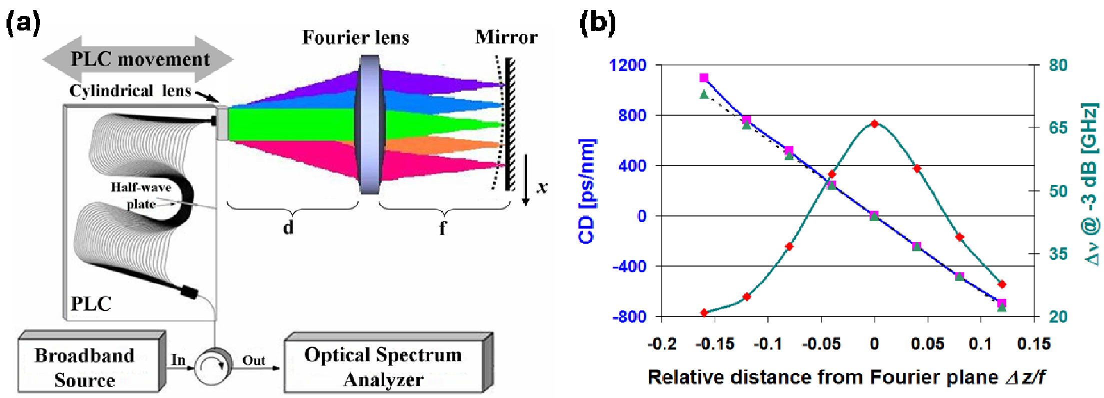

Figure 2.3 - (a) Layout of the tunable optical dispersion compensator. Changing the distance *d* between the WGR and the Fourier lens imparts a quadratic phase across the Fourier plane (seen as a dashed surface on the Fourier plane). (b) Measured CD values (Blue), Theoretical CD values (Black dashed line) and Bandwidth (Green) versus displacement Δz. As the phase curvature values at Fourier plane are larger, the narrowing effect becomes dominant bandwidth is reduced down to 20 GHz for CD values of ±1000 ps/nm.

The measured CD values (calculated from the group delay slopes), the theoretical CD values (using Eq. 2.3, with the experimental dx/dλ values), as well as the resulting -3dB channel bandwidth measures are plotted in Fig. 2.3b against the relative displacement from the lens front focal plane ***Δz/f***.

The experimental and theoretical CD values match extremely well. As the phase curvature values at Fourier plane increase, the narrowing effect becomes dominant and the bandwidth is reduced down from 65 GHz at low CD correction values to 20 GHz for extreme TODC values of ±1000 ps/nm.

In principle, there is an option of eliminating the bandwidth narrowing by using a four pass system [23,62], however such a system is more complicated and will suffer higher losses.

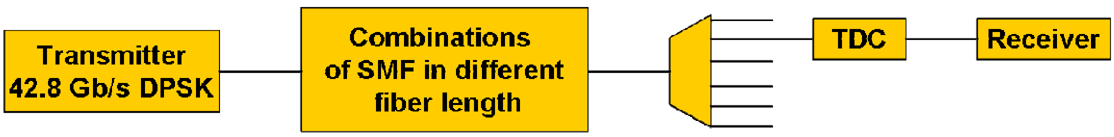

Figure 2.4 - BER measurement setup: a sequence of 42.8-Gb/s differential phase-shift keying (DPSK) 231−1 pseudorandom bit sequence at 1550.12 nm was transmitted through various fiber length with CD compensation of our TODC. the results appear in Fig 2.5.

The dispersion-compensation capability of this compact TODC was tested using a 42.8-Gb/s differential phase-shift keying (DPSK) $2^{31}-1$ pseudorandom bit sequence at 1550.12 nm, with different lengths of standard single-mode fiber (dispersion coefficient of 17 ps/nm-km) placed between the transmitter and the receiver (Fig. 2.4). Tuning the TODC was trivial, as a single micrometer movement yielded immediate eye opening at the proper distance Δz as shown in Fig. 2.5. Without the dispersing fiber, the TODC showed zero penalty over the back-to back case, as can be seen in Fig. 2.5E.

The penalty for compensation of 30-50 km fiber length was ~2 dB OSNR at 10^{-9} BER. For the 60 km fiber length the penalty increased. We attribute the greater penalty to passband narrowing at our chosen modulation format. This bandwidth narrowing changes the signal quality, as seen in the eye shape (Fig. 2.5C), resembling that of doubinary modulation [63-64].

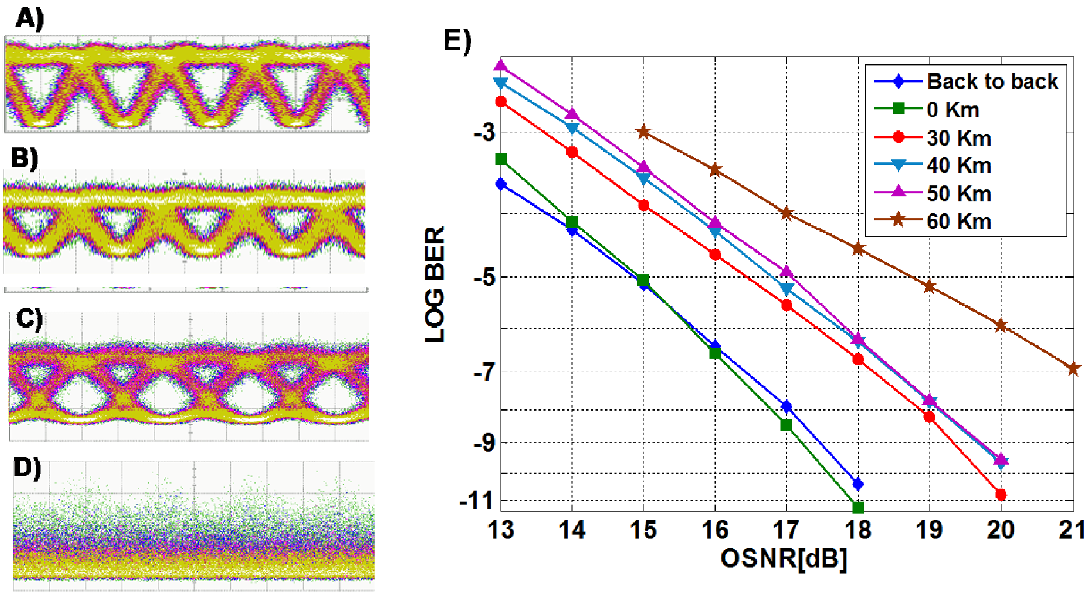

Figure 2.5 - Detected eye diagrams and BER measurments after TODC correction with signal transmitted along: A) 0 km, B) 20 km, C) 40 km and D) 40 km without TODC CD correction. E) Receiver sensitivity curves for different amounts of fiber CD in the link, compensated by the TODC.

2.3 Two dimensional PSP [48]

In this work we present a two-dimensional, amplitude and phase PSP with the ability to control each WDM channel separately and with the same high resolution as our earlier colorless PSP. This PSP was based on the combination of two crossed gratings, a high resolution AWG and a free-space bulk grating, together with the LCoS SLM. We demonstrated the ability to manipulate both spectral phase and amplitude along the conventional optical communication band (1530-1560 nm), with a resolution of 3.3 GHz and 200 MHz addressability.

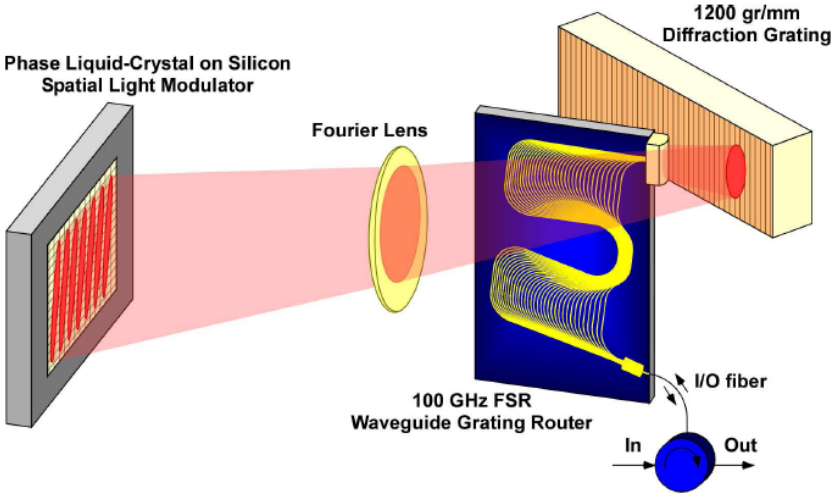

Figure 2.6 - Layout of the 2D photonic spectral processor, capable of imparting independent spectral amplitude and phase to each WDM channel with the use of a LCoS modulator array. Crossed gratings (WGR and bulk) disperse the spectrum across the two-dimensional LCoS array, enabling high resolution access to the spectral components of each channel.

The 2D PSP layout is depicted in Fig. 2.6. Light enters the same PLC used in our previous system (with a flat output) and dispersed out angularly, where a crossed bulk grating, placed between the AWG and the Fourier lens, is separating the diffraction orders of the AWG in the orthogonal direction. This arrangement results in two spatial dispersion axes: a “fast” dispersion axis with high resolution and 100 GHz FSR, and an orthogonal “slow” dispersion axis which separates the WDM channels. In order to achieve AWG order separation we must use a bulk grating with an angular dispersion greater than the diffraction spread angle. This condition can be expressed by:

$$\boldsymbol{d}\cos(\theta) \le \frac{\pi\lambda \boldsymbol{f}_{cyl}\boldsymbol{N.A}_{WG}\Delta\nu_{FSR}}{2\boldsymbol{c}} \quad (2.4)$$

We satisfy the condition set forth by Eq. (2.4) using a 1200 gr/mm holographic diffraction grating which was placed at an angle of approximately 73^0 (close to the

68.5^0 Littrow angle of such grating) in order to achieve the order separation for our 2D system. An IR-optimized ***f=100***mm cemented doublet lens performs the Fourier transform and converts the angular spectrum to spatial and projects 2D separated frequency components onto the LCoS SLM. We used our phase-only, two-dimensional LCoS reflective modulator which has 512×512 square pixels of 15 μm pitch, providing an active region of 7.68×7.68 mm.

Ideally, both gratings should be placed at the lens front focal plane so that their angular dispersion will be converted to spatial dispersion that is normally-incident onto the SLM. This could be achieved with a multi-lens solution that images the first grating onto the second [46], but such a solution increases the optical track length and component count and is hence undesirable. Instead, we placed the bulk grating in between the AWG (which is placed near the front focal plane) and the lens. This results in the grating orders being incident in a space-varying incidence angle, or curvature. This phase curvature is related to the distance of the grating from the first Fourier plane, Δz, as was shown previously in Eq. (2.3). This unwanted curved phase will result in losses for off-axis channels. However, this effect can be completely compensated in our system since our phase LCoS SLM can encode an horizontal cylindrical quadratic phase function across the aperture. In this way we can couple-back the light from all diffraction orders with constant efficiency as shown in Fig 2.7. Note that it is advantageous to displace the bulk grating from the front focal plane and not the AWG output, as the "fast" dispersion axis is more susceptible to chromatic dispersion being added onto the signal for an identical displacement.

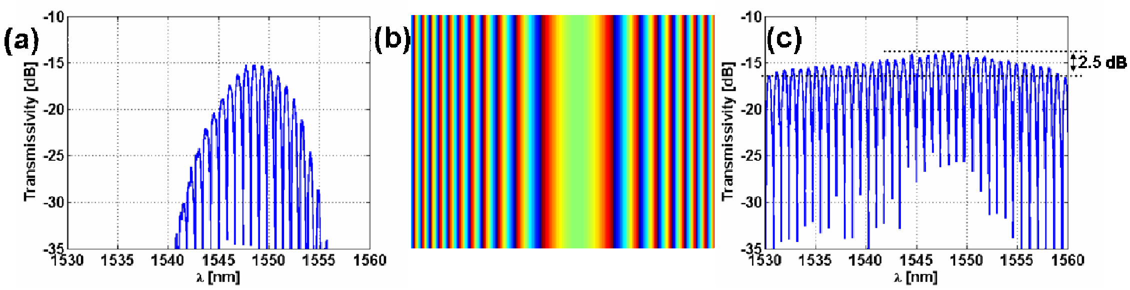

Figure 2.7 – The impact of applying horizontal curved phase along the channels in order to eliminate the losses caused by the finite separation between the AWG output facet and the bulk grating. (a) PSP output before equalization. (b) The horizontal quadratic phase that was added in order to achieve channel equalization. (c) PSP output after equalization. In the plot 40 WDM channels are shown. This was achieved by moving the SLM along the spectral plane, and stitching the overlapping results from two SLM locations.

With the horizontal curved phase applied, an intensity uniformity of 2.5 dB was achieved along 30 nm, resulting in 40 nearly equalized WDM channels. We map the spatial dispersion on the SLM by locating the center position for each laser wavelength (Fig. 2.8). In the AWG direction (fast axis) the SLM 512 columns spans a ~93-GHz wide spectrum (limited by SLM size) which correspond to spatial dispersion of 10.3[***mm/nm***]. Each column of the modulator addresses a particular center frequency, at 182 MHz shift in center frequency. The spatial dispersion in the bulk grating direction results in an offset of 15 pixels for successive diffraction orders (spaced at 100 GHz). This pitch is not constant across the spectrum, as the grating angular dispersion is not linear.

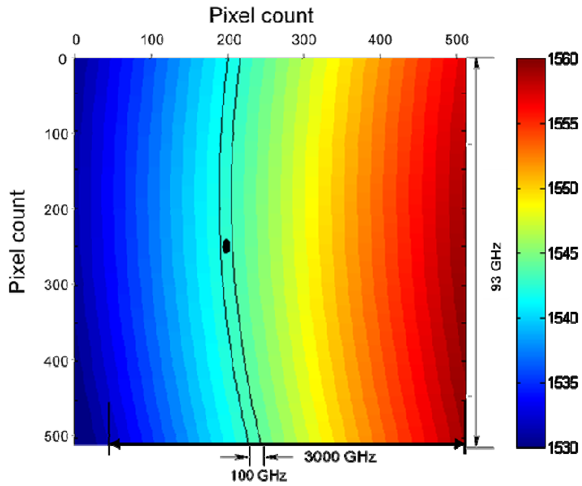

Figure 2.8 – Different wavelength locations on the SLM. The WGR provides high resolution on narrow FSR. The bulk grating separates the WGR diffraction orders. Individual channels are fully resolved on two-dimensional space. The black lines mark the borders of a specific WDM channel while the black ellipse denotes the spot size for a specific wavelength on this channel as it appears on the SLM.

The insertion loss of the PSP is -14 dB. This high loss value is partially due to phase errors in the fabricated WGR, as well as an unoptimized transition from the guided region to free space. Both issues can be corrected in a different AWG with additional fabrication process. We anticipate that system losses of ~7 dB can be achieved, limited by AWG coupling inefficiency and by losses of the 2D assembly.

With this two-dimensional PSP, numerous spectral manipulations can be envisaged, owing to its fine resolution across all channels within the C-band. In the following sections we demonstrate WDM channel spectral amplitude manipulations, spectral phase manipulations, and in-band amplitude and phase spectral manipulations.

I) Channel amplitude control – WDM blocker

As a first demonstration, we used our PSP as a channel selector by blocking or transmitting complete columns (WDM channels). Fig. 2.9 shows demonstrations of 15 randomly selected channels for attenuation. Channel selection is performed by applying a phase tilt to the rejected channel set. It should be noted that the linear phase tilt which serves as the attenuation mechanism can be prescribed either along the dispersion or along the beam height. Better attenuation performance was achieved with the former method, as the beam is wider in the fast dispersion direction.

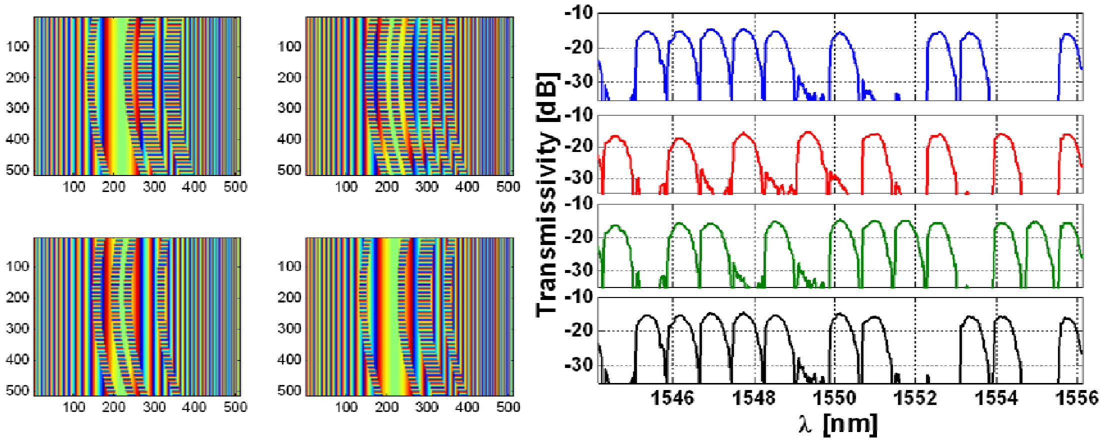

Figure 2.9 – Demonstration of channel selection with the 2D PSP. (Left) - The phase modulations as written on the SLM in the case of random selection of 15 WDM channels. Tilted phase was added on top of the curved equalization phase to attenuate channels. (Right) – Results of random selection of 15 WDM channels. A dynamic range of 20 dB is shown, limited by insufficient separation of WGR diffraction orders (or adjacent WDM channels).

II) Channel phase control –TODC and retimer

Two important applications of the PSP are TODC and channel retiming. To test the processor as a TODC, quadratic phase functions of varying radii were applied in the same way it was applied in the colorless PSP, but with ability to apply an independent quadratic phase to each selected WDM channel. We performed group delay measurements with various curvature values applied to the channels (see Fig. 2.10(a-b)). As the slopes of the group delay are equivalent to CD, it can be seen that independent CD values can be applied to each channel. Our system is able to compensate for CD values up to ±750 ps/nm for each WDM channel. Larger CD values are achievable but will result in spectral narrowing as shown in Fig. 2.11a.

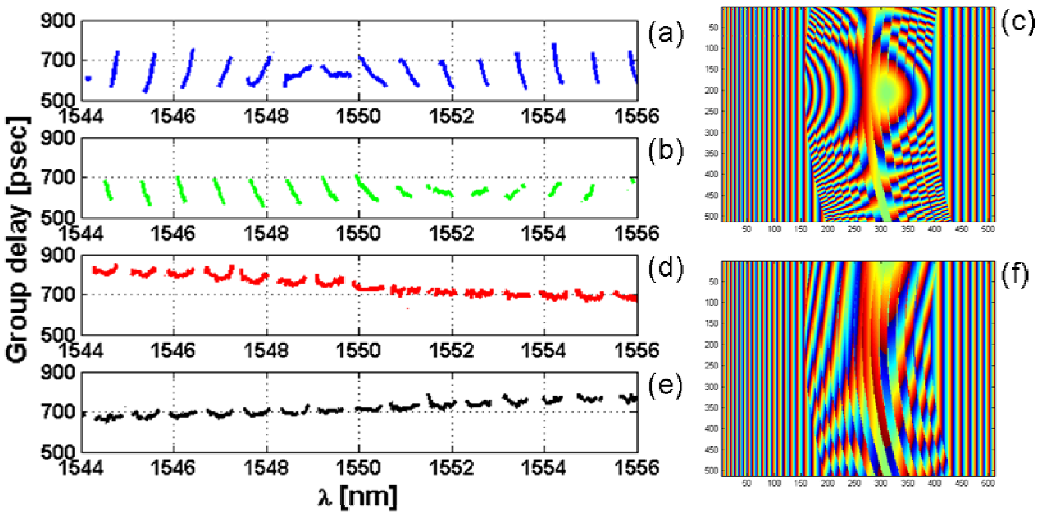

Figure 2.10 – Example of phase manipulation for 15 channels. (a-b) group delay slopes applied to each channel are equivalent to different CD compensation values. (c) The relevant phase pattern that was written on the SLM, consisting of varying quadratic phases. (d-e) Different group delay values applied to the selected 15 channels. (f) The relevant phase pattern that was written on the SLM, consisting of varying linear slopes.

A different phase manipulation is shown in Fig. 2.10(d-e). Channel retiming is achieved by applying linear phase along the spectrum, resulting in constant and controllable group delays per channel or channel retiming. Time offsets of ±100 ps are demonstrated along 15 channels. The expression for the retiming is given by [65]:

$$\tau_{GD} \equiv \frac{d\phi(\omega)}{d\omega} = -\frac{d\phi(x)}{dx}\frac{dx}{d\lambda}\frac{d\lambda}{d\omega} = -\frac{\lambda_0}{c_0}\theta\left(\frac{dx}{d\lambda}\right) \tag{2.5}$$

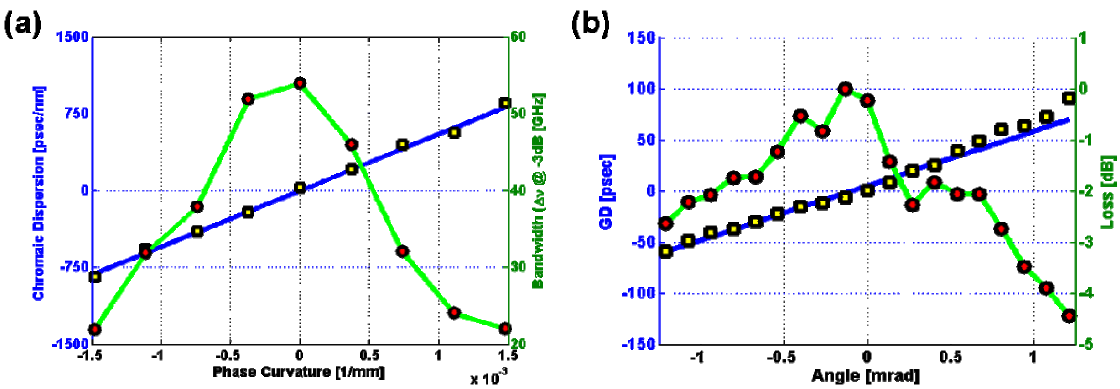

Figure 2.11 – The performance of the two-dimensional PSP when used as a TODC and as a retimer: (a) TODC performance: theoretical (Blue line) and measured (Yellow squares) CD values and bandwidth (Green) versus curvature. As the phase curvature values are larger, narrowing becomes dominant and the bandwidth is reduced down to 23 GHz FWHM for CD values of ±750 ps/nm. (b) retimer performance: theoretical (Blue line) and measured (Yellow squares) GD values and loss (Green) versus slope angle measured in milliradians. As the phase slope becomes larger, the GD increases. However, large slopes results in high coupling losses.

Where $\phi(x)=k_0 \cdot \theta \cdot x$ is the linear phase function applied along the channel, k_0 is the wave vector, and θ is the phase slope angle in radians. Applying linear phase along the spectral channel results also in losses which become larger as the slope increases as shown in Fig. 2.11b. These losses limit the amount of GD that can be achieved in the retiming mode. Thus, phase curvatures result in group delay slopes or CD values, while phase slopes result in constant group delays or retiming. TOCD range is primarily limited by spectral narrowing and retiming is limited by loss, both limitations arising from the coupling losses back to the output fiber through the PSP.

III) In-band channel manipulations – phase/amplitude carving

Fig. 2.12(a) demonstrates the use of the PSP for spectral carving by imparting unique attenuation features onto each WDM channel spectrum. This technique can be used to split the spectral channel into sub-bands or to attenuate spectral features and enhance the signal quality. Due to the high resolution of the PSP, almost any spectral shape can be prescribed for each channel, subject to the resolution constraint.

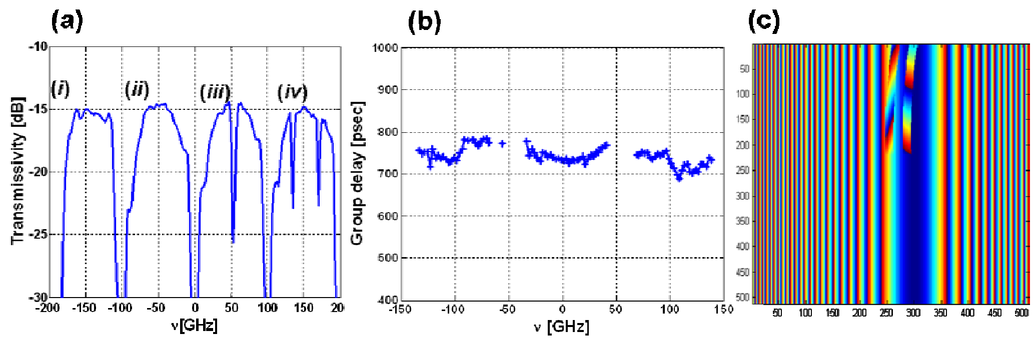

Figure 2.12 – Demonstration of inband manipulations: (a) spectral carving across the channel bandwidth for four contiguous WDM channels: (i) spectral flattening (ii) without modulation, (iii) spectrum carved to two sub-bands, (iv) spectrum carved to three sub-bands. (b) Example of half-channel group delay manipulation for 3 channels. A time split of 50 ps is obtained (c) The applied phase pattern on the SLM for the 3 half slopes case.

An interesting option which takes advantage of the high resolution of our PSP is to perform retiming of spectral components within a channel. Fig. 2.12(b) demonstrates such an example. A phase slope was applied on half of the three main channels. The result is a time delay that depends on the local slope along part of the channel [42-43]. For the left channel a positive slope was applied resulting in time delay for half of the channel, while for the right channel a negative slope was used resulting in a time advance for the half channel.

Chapter 2A.

Hybrid Guided-Wave/Free-Space Optics Photonic Spectral Processor Based on LCoS Phase Only Modulator

David Sinefeld and Dan M. Marom

Published in IEEE Photonic Technology Letters:

D. Sinefeld, and D.M. Marom, “Hybrid Guided-Wave/Free-Space Optics Photonic Spectral Processor Based on LCoS Phase Only Modulator," IEEE Photon. Technol. Lett. 7, 510-512 (2010).

Hybrid Guided-Wave/Free-Space Optics Photonic Spectral Processor Based on LCoS Phase Only Modulator

David Sinefeld and Dan M. Marom, *Senior Member, IEEE*

***Abstract*—We propose and demonstrate a photonic spectral processor for applying arbitrary spectral phase and amplitude at high resolution with a 100-GHz free-spectral range for colorless wavelength-division-multiplexing adaptive filtering applications. The system employs free-space optics for projecting the dispersed light coming out of a planar-lightwave circuit onto a phase spatial-light modulator. The processor achieves 3-GHz optical resolution over 75-GHz usable bandwidth, with 557-MHz addressable granularity.**

***Index Terms*—Optical communication, optical filters, optical planar waveguide components, optical waveguide components.**

I. Introduction

OPTICAL devices for impairment mitigation are important for maximizing the performance of optical communication systems. With increasing channel transmission rates, the broad signal spectrum is susceptible to filtering and dispersion, resulting in a degraded signal reaching the receiver. Many device classes address impairment sources by offering tunable dispersion compensation (TDC) [1], [2] or optical equalization [3], in either guided-wave or free-space optical solutions. The concept of combing a dispersive element together with spatial light modulators (SLMs) were used for pulse shaping [4], power equalization [5], [6], add–drop switch [7], amplitude and time control [8], and spectral filtering [9], [10].

Dispersion compensation can be achieved by applying a quadratic phase function across a spatially dispersed optical spectrum. When a planar lightwave circuit (PLC) device employing a waveguide grating router (WGR) for dispersing the optical signal is used, the quadratic phase has to be applied at the output curved surface of the second slab lens. Several devices based on this concept have been demonstrated, using a polymer thermo-optic lens [11], or a deformable mirror [12] as the phase modulator. Recently [13], we presented a WGR-based device using a liquid crystal on silicon (LCoS), two-dimensional phase array modulator. With the LCoS SLM, we are able to prescribe arbitrary phase as well as amplitude to the signal's spectral components. We use external free-space optics to flatten and magnify the spectrum from the curved surface to a flat field incident on the LCoS array. The beam curvature introduced by the free-space optics section compensates for the WGR's curved output plane and magnifies the signal which allows us to achieve addressable spectral granularity of 557 MHz/pixel column.

Manuscript received September 08, 2009; revised December 08, 2009; accepted January 17, 2010. First published February 02, 2010; current version published March 10, 2010. This work was supported in part by the Israel Science Foundation (Grant 1359/07) and in part by The Peter Brojde Center for Innovative Engineering.

The authors are with the Applied Physics Department, The Hebrew University of Jerusalem, Jerusalem 91904, Israel (e-mail: sinefeld@gmail.com; danmarom@cc.huji.ac.il).

Color versions of one or more of the figures in this letter are available online at http://ieeexplore.ieee.org.

Digital Object Identifier 10.1109/LPT.2010.2041548

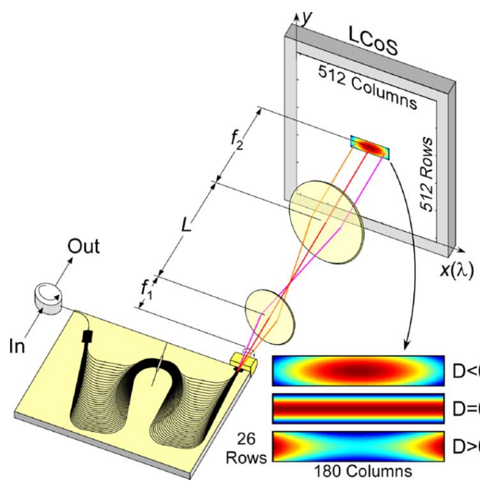

Fig. 1. Layout of the PSP. Spectrally dispersed light at the dashed curved surface are projected onto the LCoS SLM at a normal incidence angle. Inset: LCoS phase patterns sent to SLM. Horizontal curvature maps to dispersion; fixed vertical curvature is required for reduced losses. The illuminated area is small in comparison to the SLM.

In this letter, we provide further design details and updated measurement results of our photonic spectral processor (PSP). The updated results show a 17-dB loss improvement from our previous results [13], by introducing a vertical phase curvature using the SLM, to counter the beam curvature in the nondispersion direction. We now show that the optical resolution of our system is fundamentally limited by the resolving power of the WGR, providing 3-GHz resolution over a 75-GHz usable bandwidth with a 100-GHz free-spectral range (FSR). The functionality and performance of the PSP make it well suited for mitigating signal impairments and also for high resolution spectral carving or flattening.

II. System Design

The PSP layout is shown in Fig. 1. Light enters a PLC containing a high-resolution WGR through the "I/O" waveguide. Normally the light would be dispersed at the output curved surface of the second slab lens. However, since the PLC is cut through the slab lens, the refracted light focuses in air along a virtual curved surface residing off-chip (see dashed curved line in Fig. 1). The employed high-resolution WGR has been reused from [12], consisting of 34 grating arms. The on-chip slab lens radius is 3 mm, which reduces to ~2 mm after refraction at the glass–air interface.

Normally, a reflective modulator would be placed along the curved surface with an ideal curvature matching that of the WGR curvature. Mirror deviations from the WGR curvature will result in spectral phase modulation, and can be designed for chromatic dispersion (CD) compensation [12]. In our system, we replaced the curved mirror with a phase-only, two-dimensional LCoS reflective modulator in order to achieve arbitrary spectral phase modulation and fine spectral granularity. However, placing the reflective SLM directly at the curved surface would imply that the SLM should be encoded with the WGR curvature for a flat frequency response. This would result in poor diffractive efficiency due to the multiple modulo 2π phase modulation wrapping.

Therefore, we project the spectrally dispersed curved surface onto a flat plane by using a free-space beam expander using lenses f_1 and f_2, separated by a distance L. The beam expander imparts a magnification of $M = f_2/f_1$ and phase curvature of $1/R = (f_1 + f_2 - L)/f_2^2$. A typical beam expander is set at $L = f_1 + f_2$, to prevent residual curvature. However, in our case, we wish to compensate for the curved input spectral surface (dashed line in Fig. 1), which is achieved by increasing the distance L, as shown in Fig. 1, resulting in the spectral components being dispersed along the SLM plane instead of the original curved surface. We use lenses of focal lengths $f_1 = 20$ mm and $f_2 = 200$ mm separated by $L = 420$ mm, which maps the input 2-mm field curvature onto a flat surface. Our choice of lenses magnifies both the spatial dispersion and the spot sizes by a factor of $M = 10$. The magnified spectral plane extends over 2.7 mm along the horizontal axis of the SLM. It is important to note that the beam emerging from the WGR is vertically collimated by a cylindrical lens. Since the beam expander is not in collimating condition, the outcoming beam carries a residual curvature of $R = 200$ mm in the y-axis, resulting in a high power loss. A phase curvature must be added along the vertical axis of the SLM in order to achieve high system transmissivity, which was absent in our early trial [13] and yields in a 17-dB loss improvement.

Our LCoS modulator (Boulder Nonlinear Systems Model P512–1550, based on nematic liquid crystal) is optimized for 1550-nm operation and has square pixels of 15-μm pitch, resulting in ~180 columns spanning the 100-GHz-wide spectrum. Each column of the modulator addresses a particular center frequency, at 557-MHz shift in center frequency, given the system spatial dispersion of $dx/d\lambda = 3.35$ [mm/nm]. On the vertical axis, the beam is projected on 26 rows (or 390 μm). Phase modulation is achieved by prescribing an identical phase offset to all pixels in the column (on top of the curvature). Amplitude modulation can be achieved by several ways: modification of the curvature value, introduction of a linear phase ramp, or the application of a discrete phase jump, all performed in the vertical direction. System modulation speed is limited by our LCoS modulator model to 10 Hz.

The LCoS modulator supports one polarization only. Our free-space section provides ample space for a polarization diversity solution to be placed between the two lenses. However, one was not employed in the present PSP.

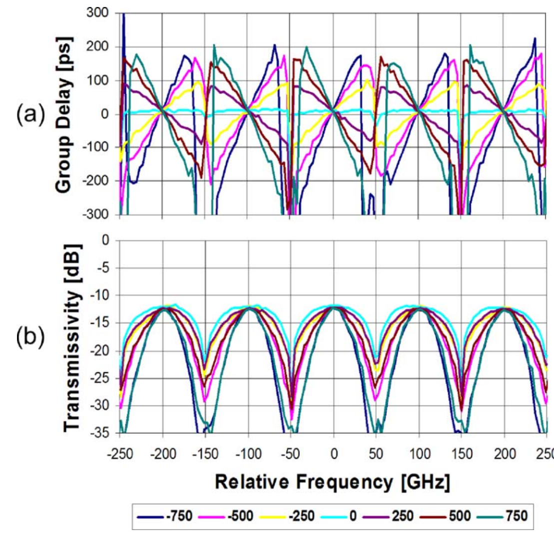

Fig. 2. Quadratic phase (CD compensation) results. (a) Group delay versus frequency. Linear slopes are observed, corresponding to seven different dispersion values (±750, ±500, ±250, and 0 ps/nm). (b) Transmissivity versus frequency. Spectral narrowing is observed for larger departures from zero dispersion. Passband and dispersion settings are repeated at 100-GHz FSR.

III. Results

The elements of the PSP, consisting of the WGR PLC, the two lenses, and the LCoS modulator were assembled on an optical table. A circulator was used to separate the input and output light to the PLC. The lens separation L was optimized to maximize and flatten the bandwidth, and the distance was very close to the designed separation. The usable bandwidth of the PSP was found to be ~75 GHz (see Fig. 2). The insertion loss of the PSP is about 12 dB comprised of 8-dB losses caused by the double-pass in the WGR [11], 2 dB due to the circulator and other fiber connectors, and 2 dB from free-space losses, losses from the SLM and high diffraction orders elimination.

To test the processor as a TDC, quadratic phase functions with varying radii were applied in the dispersion direction. The quadratic phase maps to CD values according to the equation: $\mathrm{CD} = 2\lambda_0/c_0(dx/d\lambda)^2 \cdot CV$, where $CV = 1/R$ is the phase curvature, and $dx/d\lambda$ is the spatial dispersion, achieving $\mathrm{CD} = 115\,600 \cdot CV$ [ps/nm] for our PSP implementation (where CV is measured in mm^{-1}). In order to measure the actual CD values that were applied by the PSP, we used a modulation phase shift (MPS) setup with a tunable laser. The group delay results for several CD values are shown [Fig. 2(a)]. Higher CD values result in spectral narrowing [Fig. 2(b)]. The CD values and −3-dB pass bandwidth as a function of the phase curvature are shown in Fig. 3. It can be seen that CD values are linearly dependent on phase curvature, and that narrowing effect becomes more pronounced. Bandwidth is reduced down to 30 GHz for CD values of ±750 ps/nm. Note that the passband can be artificially widened by imparting additional loss [Fig. 5(a)].

To characterize the spectral resolution of the PSP, an abrupt π phase jump was applied to one part of the signal spectrum. Spectral components near the abrupt phase transition experience a coupling loss, from which both the spatial dispersion and the resolution can be extracted (Fig. 4). The −3-dB bandwidth of the minimum resolvable spectral feature, or the optical resolution, was found to be 3 GHz. This result correlates well with the

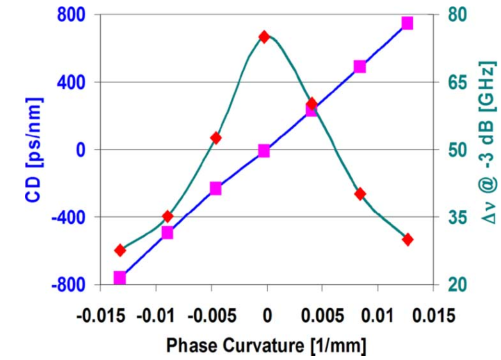

Fig. 3. CD values (blue) and bandwidth (green) versus curvature. As the phase curvature values are larger, the narrowing effect becomes dominant and the bandwidth is reduced down to 30 GHz for CD values of ±750 ps/nm.

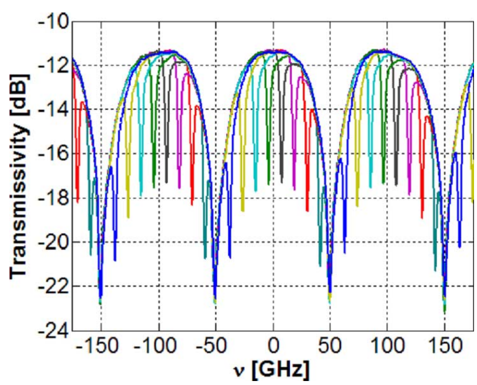

Fig. 4. Optical spectrum of PSP when testing for optical resolution. A narrow spectral dip is scanned across the spectrum. Dip width of 4.1 GHz is an artifact of the finite OSA resolution. Actual dip, measured with scanning laser, is 3 GHz wide.

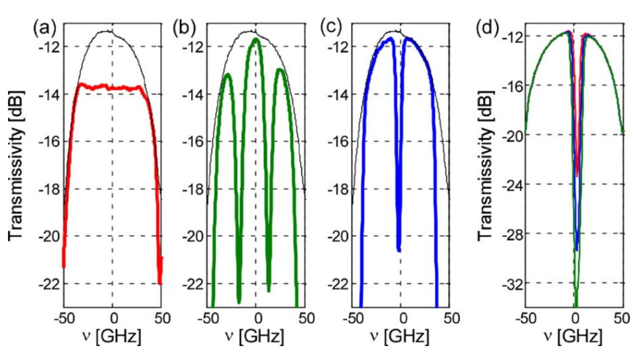

Fig. 5. Demonstration of spectral carving across the channel bandwidth, where black line denotes the native spectrum. (a) Spectral flattening; (b) spectrum carved to three sub-bands; (c) spectrum narrowed at edges and a narrow notch inserted; and (d) narrow attenuation exhibiting 22-dB dynamic range.

WGR resolvability, equaling the FSR divided by the WGR arm count (100/34, respectively).

Since the introduction of the LCoS array allows us to prescribe both spectral phase and amplitude modulation, we demonstrate this functionality by imparting attenuation features onto the channel spectrum (Fig. 5). The technique can be used to attenuate spectral features and enhance the signal quality in the time domain [10] or optimally filter a signal which has undergone distortion due to multiple spectrally misaligned channelized components. Any spectral shape, subject to the constraint of the optical resolution, can be prescribed. The dynamic range of the attenuation is greater than 20 dB [Fig. 5(d)], limited mostly by back reflections from the PLC end. However, this result is resolution dependent. When operating a high-resolution pattern, the dynamic range is lower (Fig. 4) due to the SLM spatial response.

IV. Summary

We demonstrated the functionality of the PSP, which is capable of modulating a communication signal's spectral components in amplitude and phase. The spectral resolution of the PSP is determined by the WGR, which for the present realization resolves 3-GHz features with a 75-GHz usable bandwidth and a 100-GHz FSR. The resolution can be improved with the use of a WGR with a greater number of grating arms (i.e., larger PLC). The small pixel size of the modulator allows us to address fine spectral granularity, finer than the optical resolution. Hence, we can truly extract the performance potential of the WGR with this approach.

References

[1] M. Shirasaki, "Chromatic dispersion compensator using virtually im-aged phased array," *IEEE Photon. Technol. Lett.*, vol. 9, no. 12, pp. 1598–1600, Dec. 1997.

[2] K.-M. Feng, J.-X. Cai, V. Grubsky, D. S. Starodubov, M. I. Hayee, S. Lee, X. Jiang, A. E. Willner, and J. Feinberg, "Dynamic dispersion compensation in a 10-Gb/s optical system using a novel voltage tuned nonlinearly chirped fiber Bragg grating," *IEEE Photon. Technol. Lett.*, vol. 11, no. 3, pp. 373–375, Mar. 1999.

[3] C. R. Doerr, S. Chandrasekhar, P. J. Winzer, A. R. Chraplyvy, A. H. Gnauck, L. W. Stulz, R. Pafchek, and E. Burrows, "Simple multichannel optical equalizer mitigating intersymbol interference for 40-Gb/s non return-to-zero signals," *J. Lightw. Technol.*, vol. 22, no. 1, pp. 249–256, Jan. 2004.

[4] A. Krishnan, M. Knapczyk, L. Grave de Peralta, A. A. Bernussi, and H. Temkin, "Reconfigurable direct space-to-time pulse-shaper based on arrayed waveguide grating multiplexers and digital micromirrors," *IEEE Photon. Technol. Lett.*, vol. 17, no. 9, pp. 1959–1961, Sep. 2005.

[5] J. E. Ford and J. A. Walker, "Dynamic spectral power equalization using micro-opto-mechanics," *IEEE Photon. Technol. Lett.*, vol. 10, no. 10, pp. 1440–1442, Oct. 1998.

[6] N. Riza and M. J. Mughal, "Broadband optical equalizer using fault tolerant digital micromirrors," *Opt. Express Internet J.*, vol. 11, pp. 1559–1565, Jun. 2003.

[7] J. S. Patel and Y. Silberberg, "Liquid crystal and grating-based multiple wavelength cross- connect switch," *IEEE Photon. Technol. Lett.*, vol. 7, no. 5, pp. 514–516, May 1995.

[8] N. A. Riza and N. Madamopoulos, "Synchronous amplitude and time control for an optimum dynamic range variable photonic delay line," *Appl. Opt.*, vol. 38, pp. 2309–2318, Apr. 1999.

[9] M. C. Parker, A. D. Cohen, and R. J. Mears, "Dynamic digital holographic wave- length filtering," *J. Lightw. Technol.*, vol. 16, no. 7, pp. 1259–1270, Jul. 1998.

[10] N. A. Riza and S. A. Reza, "High-dynamic-range hybrid analog-digital control broadband optical spectral processor using micromirror and acousto-optic devices," *Opt. Lett.*, vol. 33, pp. 1222–1224, Jun. 2008.

[11] C. R. Doerr, R. Blum, L. L. Buhl, M. A. Cappuzzo, E. Y. Chen, A. Wong-Foy, L. T. Gomez, and H. Bulthuis, "Colorless tunable optical dispersion compensator based on a silica arrayed-waveguide grating and a polymer thermooptic lens," *IEEE Photon. Technol. Lett.*, vol. 18, no. 11, pp. 1222–1224, Jun. 1, 2006.

[12] D. M. Marom, C. R. Doerr, M. A. Cappuzzo, E. Y. Chen, A. Wong-Foy, L. T. Gomez, and S. Chandrasekhar, "Compact colorless tunable dispersion compensator with 1000-ps/nm tuning range for 40-Gb/s data rates," *J. Lightw. Technol.*, vol. 24, no. 1, pp. 237–241, Jan. 2006.

[13] D. Sinefeld and D. M. Marom, "Colorless photonic spectral processor using hybrid guided-wave/free-space optics arrangement and LCoS modulator," in *Proc. OFC*, San Diego, CA, 2009, Paper OThB4.

Chapter 2B.

All-channel tunable optical dispersion compensator based on linear translation of a waveguide grating router

David Sinefeld, Shalva Ben-Ezra, Christopher R. Doerr and Dan M. Marom

Published in Optics Letters:

D, Sinefeld, S. Ben-Ezra, C. R. Doerr, and D. M. Marom, "All-channel tunable optical dispersion compensator based on linear translation of a waveguide grating router," Opt. Lett. 36, 1410-1412 (2011).

All-channel tunable optical dispersion compensator based on linear translation of a waveguide grating router

David Sinefeld,[1,*] Shalva Ben-Ezra,[2] Christopher R. Doerr,[3] and Dan M. Marom[1]

[1]*Applied Physics Department, Hebrew University, Jerusalem 91904, Israel*

[2]*Finisar Corporation, Nes Ziona, Israel*

[3]*Bell Laboratories, Alcatel-Lucent, 791 Holmdel-Keyport Road, Holmdel, New Jersey 07733, USA*

**Corresponding author: sinefeld@gmail.com*

Received January 7, 2011; revised February 28, 2011; accepted March 14, 2011;
posted March 17, 2011 (Doc. ID 140761); published April 13, 2011

We propose and demonstrate a compact tunable optical dispersion compensation (TODC) device with a 100 GHz free spectral range capable of mitigating chromatic dispersion impairments. The TODC is based on longitudinal movement of a waveguide grating router, resulting in chromatic dispersion compensation of ± 1000 ps/nm. We employed our TODC device for compensating 42.8 Gbit/sec differential phase-shifting keying signal, transmitted over 50 km fiber with a -2 dB power penalty at 10^{-9}.

OCIS codes: 060.2330, 130.2035.

Tunable optical dispersion compensation (TODC) devices are essential components in direct detection, high bit rate communication channels, as broad signal spectrum and narrow bit periods result in sensitivity to dispersion-induced intersymbol interference. Oftentimes, the TODC device needs to be colorless, having a free spectral range (FSR) matching the channel spacing, enabling multichannel compensation in wavelength division multiplexed (WDM) networks and reducing inventory. Colorless TODC devices can be based on ring resonators [1], sampled chirped fiber Bragg gratings [2], and Mach–Zehnder interferometers [3]. A special category of TODC devices is based on the combination of a dispersion element and a spatially controlled phase. The channel-matched FSR dispersion element can be an etalon [4], virtually imaged phased array [5], or waveguide grating router (WGR) [6], whereas the phase element may be a mirror with various selectable curvatures [7], a deformable mirror [8], a rotating cylindrical lens [9], a polymer thermo-optic lens [10], or a phase spatial light modulator (SLM) [11–13]. Common to these elements is the requirement of applying a quadratic phase function across the dispersed signal in an adjustable fashion.

Here we present a compact TODC device based on an extremely simple free space arrangement of a WGR, Fourier lens, and flat reflecting mirror [14,15], with accompanying 42.8 Gb/sec transmission results. Whereas other TODC utilized spatially controlled quadratic phase elements at the Fourier plane [7–13] or a relatively simple movement with a complex optical setup [5] impacting TODC device complexity and cost, we use a very compact arrangement and simply modify the distance between the WGR and the Fourier lens. The longitudinal displacement is equivalent to applying a radial phase at the Fourier plane and results in a curved phase front added to the dispersed spectral components. In this way we can compensate for chromatic dispersion (CD) values up to ± 1000 ps/nm. Since our WGR has a free spectral range of 100 GHz, the phase curvature is applied simultaneously to all WDM channels on the channel plan, resulting in colorless device operation. The simplicity of this system makes it effective as a TODC device for mitigating dispersion impairments, as it consumes no power once set and hence will not fail in power outages. The longitudinal displacement of the WGR from the front focal plane (distance f to lens) to an arbitrary distance d (between WGR and lens) results in a quadratic phase added to the beam at Fourier plane with curvature [16]:

$$\frac{1}{R} = \frac{1}{f}\left(1 - \frac{d}{f}\right). \tag{1}$$

As was shown in previous works [11,12,15], this curvature results in applied CD values according to

$$\mathrm{CD} = \frac{2\lambda_0}{c_0}\frac{1}{R}\left(\frac{dx}{d\lambda}\right)^2 = \frac{2\lambda_0}{c_0}\left(\frac{dx}{d\lambda}\right)^2\frac{\Delta z}{f^2} = \frac{2\lambda_0}{c_0}\left(\frac{d\theta}{d\lambda}\right)^2\Delta z, \tag{2}$$

where $\Delta z = f - d$. Hence, CD values have a linear dependence on the displacement Δz between the WGR and the Fourier lens. In this way, very simple longitudinal translation of the WGR results in different CD compensation values.

The TODC device layout and concept is depicted in Fig. 1. Light enters through an input/output waveguide to a planar lightwave circuit (PLC) containing an extremely high-resolution silica-on-silicon WGR with 0.8% index contrast waveguides that consists of 34 grating arms that are "pinched" in the middle for conserving wafer area, reducing the grating sensitivity to wafer refractive index and fabrication gradients, and enables the insertion of a half-wave plate to make the WGR polarization independent (not implemented in the present system). The angular dispersion $d\theta/d\lambda$ at the output facet of the PLC is converted to spatial dispersion with a $f = 50$ mm Fourier lens, resulting in a spatial dispersion along the x axis. A $f = 3$ mm cylindrical lens collimates the radiated light from the WGR in the guided (slab) direction to reduce the output numerical aperture. A circulator was used to separate the input and output light to the PLC. The insertion loss of the TODC device is -12.5 dB. This high loss value is partially due to phase errors in the fabricated WGR, as well as an unoptimized transition from the guided region to free space. Both issues can be corrected in a subsequent run. We anticipate system losses of ~ 5 dB can be achieved, limited by WGR coupling inefficiency.

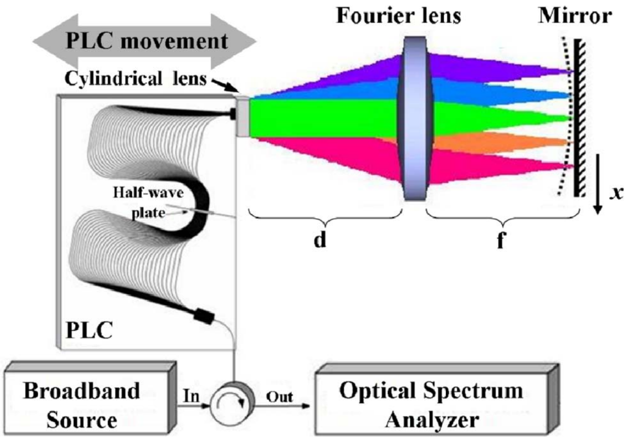

Fig. 1. (Color online) Layout of the tunable optical dispersion compensator. Changing the distance d between the WGR and the Fourier lens imparts a quadratic phase across the Fourier plane (seen as a dashed surface on the Fourier plane).

In order to determine the dispersion along the x axis ($dx/d\lambda$ value), we placed a needle in the Fourier plane and moved it along the x axis, finding for each position the corresponding attenuated wavelength component. In this way we have found that $dx/d\lambda = 5.4\,\mathrm{mm/nm}$. We repeated this measurement for both TE and TM polarizations and obtained similar results (5.4 and $5.3\,\mathrm{mm/nm}$). Since the free space arrangement does not depend on polarization, the source of the slight polarization dependence is the WGR birefringence. The effect of birefringence is a polarization-dependent splitting of the spectral passband; however, both polarizations would incur the same dispersion setting.

As a first test of the TODC device, we changed the distance d between the WGR and the Fourier lens along

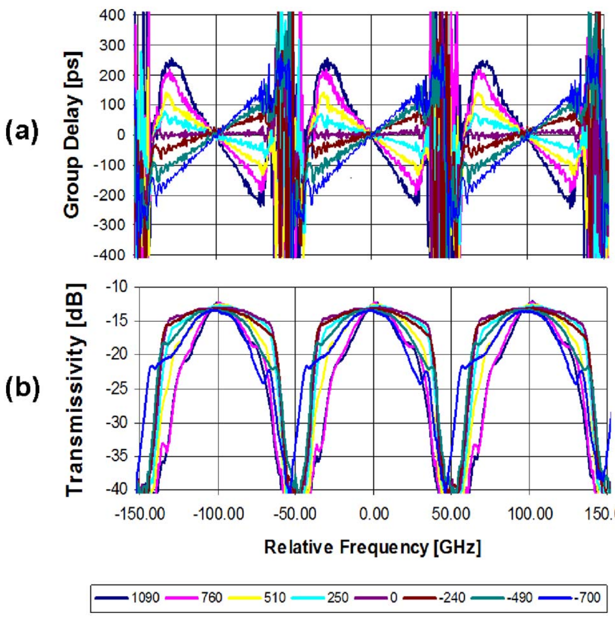

Fig. 2. (Color online) CD compensation results. (a) Group delay versus frequency. Linear slopes are observed, corresponding to eight different dispersion values between −700 and 1100 ps/nm. (b) Transmissivity versus frequency. Spectral narrowing is observed for increasing departures from zero dispersion. Passband and dispersion settings are repeated at 100 GHz FSR.

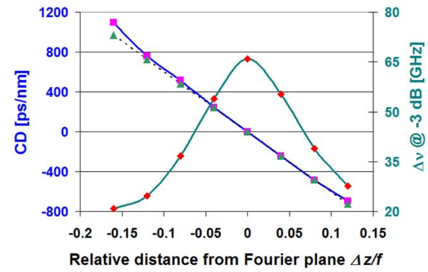

Fig. 3. (Color online) Measured CD values (blue), theoretical CD values (black dashed curve), and bandwidth (green with a peak) versus displacement Δz. As the phase curvature values at the Fourier plane are larger, the narrowing effect becomes dominant: bandwidth is reduced down to 20 GHz for CD values of $\pm 1000\,\mathrm{ps/nm}$.

14 mm travel and measured the group delay (GD) and the transmissivity at several positions. The GD varied linearly within the TODC FSR, a testament of TODC action (Fig. 2). As one can expect from such a system, the quadratic phase imposes not only CD but also an undesired spectral narrowing, due to the tilt applied to spectral components far from the channel grid. The measured CD values (calculated from the GD slopes), the theoretical CD values (using Eq. (2), with the experimental $dx/d\lambda$ values), and the resulting −3 dB channel bandwidth measures are plotted in Fig. 3 against the relative displacement from the lens front focal plane $\Delta z/f$. The experimental and theoretical CD values match extremely well. As the phase curvature values at the Fourier plane increase, the narrowing effect becomes dominant, and the bandwidth is reduced down from 65 GHz at low CD correction values to 20 GHz for extreme TODC values of $\pm 1000\,\mathrm{ps/nm}$. In principle, there is an option of eliminating the bandwidth narrowing by using a four pass system [13,17]; however, such a system is more complicated and will suffer higher losses.

Polarization-dependent loss (PDL) and polarization-mode dispersion (PMD) were measured (Fig. 4), to examine the effect of PLC birefringence. The results reveal that within the central 65 GHz, the PDL is lower than 0.3 dB and the PMD is less than 5 ps. These effects are

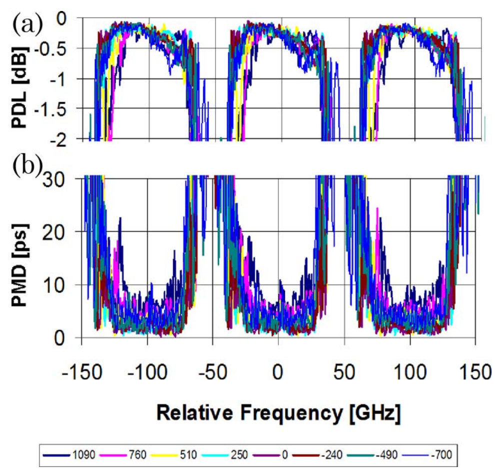

Fig. 4. (Color online) (a) Polarization-dependent loss (PDL) measured in dB versus relative frequency, (b) polarization-mode dispersion (PMD) measured in ps versus relative frequency.

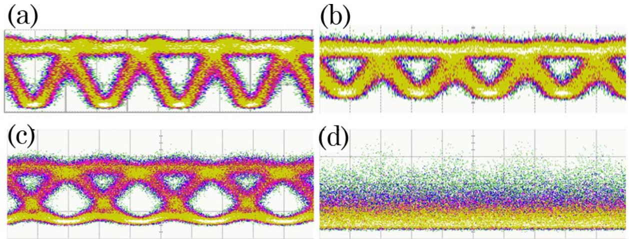

Fig. 5. (Color online) Detected eye diagrams after TODC correction with signal transmitted along (a) 0 km, (b) 20 km, (c) 40 km, and (d) 40 km without TODC CD correction.

caused solely by the birefringence of the PLC, since all the free space optics elements are polarization insensitive. Insertion of the optional half-wave plate at the pinched point of the WGR should eliminate this entirely.

The dispersion compensation capability of the TODC device was tested using a 42.8 Gb/s differential phase-shift keying $2^{31}-1$ pseudorandom bit sequence at 1550.12 nm, with different lengths of standard single-mode fiber (dispersion coefficient of 17 ps/nm-km) placed between the transmitter and the receiver. Tuning the TODC device was trivial, as a single micrometer movement yielded immediate eye opening at the proper distance Δz, as shown in Fig. 5. Without the dispersing fiber, the TODC showed zero penalty over the back-to back case, as can be seen in Fig. 6. The penalty for compensation of 30–50 km fiber length was ~2 dB optical signal-to-noise ratio (OSNR)at 10^{-9} bit error ratio (BER). For the 60 km fiber length, the penalty increased. We attribute the greater penalty to passband narrowing at our chosen modulation format. This bandwidth narrowing changes the signal quality, as seen in the eye shape [Fig. 5(c)], resembling that of doubinary modulation [18,19].

In this work we have shown a very simple, compact apparatus for TODC. In fact, actual systems that will be based on this scheme could become even more compact by use of a Fourier lens with very short focal length. Since the beam size at the output of the PLC is approximately 0.5 mm, a few millimeter focal length lens could be substituted over our 50 mm lens, resulting in a compact TODC arrangement. The PLC travel range of such a system will also be reduced, resulting in a compact system with a relatively large dispersion tuning range. Another advantage of this kind of system is that in the

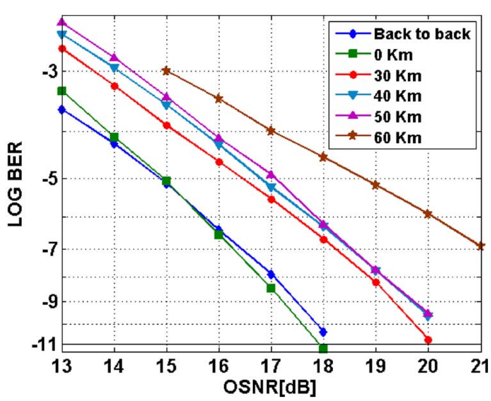

Fig. 6. (Color online) Receiver sensitivity curves for different amounts of fiber CD in the link, compensated by the TODC.

case of failure the tuning condition remains fixed. Note that the TODC might require temperature stabilization for holding the WDM grid position, an issue that was not examined in this work. However, this stabilization is identical to all WGR-based devices (e.g., a demultiplexer), as the shift does not depend on the diffraction order of the WGR (i.e., no increased temperature sensitivity).

The authors thank Moshe Tur from Tel Aviv University for using their LUNA OVA to carry out GD, PDL, and PMD measurements, and the Israel Science Foundation (ISF) (Grant 1359/07) and the Peter Brojde Center for Innovative Engineering for funding this work.

References

1. C. K. Madsen, G. Lenz, A. J. Bruce, M. A. Cappuzzo, L. T. Gomez, and R. E. Scotti, IEEE Photon. Technol. Lett. **11**, 1623 (1999).
2. K.-M. Feng, J.-X. Chai, V. Grubsky, D. S. Starodubov, M. I. Hayee, S. Lee, X. Jiang, A. E. Willner, and J. Feinberg, IEEE Photon. Technol. Lett. **11**, 373 (1999).
3. K. Takiguchi, K. Jinguji, K. Okamoto, and Y. Ohmori, IEEE J. Sel. Top. Quantum Electron. **2**, 270 (1996).
4. D. J. Moss, S. McLaughlin, G. Randall, M. Lamont, M. Ardekani, P. Colbourne, S. Kiran, and C. A. Hulse, in *Optical Fiber Communications Conference*, A. Sawchuk, ed., Vol. 70 of OSA Trends in Optics and Photonics (Optical Society of America, 2002), paper TuT2.
5. M. Shirasaki, IEEE Photon. Technol. Lett. **9**, 1598 (1997).
6. C. R. Doerr, L. W. Stulz, S. Chandrasekhar, and R. Pafchek, IEEE Photon. Technol. Lett. **15**, 1258 (2003).
7. M. Shirasaki and S. Cao, in *Optical Fiber Communications Conference*, 2001 OSA Technical Digest Series (Optical Society of America, 2001), paper TuS1.
8. D. Marom, C. Doerr, M. Cappuzzo, E. Chen, A. Wong-Foy, L. Gomez, and S. Chandrasekhar, J. Lightwave Technol. **24**, 237 (2006).
9. M. Durst, D. Kobat, and C. Xu, Opt. Lett. **34**, 1195 (2009).
10. C. R. Doerr, R. Blum, L. L. Buhl, M. A. Cappuzzo, E. Y. Chen, A. Wong-Foy, L. T. Gomez, and H. Bulthuis, IEEE Photon. Technol. Lett. **18**, 1222 (2006).
11. D. Sinefeld and D. M. Marom, in *Optical Fiber Communications Conference*, OSA Technical Digest (CD) (Optical Society of America, 2009), paper OThB4.
12. D. Sinefeld and D. M. Marom, IEEE Photon. Technol. Lett. **22**, 510 (2010).
13. K. Suzuki, N. Ooba, M. Ishii, K. Seno, T. Shibata, and S. Mino, in *Optical Fiber Communications Conference*, OSA Technical Digest (CD) (Optical Society of America, 2009), paper OThB3.
14. D. Sinefeld, C. R. Doerr, and D. M. Marom, in *Optical Fiber Communications Conference* (Optical Society of America, 2011), paper OWM6.
15. K. Seno, N. Ooba, K. Suzuki, T. Watanabe, K. Watanabe, and S. Mino, IEEE Photon. Technol. Lett. **21**, 1701 (2009).
16. J. W. Goodman, *Introduction to Fourier Optics*, 3rd ed. (Roberts, 2005).
17. D. T. Neilson, R. Ryf, F. Pardo, V. A. Aksyuk, M. E. Simon, D. O. Lopez, D. M. Marom, and S. Chandrasekhar, J. Lightwave Technol. **22**, 101 (2004).
18. T. Ono, Y. Yano, K. Fukuchi, T. Ito, H. Yamazaki, M. Yamaguchi, and K. Emura, J. Lightwave Technol. **16**, 788 (1998).
19. D. Boivin, M. Hanna, and J. R. Barry, IEEE Photon. Technol. Lett. **17**, 1331 (2005).

Chapter 2C.

A photonic spectral processor employing two-dimensional WDM channel separation and a phase LCoS modulator

David Sinefeld, Christopher R. Doerr and Dan M. Marom

Published in Optics Express:

D. Sinefeld, C. R. Doerr, and D. M. Marom, "A photonic spectral processor employing two-dimensional WDM channel separation and a phase LCoS modulator," Opt. Express 19, 14532-14541 (2011).

A photonic spectral processor employing two-dimensional WDM channel separation and a phase LCoS modulator

David Sinefeld,[1,*] Christopher R. Doerr,[2] and Dan M. Marom[1]

[1]*Applied Physics Department, Hebrew University, Jerusalem 91904, Israel*
[2]*Bell Laboratories, Alcatel-Lucent, 791 Holmdel-Keyport Rd., Holmdel, NJ 07733, USA*
[*]*sinefeld@gmail.com*

Abstract: We present a Photonic Spectral Processor (PSP) that provides both fine spectral resolution and broad bandwidth support by dispersing light over two-dimensional space using the crossed-grating approach. The PSP uses a hybrid guided wave/free-space optics arrangement, where a waveguide grating router implemented in silica waveguides disperses the light in one dimension with a 100 GHz FSR and a bulk 1200 gr/mm diffraction grating disperses the light along the second (crossed) dimension. The diffracted light is focused by a lens onto a liquid-crystal on silicon, two-dimensional, phase-only, spatial light modulator, which we use to prescribe phase and amplitude to the signal's spectral components. With the 2-D PSP arrangement we are able to address frequency components at 0.2 GHz/column with an optical resolution of 3.3 GHz covering 40 C-band channels.

OCIS codes: (060.2330) Fiber optics communications; (130.2035) Dispersion compensation devices; (130.7408) Wavelength filtering devices.

References and links

1. M. A. F. Roelens, S. Frisken, J. A. Bolger, D. Abakoumov, G. Baxter, S. Poole, and B. J. Eggleton, "Dispersion trimming in a reconfigurable wavelength selective switch," J. Lightwave Technol. **26**(1), 73–78 (2008).
2. D. T. Neilson, R. Ryf, F. Pardo, V. A. Aksyuk, M. E. Simon, D. O. Lopez, D. M. Marom, and S. Chandrasekhar, "MEMS-based channelized dispersion compensator with flat passbands," J. Lightwave Technol. **22**(1), 101–105 (2004).
3. D. T. Neilson, H. Tang, D. S. Greywall, N. R. Basavanhally, L. Ko, D. A. Ramsey, J. D. Weld, Y. L. Low, F. Pardo, D. O. Lopez, P. Busch, J. Prybyla, M. Haueis, C. S. Pai, R. Scotti, and R. Ryf, "Channel equalization and blocking filter utilizing microelectromechanical mirrors," IEEE J. Sel. Top. Quantum Electron. **10**(3), 563–569 (2004).
4. S. Sohma, K. Mori, H. Masuda, A. Takada, K. Seno, K. Suzuki, and N. Ooba, "Flexible chromatic dispersion compensation over entire L-band for over 40-Gb/s WDM transparent networks using multichannel tunable optical dispersion compensator," IEEE Photon. Technol. Lett. **21**(17), 1271–1273 (2009).
5. M. Shirasaki, "Chromatic dispersion compensator using virtually imaged phased array," IEEE Photon. Technol. Lett. **9**(12), 1598–1600 (1997).
6. C. R. Doerr, R. Blum, L. L. Buhl, M. A. Cappuzzo, E. Y. Chen, A. Wong-Foy, L. T. Gomez, and H. Bulthuis, "Colorless tunable optical dispersion compensator based on a silica arrayed-waveguide grating and a polymer thermooptic lens," IEEE Photon. Technol. Lett. **18**(11), 1222–1224 (2006).
7. D. M. Marom, C. R. Doerr, M. A. Cappuzzo, E. Y. Chen, A. Wong-Foy, L. T. Gomez, and S. Chandrasekhar, "Compact colorless tunable dispersion compensator with 1000-ps/nm tuning range for 40-Gb/s data rates," J. Lightwave Technol. **24**(1), 237–241 (2006).
8. D. Sinefeld and D. M. Marom, "Colorless photonic spectral processor using hybrid guided-wave/free-space optics arrangement and LCoS modulator," in *Proceedings of Optical Fiber Communication Conference and Exposition* (Optical Society of America, 2009), paper OThB4.
9. D. Sinefeld and D. M. Marom, "Hybrid guided-wave/free-space optics photonic spectral processor based on LCoS phase only modulator," IEEE Photon. Technol. Lett. **22**(7), 510–512 (2010).
10. K. Suzuki, N. Ooba, M. Ishii, K. Seno, T. Shibata, and S. Mino, "40-wavelength channelized tunable optical dispersion compensator with increased bandwidth consisting of arrayed waveguide gratings and liquid crystal on silicon," in *Proceedings of Optical Fiber Communication Conference and Exposition* (Optical Society of America, 2009), paper OThB3.

#149409 - $15.00 USD Received 16 Jun 2011; revised 30 Jun 2011; accepted 30 Jun 2011; published 13 Jul 2011

11. K. Seno, N. Ooba, K. Suzuki, T. Watanabe, K. Watanabe, and S. Mino, "Tunable optical dispersion compensator consisting of simple optics with arrayed waveguide grating and flat mirror," IEEE Photon. Technol. Lett. **21**(22), 1701–1703 (2009).
12. D. Sinefeld, S. Ben-Ezra, C. R. Doerr, and D. M. Marom, "All-channel tunable optical dispersion compensator based on linear translation of a waveguide grating router," Opt. Lett. **36**(8), 1410–1412 (2011).
13. D. Sinefeld and D. M. Marom, "Spectral processor implemented with hybrid free-space and guided-wave optics and active LCoS modulator," in *Proceedings of IEEE 25th Convention of Electrical and Electronics Engineers in Israel*, 380–383 (2008).
14. K. Seno, K. Suzuki, N. Ooba, K. Watanabe, M. Ishii, H. Ono, and S. Mino, "Demonstration of channelized tunable optical dispersion compensator based on arrayed-waveguide grating and liquid crystal on silicon," Opt. Express **18**(18), 18565–18579 (2010).
15. T. K. Chan, J. Karp, R. Jiang, N. Alic, S. Radic, C. F. Marki, and J. E. Ford, "1092 channel 2-D array demultiplexer for ultralarge data bandwidth," J. Lightwave Technol. **25**(3), 719–725 (2007).
16. V. R. Supradeepa, C. B. Huang, D. E. Leaird, and A. M. Weiner, "Femtosecond pulse shaping in two dimensions: towards higher complexity optical waveforms," Opt. Express **16**(16), 11878–11887 (2008).
17. D. Sinefeld, C. R. Doerr, and D. M. Marom, "Photonic spectral processor employing two-dimensional WDM channel separation and a phase LCoS modulator," in *Proceedings of Optical Fiber Communication Conference and Exposition* (Optical Society of America, 2010), paper OMP5.
18. K. Seno, K. Suzuki, N. Ooba, T. Watanabe, M. Itoh, S. Mino, and T. Sakamoto, "50-wavelength channel-by-channel tunable optical dispersion compensator using combination of arrayed-waveguide and bulk gratings," in *Optical Fiber Communication Conference and Exposition*, (Optical Society of America, 2010), paper OMT7.
19. K. Seno, K. Suzuki, N. Ooba, T. Watanabe, M. Itoh, S. Mino, and T. Sakamoto, "50-wavelength channel-by-channel tunable optical dispersion compensator using a combination of AWG and bulk grating," IEEE Photon. Technol. Lett. **22**(22), 1659–1661 (2010).
20. C. K. Madsen and J. H. Zhao, *Optical filter design and analysis: A signal processing approach* (Wiley-Interscience, 1999).
21. J. Leuthold, D. Marom, S. Cabot, J. Jaques, R. Ryf, and C. Giles, "All-optical wavelength conversion using a pulse reformatting optical filter," J. Lightwave Technol. **22**(1), 186–192 (2004).
22. S. Sygletos, R. Bonk, T. Vallaitis, A. Marculescu, P. Vorreau, J. Li, R. Brenot, F. Lelarge, G.-H. Duan, W. Freude, and J. Leuthold, "Filter assisted wavelength conversion with quantum-dot SOAs," J. Lightwave Technol. **28**(6), 882–897 (2010).
23. H. Schenk, H. Gruger, F. Zimmer, W. Scherf, and A. Kenda, "Optical MEMS for advanced spectrometers," in *Proceedings of IEEE/LEOS Conf. on Optical MEMS*, 117–118 (2005).

1. Introduction

Optical devices independently controlling the transmission of individual channels are important for maximizing the performance of WDM optical communication systems. Channel power equalizers are required for maintaining the same OSNR across all amplified channels in a long-haul system. Dispersion compensators are essential in communication systems employing direct or differential detection, and can reduce the processing overhead in coherent reception systems. With increasing channel transmission rates, the broad signal spectrum becomes more susceptible to filtering and dispersion, resulting in a degraded signal reaching the receiver. One promising class of impairment mitigation devices uses spatial dispersion to separate the light's frequency components together with a spatial light modulator (SLM) in applying an adaptive filtering function [1–5]. The optical performance of these spectral processing devices depends on the spectral resolution and spectral addressability, which are a function of the dispersing optics solution and the SLM technology. Colorless devices use an engineered dispersing element with a free-spectral range (FSR) matching the channel plan [6–12], imparting identical functionality to every channel but with very high resolution. Broadband devices use dispersing elements with a FSR matching or exceeding the whole communication band, which limits the optical resolution of the system [13-14]. These devices demonstrate that the optical dispersion arrangements provide a finite space-bandwidth product that can be allocated to either broad bandwidth at coarse resolution or narrow bandwidth at fine resolution. This space-bandwidth limitation can be overcome by dispersing over two-dimensional space, capitalizing on the additional transverse spatial dimension available with free-space optics. The typical crossed-dispersion optics solution utilizes two gratings where the first has a small FSR with fine resolving capability, and the second crossed grating has a large FSR that separates the diffraction orders of the first grating. This kind of arrangement was introduced before as a solution for a high resolution demultiplexer [15] as well as for pulse shaping [16].

#149409 - $15.00 USD Received 16 Jun 2011; revised 30 Jun 2011; accepted 30 Jun 2011; published 13 Jul 2011

Last year, we presented a two-dimensional, amplitude and phase, photonic spectral processor (PSP) with the ability to control each WDM channel in separately [17], and had the same high resolution as our earlier colorless PSP [9]. This PSP was based on the combination of two crossed gratings, a high resolution waveguide grating router (WGR) and a free-space bulk grating, together with a liquid crystal on silicon (LCoS), two-dimensional, pixelated phase modulator. An identical arrangement was simultaneously inroduced by Seno at al [18, 19], but their work demonstrated only tunable dispersion compensation. In this work we discuss the full design consideration of such a two dimensional system, with the addition of new and improved results over those reported in [17], demonstrating the ability to manipulate both spectral phase and amplitude along the conventional optical communication band (1530-1560 nm), with a resolution of 3.3 GHz and 0.2 GHz addressability.

2. System design considerations

Our PSP is based on a hybrid guided wave / free-space optics arrangement, where a WGR implemented in silica waveguides disperses the light in one dimension with a 100 GHz FSR and a bulk 1200 gr/mm diffraction grating disperses the light along the second (crossed) dimension and separates the diffraction orders of the WGR grating. The diffracted light is then focused by a Fourier lens onto an LCoS, two-dimensional phase SLM. With the LCoS SLM we are able to prescribe phase and amplitude to the signal's spectral components.

The PSP layout and concept is depicted in Fig. 1. Light enters a planar lightwave circuit (PLC) containing an extremely high resolution WGR through the input/output (I/O) waveguide. The WGR was fabricated in silica-on-silicon technology with 0.8% index contrast waveguides and consists of 34 grating arms that are "pinched" in the middle for conserving wafer area, reducing the grating sensitivity to wafer refractive index gradients, and enables the insertion of a half-wave plate to make the WGR polarization-independent (not performed in this case as both the LCoS and bulk grating are polarization dependent). The output of the WGR is unconventional: instead of employing a second slab-lens region that demultiplexes to output waveguides, the grating arms terminate at the PLC edge and the light radiates to free-space. An f = 3mm cylindrical lens that is affixed at the PLC edge collimates the light in the guided direction.

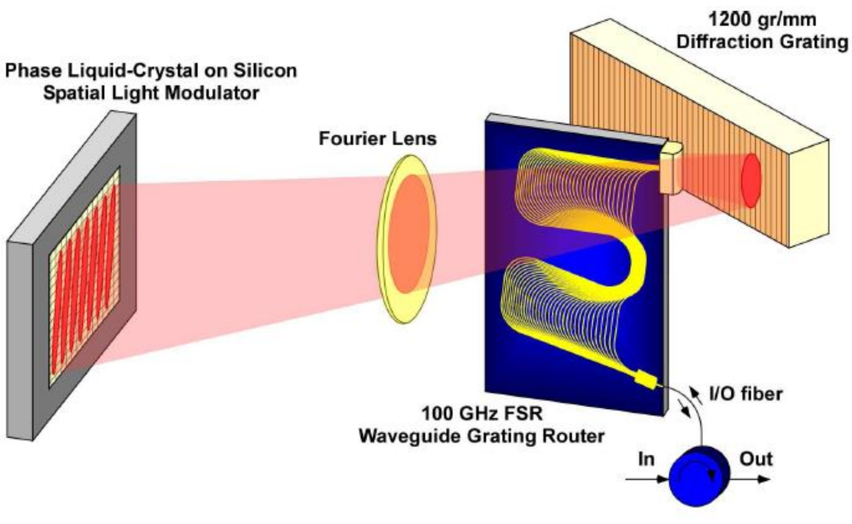

Fig. 1. Layout of the two-dimensional photonic spectral processor, capable of imparting independent spectral amplitude and phase to each WDM channel with the use of a LCoS modulator array. Crossed gratings (WGR and bulk) disperse the spectrum across the two-dimensional LCoS array, enabling high resolution access to the spectral components of each channel.

In a simple, colorless system [9], a Fourier lens is placed after the WGR output to observe the spatially-dispersed spectra at the lens back focal plane. In that case, the dispersed spectrum of all the WDM channels overlap onto each other, due to the WGR's 100 GHz FSR, and would be the basis for a colorless device. In our current 2D processor we place a crossed bulk grating between the WGR and the lens, separating the diffraction orders of the WGR in the orthogonal direction. This arrangement results in two spatial dispersion axes: a "fast" dispersion axis which has high resolution and 100 GHz FSR, and an orthogonal "slow" dispersion axis which separates the WDM channels. The diffraction spread angle of the beam in the "slow" axis is determined by the collimated size of the beam output after the cylindrical lens, according to:

$$\Delta\theta_{spot} = \frac{2\lambda}{\pi w_0} = \frac{2\lambda}{\pi f_{cyl} N.A._{WG}} \tag{1}$$

where $2w_0$ is the collimated size of the beam output, $\lambda = 1.55\mu m$ is the center wavelength, $f_{cyl} = 3\ mm$ is the cylindrical lens focal length, and $N.A._{WG} = 0.12$ is the waveguide output numerical aperture. To achieve WGR order separation we must use a bulk grating with an angular dispersion $(d\theta/d\nu)_{BG}$ greater than the diffraction spread angle:

$$\Delta\nu_{FSR} \cdot \left(\frac{d\theta}{d\nu}\right)_{BG} \geq \Delta\theta_{spot} \tag{2}$$

Using $\Delta\theta_{spot}$ from Eq. (1), and $\Delta\nu_{FSR} = 100\ GHz$ of the WGR, we can calculate the required dispersion in the "slow" dispersion axis. We utilize near Littrow mounting for our bulk grating. In this case the angular dispersion is determined by:

$$\left|\left(\frac{d\theta}{d\nu}\right)_{BG}\right| = \frac{\lambda^2}{c}\left(\frac{d\theta}{d\lambda}\right)_{BG} = \frac{\lambda^2}{c \cdot d\cos(\theta)} \tag{3}$$

where d is the grating period, λ is the wavelength, c is the speed of light and θ is the incidence/diffraction angle of the bulk grating. Combining Eqs. (1)–(3) results in the condition:

$$d\cos(\theta) \leq \frac{\pi\lambda f_{cyl} N.A._{WG} \Delta\nu_{FSR}}{2c} \tag{4}$$

We satisfy the condition set forth by Eq. (4) using a 1200 gr/mm holographic diffraction grating which was placed at an angle of approximately 73° (close to the 68.5° Littrow angle of such grating) in order to achieve the order separation for our 2D system. An IR-optimized $f = 100$mm cemented doublet lens performs the Fourier transform and converts the angular spectrum to spatial and projects 2D separated frequency components onto the LCoS SLM. We used a phase-only, two-dimensional LCoS reflective modulator manufactured by Boulder Nonlinear Systems and placed it at the spectral plane. The LCoS modulator has 512 × 512 square pixels of 15 µm pitch, providing an active region of 7.68 × 7.68 mm.

Ideally, both gratings should be placed at the lens front focal plane so that their angular dispersion will be converted to spatial dispersion that is normally-incident onto the SLM. This could be achieved with a multi-lens solution that images the first grating onto the second [16], but such a solution increases the optical track length and component count and is hence undesirable. Instead, we place the bulk grating in between the WGR (which is placed near the front focal plane) and the lens. This results in the grating orders being incident in a space-varying incidence angle, or curvature. This phase curvature is related to the distance of the grating from the first Fourier plane, Δz, according to the expression [12]:

$$\frac{1}{R} = \frac{\Delta z}{f^2} \tag{5}$$

#149409 - $15.00 USD   Received 16 Jun 2011; revised 30 Jun 2011; accepted 30 Jun 2011; published 13 Jul 2011

where f is the focal length of the Fourier lens, and R is the phase radii. This unwanted curved phase will result in losses for off-axis channels. However, this effect can be completely compensated in our system since our phase LCoS SLM can encode a cylindrical quadratic phase function across the aperture. In this way we can couple-back the light from all diffraction orders with constant efficiency as shown in Fig. 2. Note that it is advantageous to displace the bulk grating from the front focal plane and not the WGR output, as the “fast” dispersion axis is more susceptible to chromatic dispersion being added onto the signal for an identical displacement [12].

3. System characteristics and basic performance

The elements of the two-dimensional PSP, consisting of the WGR PLC, bulk grating, lens, and the LCoS modulator were assembled on an optical table as shown in Fig. 1. A curved phase along the SLM slow-axis direction equalized the insertion loss along the different channels as discussed previously (see Fig. 2).

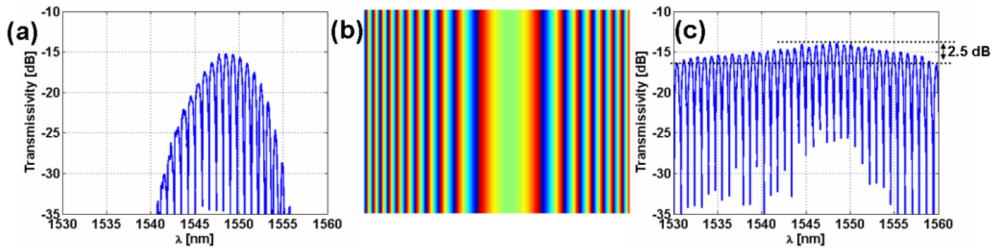

Fig. 2. The impact of applying horizontal curved phase along the channels in order to eliminate the losses caused by the finite separation between the WGR output facet and the bulk grating. (a) PSP output before equalization. (b) The horizontal quadratic phase that was added in order to achieve channel equalization. (c) PSP after equalization. In the plot 40 WDM channels are shown. This was achieved by moving the SLM along the spectral plane, and stitching the overlapping results from two SLM locations.

An intensity uniformity of 2.5 dB is achieved along 30 nm, resulting in 40 nearly equalized WDM channels. We should note that since our SLM is not physically large enough to span the entire c-band (it is sufficient for only 30 WDM channels), we had to transversely reposition the SLM and stitch together two spectra in order to record all the 40 channels as shown in Fig. 2. This result was measured without any other change in the optical setup, which means it could be easily achieved with a larger SLM. An alternative solution is to use a shorter focal length Fourier lens, but there was insufficient clearance for such an approach with a reflection grating.

To characterize the spatial dispersion, beam size and resolution of the PSP, a narrow line laser was tuned across the c-band, and its transmitted power through the system was recorded. For every wavelength, a 0-π vertical phase step transition pattern was applied, the location of this phase jump being scanned along the rows of the SLM (Fig. 3(b)). A similar horizontal phase step pattern was subsequently scanned along the columns of the SLM (Fig. 3(e)). Both step phase patterns were applied on top the base curved phase (Fig. 3(c) and 3(f)), which is always required for channel equalization. When the phase step occurs at the center of the laser line spot (in either horizontal or vertical direction), destructive interference between the two equal halves of the beam results in minimal output power coupling, thus identifying the beam position for every wavelength. Similarly, the onset and ending of the output power fluctuation measure the beam extent in the horizontal and vertical axes directions (as shown in Fig. 3(a), and 3(d)).

The spatial dispersion mapping is identified by locating the center position for each laser wavelength. In the WGR direction (fast axis) the SLM 512 columns spans a ~93-GHz wide spectrum (limited by SLM size) which correspond to spatial dispersion of 10.3[*mm/nm*]. Each column of the modulator addresses a particular center frequency, at 182 MHz shift in center frequency. The spatial dispersion in the bulk grating direction results in an offset of 15 pixels for successive diffraction orders (spaced at 100 GHz). This pitch is not constant across the

#149409 - $15.00 USD Received 16 Jun 2011; revised 30 Jun 2011; accepted 30 Jun 2011; published 13 Jul 2011

spectrum, as the grating angular dispersion is not linear. Figure 3(g) shows a mapping of the incident wavelengths onto the LCoS array. There is a slight deviation from linear dispersion on account of the bulk grating being offset from the lens focal plane. Due to the limited size of our LCoS SLM, only 30 WDM channels spaced at 100GHz can be modulated and reflected back at a time.

Using the same method, we measured the vertical and horizontal size of a single laser spot on the SLM. The vertical beam width was 18 pixels along the WGR (fast) dispersion direction at −3 dB. This determines the resolution of the system which equals $18 \times 0.182 = 3.3$ *GHz*. One should note the distinction between spectral resolution and addressability: the resolution defines the smallest feature that can be controlled with the system, while the addressability defines the amount of minimal change in the center wavelength of any spectral feature controlled with the PSP. Scanning the SLM in the bulk (slow) direction gave a beam width of 15 pixels (full width measured at 0 dB level in the horizontal direction as shown in Fig. 3(d)), which is exactly the separation between diffraction orders along the SLM. This result demonstrates that each diffraction order is just barely resolved in our implementation.

After defining the spatial dispersion mapping, we can assign spectral modulation to the dispersed components (subject to resolution limitations). Phase modulation to a spectral component is achieved by prescribing an identical phase to all pixels within the beam corresponding to the spectral component (18 pixels height) in the WGR direction. Amplitude modulation is achieved by setting a linear phase ramp along the column which reduces the coupling back to the PLC. Any spectral amplitude and phase combination can be achieved by combining a tilt for amplitude and absolute offset for phase, limited only by the resolution of the system.

The insertion loss of the PSP is −14 dB. This high loss value is partially due to phase errors in the fabricated WGR, as well as an unoptimized transition from the guided region to free space. Both issues can be corrected in a subsequent run. We anticipate that system losses of ~7 dB can be achieved, limited by WGR coupling inefficiency and by losses of the 2D assembly. Thermal fluctuations in the system which may change slightly the position of the grid lines can be compensated with the written phase functions on the SLM and should not adversely affect the performance.

The PSP that we implemented supports one polarization only, due to our choice of grating and the LCoS SLM. Solutions providing support for both polarizations are discussed in Section 5.

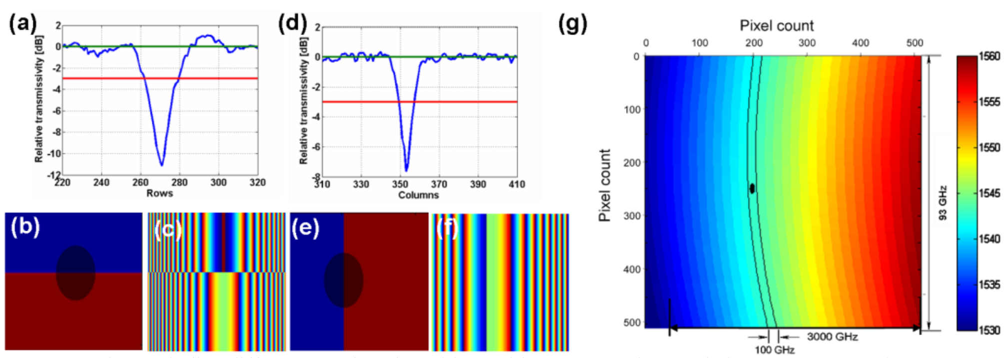

Fig. 3. Finding different wavelength positions with a 0-π step phase technique: (a-c) - Scanning the SLM with a phase step along the WGR direction results in the vertical position and size of the spot at specific wavelengths. The phase step is applied on top of the curved phase in order to reduce losses. The beam width (18 pixels) determines the spectral resolution of the system. (d-f) – The same procedure when the phase step is applied in the bulk grating direction. The result determines the size of each WDM channels on the SLM, where the green line mark 0 dB level. (g) Different wavelength locations on the SLM. The WGR provides high resolution on narrow FSR. The bulk grating separates the WGR diffraction orders. Individual channels are fully resolved on two-dimensional space. The black lines mark the borders of a specific WDM channel while the black ellipse denotes the spot size for a specific wavelength on this channel as it appears on the SLM.

#149409 - $15.00 USD Received 16 Jun 2011; revised 30 Jun 2011; accepted 30 Jun 2011; published 13 Jul 2011

4. PSP demonstrations

Numerous spectral manipulations can be envisaged with the two-dimensional PSP, owing to its fine resolution across all channels within the C-band. We demonstrate in the following WDM channel spectral amplitude manipulations, spectral phase manipulations, and in-band amplitude and phase spectral manipulations.

4.1 Channel amplitude control – WDM blocker

As a first demonstration, we used our PSP as a channel selector by blocking or transmitting complete columns (WDM channels). Figure 4 shows demonstrations of 15 randomly selected channels for attenuation. Channel selection is performed by applying a phase tilt to the rejected channel set. It should be noted that the linear phase tilt which serves as the attenuation mechanism can be prescribed either along the dispersion or along the beam height. Better attenuation performance was achieved with the former method, as the beam is wider in the fast dispersion direction.

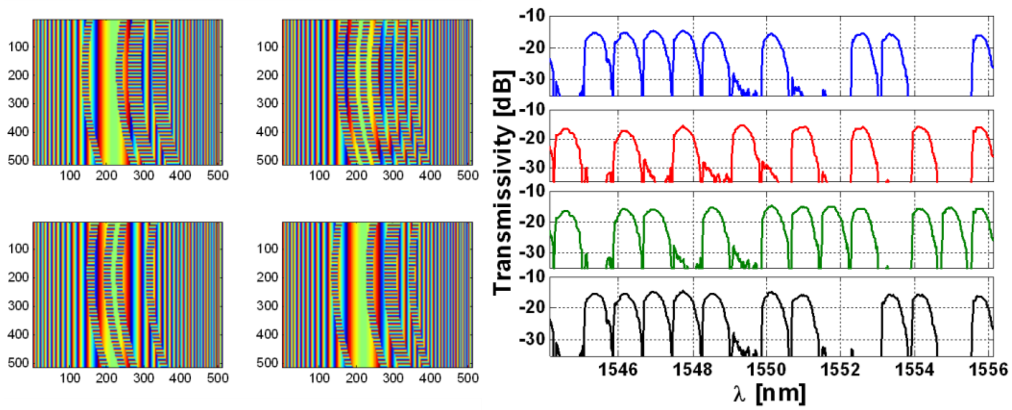

Fig. 4. Demonstration of channel selection with the 2D PSP. (Left) - The phase modulations as written on the SLM in the case of random selection of 15 WDM channels. Tilted phase was added on top of the curved equalization phase to attenuate channels. (Right) – Results of random selection of 15 WDM channels. A dynamic range of 20 dB is shown, limited by insufficient separation of WGR diffraction orders (or adjacent WDM channels).

4.2 Channel phase control –TODC and retimer

Two important applications of the PSP are tunable optical dispersion compensation (TODC) and channel retiming. To test the processor as a TODC, quadratic phase functions of varying radii were applied in the high dispersion direction to different channels (Fig. 5e), which result in different group delay slopes across each channel, hence chromatic dispersion (CD). An independent quadratic phase is applied to each selected. The quadratic phase maps to CD values according to:

$$CD \equiv \frac{2\pi c}{\lambda^2}\frac{d^2\phi(\omega)}{d\omega^2} = \frac{\lambda_0^2}{2\pi c_0}\frac{d^2\phi(x)}{dx^2}\left(\frac{dx}{d\lambda}\right)^2 = \frac{\lambda_0}{c_0}\frac{1}{R}\left(\frac{dx}{d\lambda}\right)^2 \tag{6}$$

where $\phi(x) = k_0 \cdot x^2/2R$ is the parabolic approximation to a curved phase, λ_0 is the wavelength in vacuum, c_0 is the speed of light, k_0 is the wave vector, $1/R$ is the applied curvature, $dx/d\lambda$ is the spatial dispersion and CD is the chromatic dispersion in units of ps/nm.

We performed group delay measurements with various curvature values applied to the channels (see Fig. 5(a) and 5(b)). As the slopes of the group delay are equivalent to CD, it can be seen that independent CD values can be applied to each channel. Our system is able to

#149409 - $15.00 USD Received 16 Jun 2011; revised 30 Jun 2011; accepted 30 Jun 2011; published 13 Jul 2011

compensate for CD values up to ± 750 ps/nm for each WDM channel. Larger CD values are achievable but will result in spectral narrowing [9] as shown in Fig. 6(a).

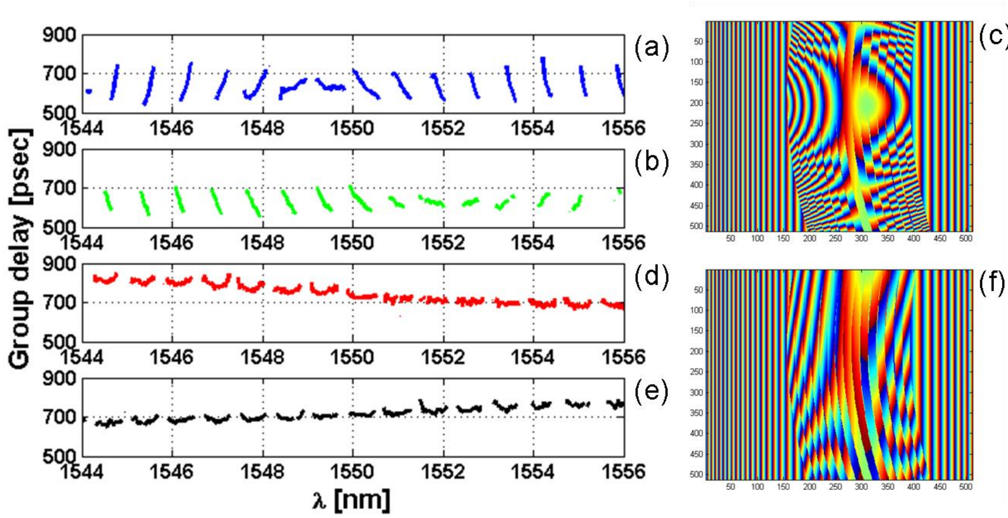

Fig. 5. Example of phase manipulation for 15 channels. (a-b) group delay slopes applied to each channel are equivalent to different CD compensation values. (c) The relevant phase pattern that was written on the SLM, consisting of varying quadratic phases. (d-e) Different group delay values applied to the selected 15 channels. (f) The relevant phase pattern that was written on the SLM, consisting of varying linear slopes.

A different phase manipulation is shown in Fig. 5(d) and 5(e). Channel retiming is achieved by applying linear phase along the spectrum, resulting in constant and controllable group delays per channel or channel retiming. Time offsets as large as ± 100 ps are demonstrated along 15 channels. The expression for the retiming is given by [20]:

$$\tau_{GD} \equiv \frac{d\phi(\omega)}{d\omega} = -\frac{d\phi(x)}{dx}\frac{dx}{d\lambda}\frac{d\lambda}{d\omega} = -\frac{\lambda_0}{c_0}\theta\left(\frac{dx}{d\lambda}\right) \tag{7}$$

where $\phi(x) = k_0 \cdot \theta \cdot \cdot x$ is the linear phase function applied along the channel, k_0 is the wave vector, and θ the phase slope angle in radians (under small angle approximation).

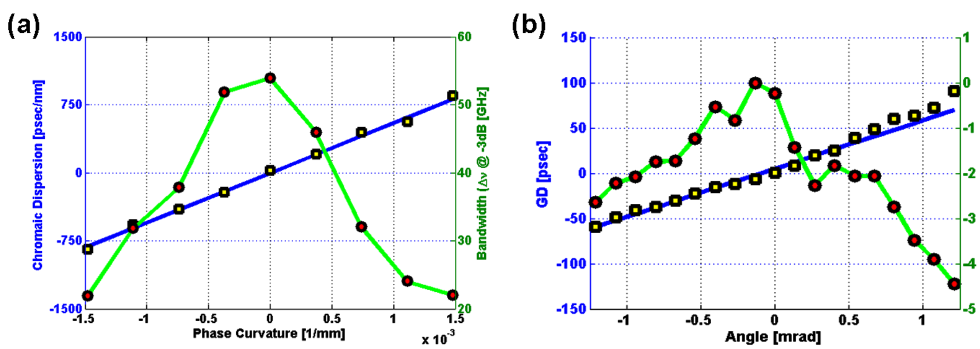

Fig. 6. The performance of the two-dimensional PSP when used as a TODC and as a retimer. (a) TODC performance: theoretical (Blue line) and measured (Yellow squares) CD values and bandwidth (Green) versus curvature. As the phase curvature values are larger, narrowing becomes dominant and the bandwidth is reduced down to 23 GHz FWHM for CD values of ± 750 ps/nm. (b) retimer performance: theoretical (Blue line) and measured (Yellow squares) GD values and loss (Green) versus slope angle measured in milliradians. As the phase slope becomes larger, the GD increases. However, large slopes results in high coupling losses.

#149409 - $15.00 USD Received 16 Jun 2011; revised 30 Jun 2011; accepted 30 Jun 2011; published 13 Jul 2011

Applying linear phase along the spectral channel results also in losses which become larger as the slope increases as shown in Fig. 6b. Those losses limit the amount of GD that can be achieved in the retiming mode. Thus, phase curvatures result in group delay slopes or CD values, while phase slopes result in constant group delays or retiming. TOCD range is primarily limited by spectral narrowing and retiming is limited by loss, both limitations arising from the coupling losses back to the output fiber through the PSP.

4.3 In-band channel manipulations – phase/amplitude carving

Since the spectral components of the communication C-band are dispersed along the two dimensional SLM, independent phase and amplitude spectral manipulations can be prescribed within each WDM channel.

Figure 7(a) demonstrates the use of the PSP for spectral carving by imparting unique attenuation features onto each WDM channel spectrum. This technique can be used to split the spectral channel into sub-bands or to attenuate spectral features and enhance the signal quality. Due to the high resolution of the PSP, almost any spectral shape can be prescribed for each channel, subject to the resolution constraint.

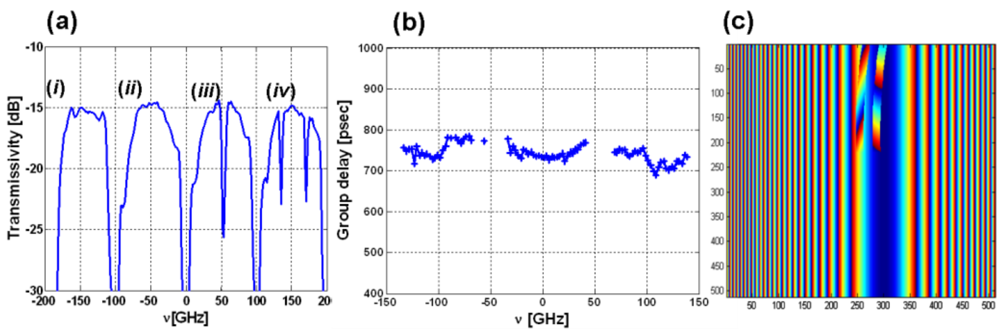

Fig. 7. Demonstration of inband manipulations: (a) spectral carving across the channel bandwidth for four contiguous WDM channels: (i) spectral flattening (ii) without modulation, (iii) spectrum carved to two sub-bands, (iv) spectrum carved to three sub-bands. (b) Example of half-channel group delay manipulation for 3 channels. A time split of 50 psec is obtained (c) The applied phase pattern on the SLM for the 3 half slopes case.

An interesting option which takes advantage of the high resolution of our PSP is to perform retiming of spectral components within a channel. Figure 7-(b) demonstrates such an example. A phase slope was applied on half of the three main channels. The result is a time delay that depends on the local slope along part of the channel [21-22]. For the left channel a positive slope was applied resulting in time delay for half of the channel, while for the right channel a negative slope was used resulting in a time advance for the half channel

5. Solutions for supporting dual polarizations

As mentioned previously, the current arrangement of our two-dimensional PSP operated for only a single polarization, due to the SLM and bulk grating.

There are two possible schemes in order to overcome this limitation which will result in a polarization-insensitive PSP. The first is by using components which are polarization insensitive. In this case one might substitute a MEMS based SLM [23] combined with a low-polarization dependent grating. An alternative approach is to design a system with polarization diversity as shown in Fig. 8.

In this solution, two PLC's are aligned together before the bulk grating. A polarization beam splitter and a polarization rotator are added to ensure that both polarizations are aligned after the WGR output. Since the angular dispersion of the two WGR is identical, the Fourier lens will project the spectral component onto the same position on the SLM, hence the same SLM can be used for applying phase and amplitude modulation to the various spectral components for both polarizations.

#149409 - $15.00 USD Received 16 Jun 2011; revised 30 Jun 2011; accepted 30 Jun 2011; published 13 Jul 2011

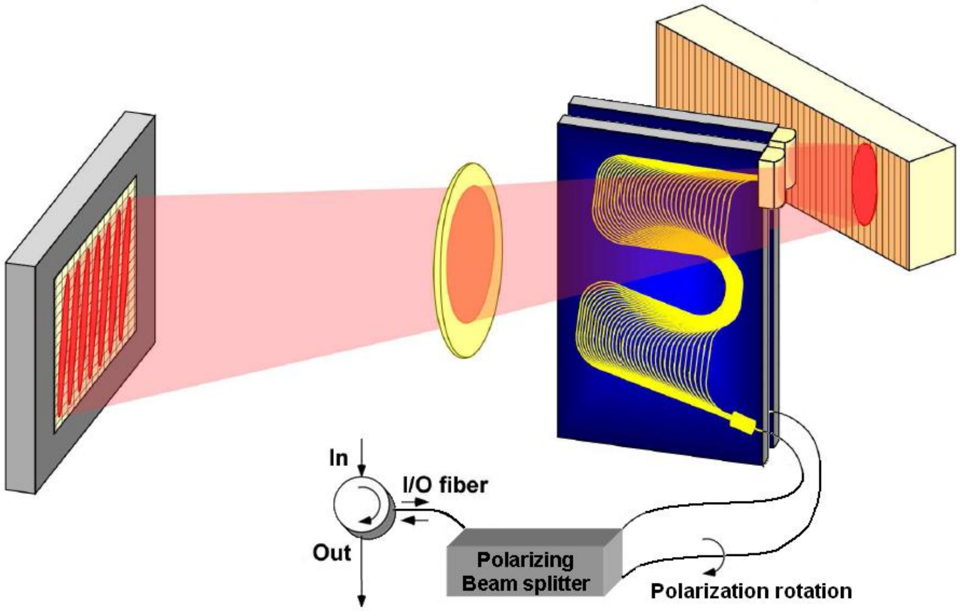

Fig. 8. Layout of a potential polarization insensitive PSP solution based on two PLC aligned together before the bulk grating. A polarizing beam splitter is used to separate the two incoming polarizations and a polarization rotator is added to ensure that both polarizations are aligned after the WGR output.

6. Summary

We demonstrated the functionality of our two-dimensional photonic spectral processor, which is capable of modulating a communication signal’s spectral components in amplitude and phase. Our system’s high resolution and full control along the entire C-band brings tremendous possibilities for wavelength manipulations useful in controlling and improving WDM signals in optical communication systems.

The two-dimensional PSP realized in our lab was assembled on an optical table using conventional optomechanical mounts. The arrangement would have to be compactly packaged for a more practical realization that can be deployed in the field. Such a realization would have to address the dual polarization support, as described in Section 5, as well as clever folding solutions such that the system’s optical height is reduced. Currently the size of the WGR is the limiting factor in the vertical direction. A 90° rotating prism could be inserted in the optical system to orient the PLC in the horizontal direction, thereby achieving a slender optical system.

#149409 - $15.00 USD Received 16 Jun 2011; revised 30 Jun 2011; accepted 30 Jun 2011; published 13 Jul 2011

Chapter 3.
Three PSP applications

In addition to the different variations of the PSP, different applications were developed. In the following section 3 different implementations of the 3 PSP variations will be discussed. The first paper describe the usage of a high resolution PSP for employing full Nyquist WDM (N-WDM) filtering [66]. The second paper describe generation of WDM colored pulse stream by combination of two different passive PSP setups [67]. The third paper describe a ring laser which is based on the two dimensional PSP setup [68].

In the following section we will describe these systems and their results.

6.1 N-WDM Filter Shaping with a high resolution PSP [66]

In this work we employ our high resolution, colorless PSP with a spectral addressability of 100 MHz along 100 GHz bandwidth, for multi-channel, high resolution reshaping of Gaussian channel response to square-like shape, compatible with Nyquist WDM requirements.

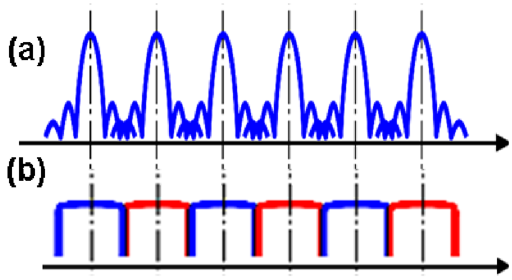

Figure 3.1 - comparison between conventional and Nyquist WDM: (a) Conventional WDM with low spectral utilization. (b) Nyquist WDM with dense spectral packing.

High spectral efficiency modulation formats and dense packing of wavelength-division multiplexing channels are key techniques for maximizing the transmission capacity over the available optical gain window. One of the promising approaches for such dense spectral utilization is called Nyquist WDM (N-WDM). (Fig 3.1). The square-like spectral form of N-WDM is amenable to non-overlapping and contiguous packing. This formats support the construction of terabit super-channels that propagate between endpoints with no intermediate filtering elements [69]. N-WDM transmission experiments [70-71] typically employ filters originally designed for channel add-drop. As such their performance attributes fall short of those required to optimally support N-WDM.

In this work we capitalize on the high-resolution filtering attributes of our PSP which is an enhanced version of our former device [41], and use it in cascade with a multiplexing filter having Gaussian pass band characteristics. We adjust the PSP for spectral reshaping to generate a square-like spectrum, conforming to the N-WDM requirements.

We used the same PSP as in our former work, with a flat spectral response over the entire FSR, and a spectral resolution of ~3 GHz. In order to achieve even better addressability, we replaced our BNS SLM with a new Holoeye LCoS SLM which has 1920×1080 pixels of 8 μm pitch which result in addressability of 100 MHz per SLM column. This arrangement yields a flat spectral response over the entire FSR, in contrast to our previous PSP implementation (with the curved output) [41]. The required square-like spectral filter response in N-WDM is the cumulative transfer function of the multiplexing components. Hence, we need to take into account the response of the multiplexer, typically of Gaussian shape. A typical optical N-WDM implementation would thus separately multiplex the even and odd channels, shape each group to square-like channel response with a 50% spectral duty cycle, and passively combine the two interleaved halves (Fig. 3.2a).

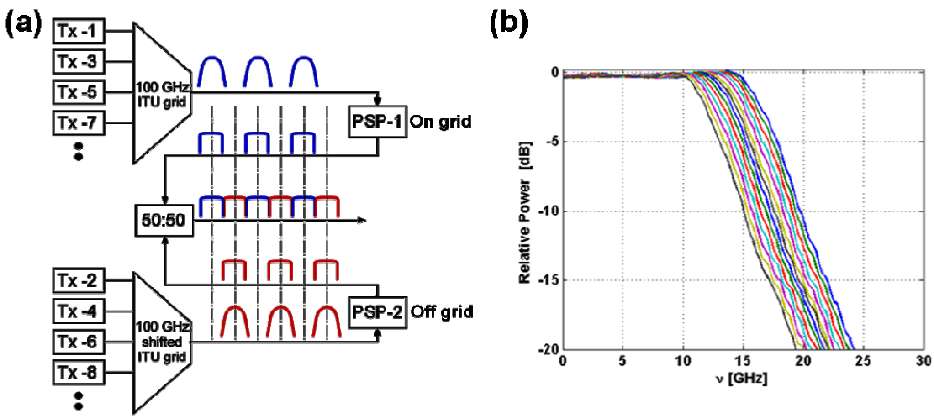

Figure 3.2 - (a) Proposed method for generating a Nyquist-WDM super-channel: odd square channels (marked in blue) are generated using an on-grid PSP filtering the output of a 100 GHz ITU grid demultiplexer, while even square channels (marked in red) are generated using an off-grid PSP filtering the output of a 100 GHz shifted ITU grid demultiplexer. (b) Experimental results of PSP filter width change, one column at a time.

For the N-WDM filtering application, the 100 MHz addressability dictates the precision at which the filter bandwidth can be set, and the 3 GHz resolution sets the roll-off shape (deviation from ideal square-like filter response). This is experimentally shown in Fig. 3.2b, where the filter edge is displaced in increments as fine as 100 MHz. The roll-off shape is always maintained, and determined by the spectral resolution, regardless to the filter bandwidth, with a decrease from -0.5dB to -10dB in 3 GHz bandwidth. In order to generate filtering for both on/off grid channels with the same PSP, a flat spectral response is required, as experimentally achieved (purple dashed curve in Fig 3.3a-b). As a first demonstration of the flattening abilities of the PSP, we used an etalon-based tunable spectral filter with a Lorentzian line shape which was placed after an amplified spontaneous emission source. The filter response is plotted in Fig. 3.3a-b as a dashed black curve. The PSP was placed afterwards, and flattened the spectral response by applying an inverse attenuation function over prescribed bandwidths. In this fashion we show square-like spectral response for 30, 40 and 50 GHz bandwidths with <0.5 dB ripple (Fig. 3.3a). As we prescribe larger bandwidths, the overall filter attenuation at center must be increased (see Fig. 3.3b) in order to achieve flat equalization over bandwidth target. The temporal response of the flattened spectrum was characterized by filtering ultrashort pulses (100 fs) emitted from a Spectra Physics Tsunami + Opal mode locked laser (λ=1.55 μm, 80 MHz rate). The laser output was fiber coupled and traversed the etalon filter and the PSP, allowing transmission of the single flattened channel only.

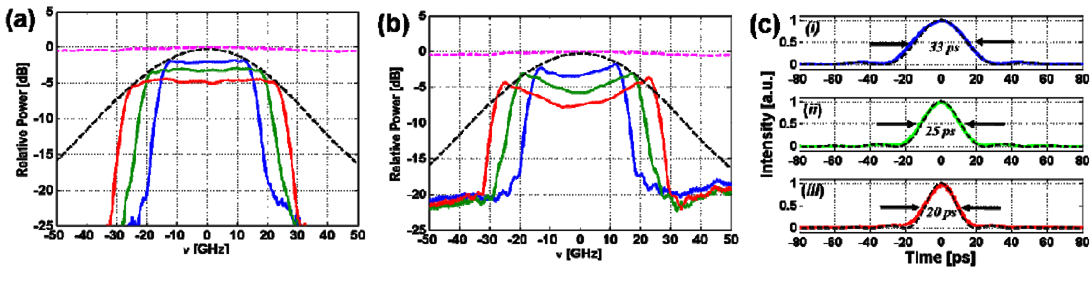

Figure 3.3 - (a-b) Experimental results of rectangular spectral filter response, compensating a commercial multiplexing filter (marked with dashed black line) for three selected bandwidths: 30, 40 and 50 GHz. (a) The cascaded flattened spectrum for three bandwidths. As the bandwidth becomes larger, overall filter attenuation must be increased in order to achieve equalization. (b) Encoded PSP response without the multiplexer (different colors match those of Fig. 3.3a). The dashed purple line denotes the PSP response without any spectral shaping, showing a flat response along the entire usable bandwidth. (c) Time-domain measurements of (i) 30 GHz, (ii) 40 GHz and (iii) 50 GHz carved spectra, resulting in 33, 25 and 20 ps width sinc^2 shaped pulse intensities, respectively, measured with a high-speed sampling scope.

With the PSP, we applied the same cascaded spectral responses that were measured and shown in Fig 3.3a. The temporal response of 30, 40 and 50 GHz channel bandwidths were measured using a high speed sampling (HSS) scope, resulting in $sinc^2$ shaped intensity pulses with widths of 33, 25 and 20 ps respectively (Fig 3.3c).

In order to demonstrate the ability to operate simultaneously for all WDM channels spaced at FSR, a combination of flattened 50 GHz on-grid and off-grid channels is needed. Although two different 100 GHz multiplexers are required (on and off grid), it is still desirable to use identical PSP in both channel sets. The PSP AWG is designed with 100 GHz FSR aligned for on-grid operations. When placed in cascade with an on-grid multiplexer, the central 50 GHz are flatten by applying varying tilted phases with the LCoS SLM, and a large constant phase tilt outside the central band for high attenuation (Fig. 3.4a). For off-grid channel flattening, the outer parts of the FSR are shaped using the varying tilted phase, where the central part is blocked by the large attenuation (Fig 3.4b). This demonstrates the coherent combining of frequency components separated to two different diffraction orders at the FSR edge.

In order to demonstrate optical N-WDM channel filtering, we used a Finisar WaveShaper (1000S) to simulate multiplexed Gaussian WDM channel spectra both on and off grid. Both multiplexer responses were compensated by the PSP functions, resulting in rectangular spectral shaping having 50% duty cycle (Figs. 3.4c). The two branches can then be passively combined, resulting in the entire spectrum being occupied with no spectral gaps and <1 dB ripple.

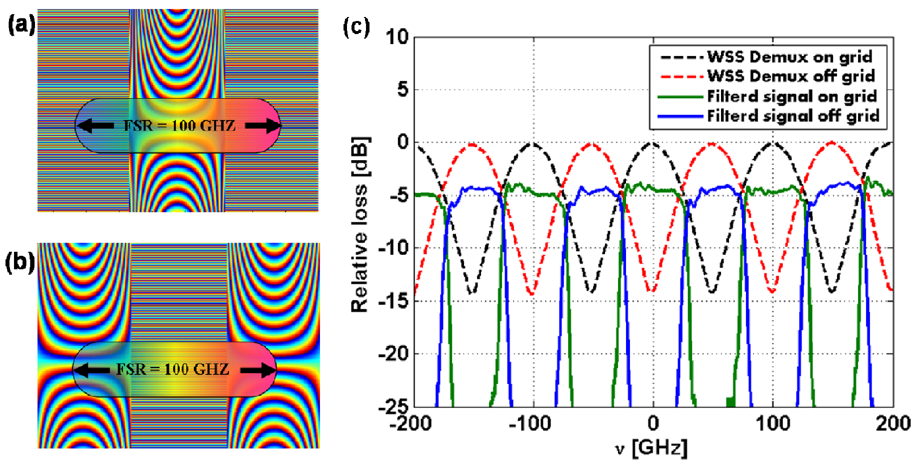

Figure 3.4 - (a) SLM pattern for on-grid channel filtering with varying phase tilts along the central 50 GHz and large constant phase tilt outside and (b) SLM pattern for the off-grid channel filtering with varying phase tilts along the outer 50 GHz and large constant phase tilt along the center. (c) Passively-combined filtered on-grid and off-grid components of each branch, resulting in full spectral coverage with <1 dB ripple.

6.2 Generation of WDM adaptive-rate pulse bursts [67]

In this work we demonstrate passive generation of optical pulse-trains with each pulse having distinct center carrier and spectra using tunable group delay (GD) staircase transfer functions. The GD steps result from opposite and equal magnitude GD slopes from narrow-band and wide-band tunable optical dispersion compensators. We use this technique to split the spectrum of a femtosecond pulse to a pulse burst with precise control of pulse time separation.

Chirped pulses are useful in converting an ultrafast optical signal by way of parametric wave mixing to a frequency mapped signal, performing temporal imaging and serial-to-parallel conversion [72-73]. Some applications preferably require a discrete colored pulse train such as photonic ADC [74-79], as opposed to a continuous carrier sweep. This can be achieved by a photonic spectral processor (PSP) [48, 80], which uses a phase spatial light modulator (SLM), which can be used for applying different phase slopes to different spectral channels. However, adding phase slopes to the spectrum using the PSP approach results in losses which increase with the associated time delay [48], and the use of an active SLM component to generate the desired group delay (GD) function is expensive.

Our proposed method for generating a WDM pulse burst with passive components only is based on realizing a transfer function consisting of a GD staircase, by cascading a continuous CD element with a narrow FSR WDM dispersion compensator of opposite GD slope, as shown in Fig .3.5

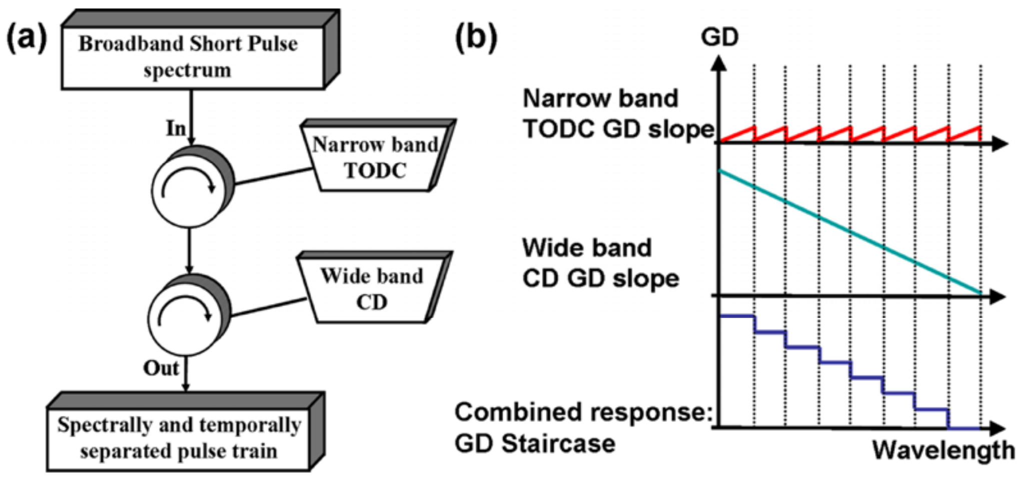

Figure 3.5 - Layout of the tunable group delay system: (a) System arrangement. (b) Narrow band TODC and wide band TODC GD slopes and the resultant GD staircase.

Continuous (or wideband) CD is characterized by fixed GD slope versus wavelength, with the slope defining the CD. Finite (or narrowband) FSR CD has sawtooth GD vs. wavelength pattern. Their cascade, when the slopes are equal in magnitude and opposite in sign, create GD stairs where the step height, ΔGD, is given by:

$$\Delta GD[ps] = CD[ps/nm] \cdot \Delta\lambda[nm] \tag{6.1}$$

where Δλ is the FSR. If an ultrashort pulse traverses the staircase transfer function, it will be filtered to a burst of subpulses, each being transform limited, delayed in time, and of contiguous spectral extent. Furthermore, if both the wideband and narrow band CD are made tunable, then the pulse burst is also rate adaptable, with the rate being the inverse of ΔGD.

We use our passive narrowband TODC [60] (Fig. 3.6a) to generate a periodic GD sawtooth pattern by moving the AWG towards the Fourier lens. We apply the same technique towards realization of a wideband TODC. Wideband support was achieved by replacing the AWG with a bulk grating (Fig. 3.6b). Since the bulk grating's angular dispersion is much smaller, and to eliminate spatiotemporal coupling effects, the system is double passed (by reflecting off a folding mirror and experiencing four grating diffraction events). The narrowband TODC has a 100 GHz (0.81 nm) FSR, yielding m≅1900, with output waveguides at pitch of p=16 μm, leading to angular dispersion of dθ/dλ=120 mrad/nm. In contrast, the wideband TODC with an 1100 gr/mm grating mounted near Littrow has dθ/dλ=5.7 mrad/nm. Due to the CD dependence on angular dispersion squared (Eq. 2.2), the wideband TODC has to translate 220 times as much for an identical CD setting.

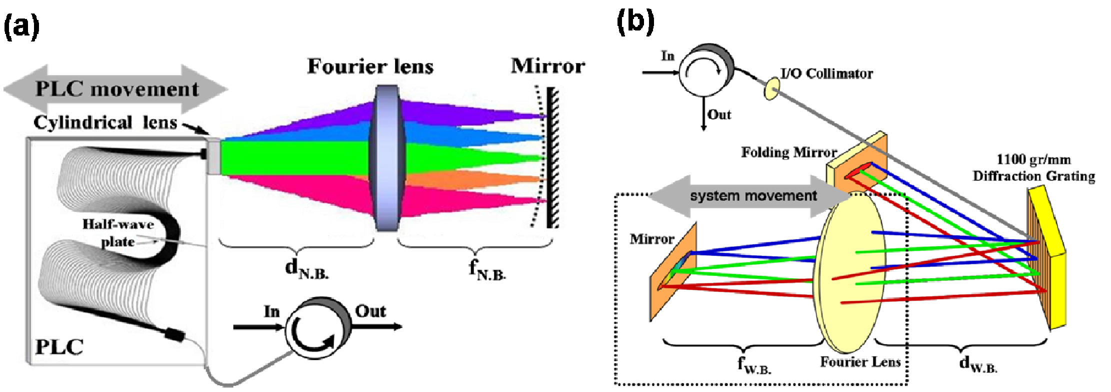

Figure 3.6 - (a) Narrow band TODC based on high resolution dispersion from an AWG. Changing the grating-lens distance, $d_{N.B.}$, results in quadratic spectral phase or GD slope. (b) Wideband TODC of similar nature with a bulk diffraction grating. The system is double-passed to maximize the CD capacity and avoid spectral narrowing.

The tuning ability and accuracy of the system is shown in Figs. 3.7(a-c). The dispersion of the wideband and the narrowband systems was set to ±18.75 (blue) and ±50 ps/nm (green). The combination of the narrowband TODC GD slopes (Fig. 3.7a) with the wideband TODC slopes (Fig. 3.7b) resulted in the desired GD staircase pattern (Fig. 3.7c). Since the narrowband FSR is 0.81 nm, the GD staircase step height is ~15 ps (40 ps) for GD slopes of ±18.75 ps/nm (±50 ps/nm), resulting 66.6 GHz (25 GHz) pulse bursts. The two GD staircase patterns were used to filter ultrashort (100fs) pulses at λ_0=1.55 μm from a mode-locked laser (MLL). We used Spectra Physics Tsunami + Opal MLL, with a pulse rate of 80 MHz and average power of 300 mW. Each filtered ultra-short pulse generates a finite duration WDM pulse burst. A continuous WDM pulse sampling sequence can be generated by employing a higher repetition rate MLL. The generated pulse bursts were measured with a high-speed optical sampling scope (65 GHz effective bandwidth), having inter-pulse spacings of 15 and 40 ps (Fig. 3.8). The narrowband TODC has a spectral filtering bandwidth of ~60 GHz, leading to filtered, transform limited pulses of ~17 ps duration full-width-half-max (FWHM). For the 25 GHz pulse burst, this corresponds to a pulse burst duty cycle of 0.33.

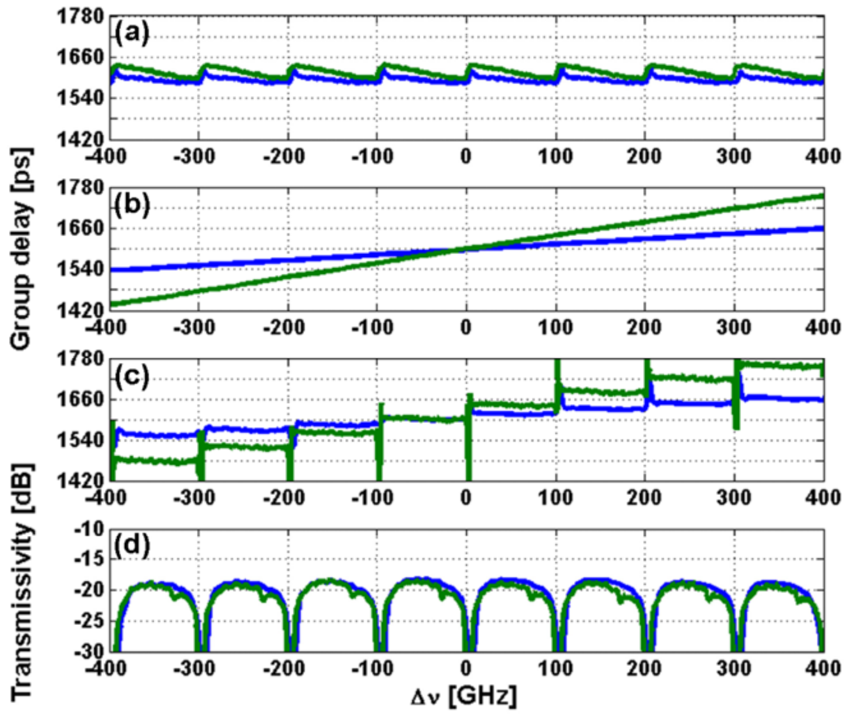

Figure 3.7 - Plots of measured GD with slopes of ±18.75 ps/nm (blue) and ±50 ps/nm (green). (a) Narrow band TODC. (b) Wide band TODC. (c) The combined TODC arrangement with the GD staircase pattern. with step heights of 15 ps (blue) and 40 ps (green) (d) IL of the combined TODC arrangement in both cases.

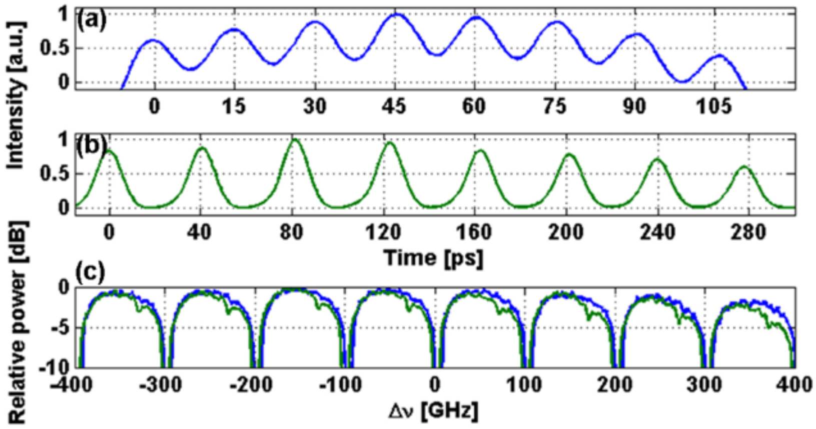

Figure 3.8 - High-speed oscilloscope measurements of the WDM pulse bursts that were generated with group delay system: (a) 15 ps spaced pulses. (b) 40 ps spaced pulses. (c) OSA measurement of the relative power of the filtered MLL spectrum for both 15 ps (blue) and 40 ps (green) spaced pulses.

For both pulse bursts, no loss degradation was observed, and the loss was relatively uniform along all pulses (Fig 3.7d). With a PSP approach [48], where each pulse is independently delayed, there will be delay-dependent losses along the spectrum.

To show that the pulse burst is truly wavelength distinguishable, we used a WDM channel filter allowing the transmission of one WDM channel at a time for selecting individual pulses from the pulse burst. While keeping the time frame along the whole measurements, we performed both temporal measurements with the high speed scope, and spectral measurement using an optical spectrum analyzer (OSA), resulting in a direct correspondence between pulse position and spectrum (Fig. 3.9).

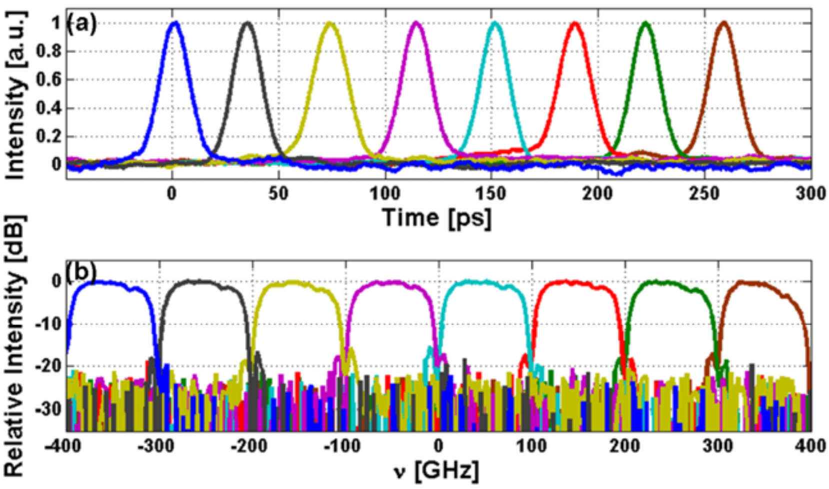

Figure 3.9 - Validation experiment of unique pulse center carrier and spectrum by WDM channel filtering, and subsequent high-speed scope measurements and corresponding OSA measurements, collected and normalized for each filtered pulse separately. (a) Temporal measurements. (b) spectral measurements. The colors in (a) and (b) are matched, showing that each pulse has distinguished spectral content.

6.3 Tunable fiber ring laser based on the 2D PSP [68]

In this work we present a novel mechanism of tunable fiber laser based on our two dimensional PSP. With this arrangement we have demonstrated a tunable laser with a tuning resolution of 200 MHz along 30 nm. In order to operate and measure the output power of the laser, we connected the circulator output signal to an erbium doped fiber amplifier (EDFA) and than coupled it back to the circulator input, forming a ring laser spectrally controlled by the 2D PSP. A tap splitter allows lasing extraction from the cavity (Fig 3.10).

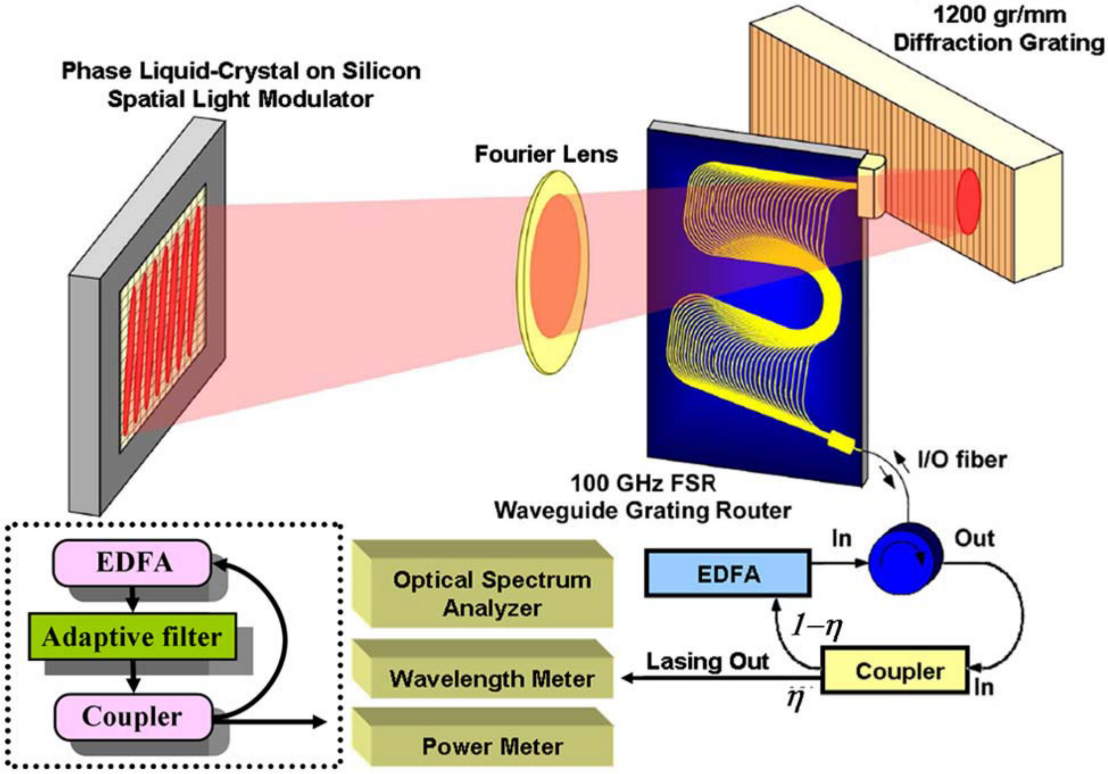

Figure 3.10 - Layout of the two-dimensional laser amplified light goes through crossed AWG and bulk grating, which disperse the spectrum across the two-dimensional LCoS array, enabling high resolution access to the spectral components along the communication c-band. Inset: layout of a ring laser based on an adaptive filter and gain module inside the cavity.

Wavelength selection is performed by attenuating all spectral components but the one where lasing is to occur [81-82]. Attenuation is achieved by prescribing a linear phase across the beam, thus increasing the coupling loss back to the fiber. Using this method, we can eliminate all the spectral components except from specific line, by applying tilted phase for all the SLM except for small "opened" window (Fig 3.11a). Changing the horizontal position of the window results in large change in the output wavelength (100 GHz Steps), since the lasing occurs from different channels of the

AWG (Fig 3.11b). Changing the vertical position of the window along the channel, results in high resolution changes in the output wavelength (step size of ~180 MHz) the result is shown in Fig 3.11c. In this way we can coarsely tune the wavelength by selecting a different WGR diffraction order (separated by the bulk grating) or finely tune the wavelength by selecting within the WGR diffraction order. The smallest spectral window that can be prescribed is limited by the optical resolution of the system. Since a single laser spot is lying on 18 pixels with an addressability of 182 MHz per pixel, we can achieve a minimal spectral width of ~3 GHz.

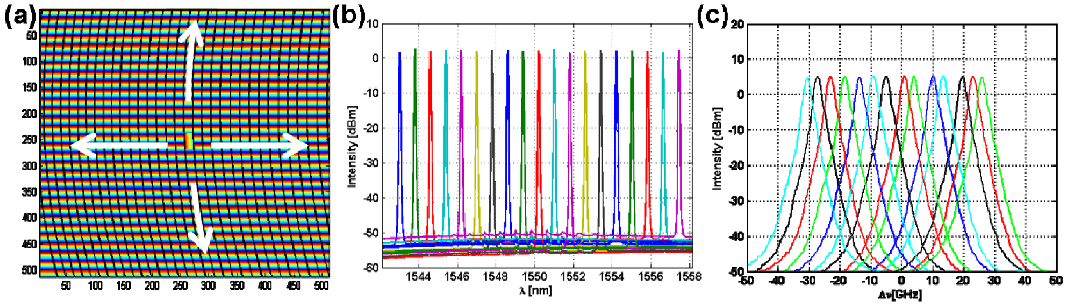

Figure 3.11 - Output of the fiber laser – (a): The applied LCoS phase, attenuating all spectral components except the lasing line. The white arrows mark low resolution scan (horizontal translation of the opened spectral window) and high resolution scan (vertical translation of the opened spectral window). (b) laser lines from different diffraction orders of the AWG. (c) laser lines from different locations at the same diffraction order of the AWG.

Since the insertion loss of the 2D PSP is ~ 14 dB, we used an EDFA amplification of 22 dB in order to achieve constant output along the spectrum (Fig. 3.11b). This gain value leads to a saturated output power level of the EDFA, which enables equal power emission at any wavelength.

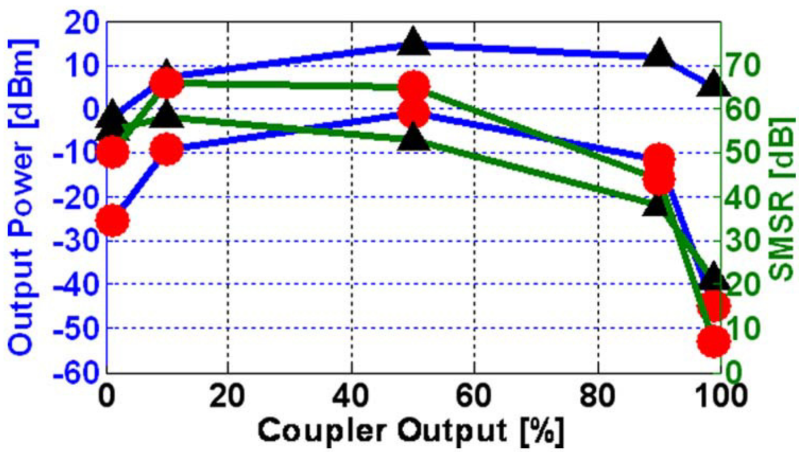

Figure 3.12 - Output Power (blue line) and SMSR (green line) of the fiber laser vs. output tap value, measured in various combinations: a) EDFA before the coupler (results mark with black triangles); (b) EDFA after coupler, (results mark with red circles).

The optical output power of the laser, measured at -7 dBm, was limited by the 1% tap. The Side-Mode Suppression Ratio (SMSR) is more than 50 dB. In order to find the best way to operate the ring laser we change the tap splitter values and position. We used 3 couplers with splitting values of: 1/99, 10/90 and 50/50 with 5 output options: 1%, 10%, 50%, 90% and 99%. We also replaced the position of the EDFA and the tap splitter.

In each of the above arrangement we measured both the output power and the SMSR. The results are shown in Fig 3.12. The highest output power was measured with the 50% output tap with the EDFA before the coupler.

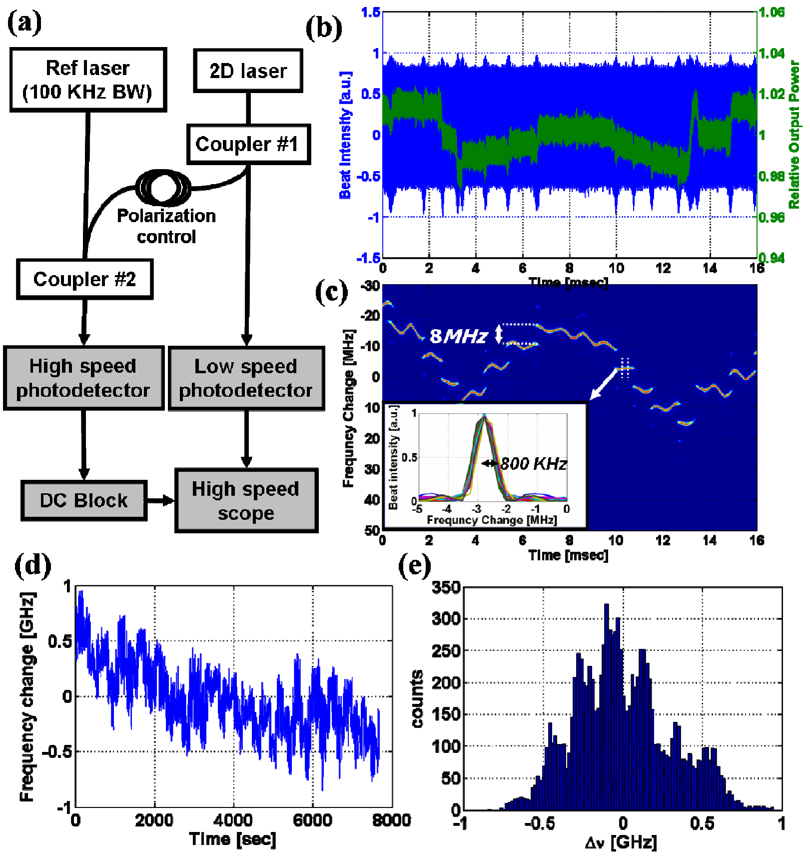

Figure 3.13 - Measuring laser line width: (a) Setup for line width measurement using a high speed detector to measure the beating between a reference laser and the 2D laser, while a slow detector measures the direct output power of the 2D laser. (b) Registered powers of the beat frequency (blue) and the output power (green), with correlation between intensity spikes and mode hops. (c) Spectrogram of the interferometric measurement showing mode hops occurring every 1-3 milliseconds. Frequency hop is approximately 8 MHz. Inset: cross-section of the spectrogram showing instantaneous laser linewidth of 800 KHz. (d) Results of 10000 measurements of laser relative lasing frequency taken along 8000 seconds. The central frequency changes are due to mode hoping and thermal drift. (e) Histogram of the above 10000 measurements showing the long term frequency excursion of the laser output.

The spectral plots of the laser output, as shown in Fig 3.11b, do not reflect the actual laser line width, rather the OSA resolution limit. To properly measure the laser line width, we mixed our fiber laser output with that of a reference 100 KHz linewidth external cavity laser. The reference laser was set to a slightly different wavelength resulting in an intermediate frequency beating between the two lasers. This was detected with a high speed photodetector connected to a high speed real-time scope (Fig. 3.13a).

In addition, a slow detector was connected directly to the fiber laser to track its output power. The detected power results are shown in Fig 3.13b. A spectrogram of the beat intensity measurement (Fig. 3.13c) shows that every few milliseconds a mode hopping event occurs inside the ring laser, with a lasing frequency hop of approximately 8 MHz. This correlates to a fiber cavity length of 38 meters which is reasonable due to the EDFA fiber length. A vertical cross section of the spectrogram (shown in the inset of Fig. 3.13c) shows the instantaneous laser line width is approximately 800 KHz. This narrow linewidth can be utilized in self-homodyne sensing applications. However, the rapid mode hopping likely precludes the laser’s use in other coherent reception applications, and in application requiring high intensity stability. A histogram of 10000 relative frequency measurements taken with ~1 second interval in an uncontrolled environment, gives the long duration lasing wavelength stability bandwidth of 1.3 GHz (Fig 3.13d-e). This bandwidth is smaller than the 3 GHz filter window, since the lasing preferentially occurs close to the filter peak where losses are minimal.

Chapter 3A.

Nyquist-WDM filter shaping with a high-resolution colorless photonic spectral processor

David Sinefeld, Shalva Ben-Ezra and Dan M. Marom

Published in Optics Letters:

D. Sinefeld, S. Ben-Ezra, and D. M. Marom, "Nyquist-WDM filter shaping with a high-resolution colorless photonic spectral processor," Opt. Lett. 38, 3268-3271 (2013).

Nyquist-WDM filter shaping with a high-resolution colorless photonic spectral processor

David Sinefeld,[1,]* Shalva Ben-Ezra,[2] and Dan M. Marom[1]

[1]*Applied Physics Department, Hebrew University, Jerusalem 91904, Israel*

[2]*Finisar Corporation, Nes Ziona, Israel*

**Corresponding author: sinefeld@gmail.com*

Received May 8, 2013; revised July 26, 2013; accepted July 29, 2013;
posted July 30, 2013 (Doc. ID 190284); published August 21, 2013

We employ a spatial-light-modulator-based colorless photonic spectral processor with a spectral addressability of 100 MHz along 100 GHz bandwidth, for multichannel, high-resolution reshaping of Gaussian channel response to square-like shape, compatible with Nyquist WDM requirements.

OCIS codes: (060.2330) Fiber optics communications; (130.7408) Wavelength filtering devices.
http://dx.doi.org/10.1364/OL.38.003268

High-spectral-efficiency modulation formats and dense packing of wavelength division multiplexing (WDM) channels are key techniques for maximizing the transmission capacity over the available optical gain window. Two different approaches are actively being investigated for placing the signals at the packing limit, when the baud rate equals the channel spacing: coherent optical orthogonal frequency-division multiplexing (CO-OFDM) and Nyquist WDM (N-WDM). In CO-OFDM, the subcarriers are synchronously modulated with rectangular pulses in time, creating sinc-like spectra. The modulation rate equals the carrier separation such that the sinc nulls fall on neighboring carriers. While the spectral components of neighboring channels overlap, channel crosstalk can be averted by proper filtering and signal processing (SP) at the receivers. In N-WDM, the signal is modulated with sinc pulses in time, suggesting strong intersymbol interference (ISI) due to overlapping neighboring pulses. By receiver sampling at the sinc peak position, ISI can be avoided due to the constant zero spacing property of the sinc function. The square-like spectral form of N-WDM is amenable to nonoverlapping and contiguous packing. N-WDM and CO-OFDM can be seen as complementary schemes, overlapping in either the time or frequency domain. In theory, both modulation formats can reach the same sensitivity performance; however, in practical scenarios, N-WDM requires less receiver bandwidth (due to its limited spectral extent) and slower analog-to-digital converters [1]. These formats support the construction of terabit superchannels that propagate between endpoints with no intermediate filtering elements [2,3].

Both CO-OFDM and N-WDM require careful control over the modulated signal form, to reach their desired attributes. This can be obtained by electrically shaping the modulator driving signals through transmitter digital SP circuitry and digital-to-analog converters [4,5]. However, the electrical SP tasks are both power-consuming and costly. Alternatively, all-optical techniques have been proposed, which are based on passive filtering arrangements, which are further not rate limited to electronic SP abilities. OFDM receivers and transmitters [6–9] have been realized through interference-based devices. N-WDM transmission experiments [10–13] typically employ filters originally designed for channel add–drop. As such their performance attributes fall short of those required to optimally support N-WDM.

In this Letter, we capitalize on the high-resolution filtering attributes of a photonic spectral processor (PSP), which is an enhanced version of our former device [14], and use it in cascade with a multiplexing filter having Gaussian passband characteristics (see Fig. 1). We adjust the PSP for spectral reshaping to generate a square-like spectrum, conforming to the N-WDM requirements.

The key to the fine optical resolution of our PSP is its operation over a small free spectral range (FSR), in this case 100 GHz. The dispersive medium is an arrayed waveguide grating (AWG) planar lightwave circuit (PLC), having 34 grating arms fabricated in silica-on-silicon technology with 0.8% index contrast. The output of the AWG is unconventional: instead of employing a second slab-lens region that demultiplexes to output waveguides, the grating arms terminate at the PLC edge at fixed pitch, and the light radiates normally into free space. This forms a phased-array output that experiences angular dispersion on account of wavelength-dependent phase delays. An $f = 3$ mm cylindrical lens that is affixed at

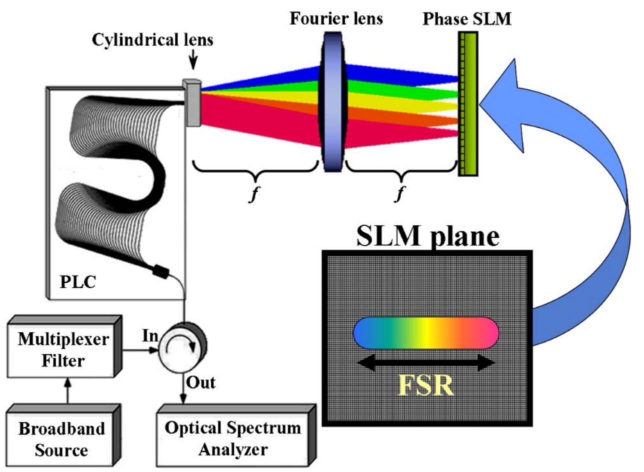

Fig. 1. Experimental layout making use of the PSP for shaping to a rectangular spectrum with the liquid crystal on silicon (LCoS) spatial light modulator (SLM). The SLM applies linear phase tilts to each spectral component for encoding coupling losses to the desired spectral shape.

the PLC edge collimates the light in the guided direction. The optical resolution of the AWG is the FSR divided by the waveguide arm count, resulting in ~3 GHz spectral resolution. The same resolution can be obtained with an AWG having larger FSR, but would require a larger waveguide count (and larger AWG device layout). Likewise, we can obtain finer resolution with the same FSR if we increase the waveguide count (again at the expense of a larger AWG). For our purposes here, the 3 GHz suffices to demonstrate the square filtering function.

The angularly dispersed output radiated light is projected with a Fourier lens using a simple *f*-*f* arrangement onto a liquid crystal on silicon (LCoS,) two-dimensional phase spatial light modulator (SLM) that is controlled by a computer. The resulting PSP is therefore a hybrid guided-wave/free-space optics device. The reflective LCoS SLM is placed at the Fourier plane, where the spectral components of the incident optical signal are spatially dispersed and manipulated. This arrangement yields a flat spectral response over the entire FSR, in contrast to our previous PSP implementation [14], where the grating arms terminated in a slab lens and then radiated into free space. This required a complicated telescopic free-space arrangement, which experienced spectral apodization. Due to the periodic nature of the dispersion (originating from the FSR property of the AWG), spectral elements that are shifted by FSR multiples overlap in space and the same channel response is achieved every FSR (the colorless property, when the FSR equals the channel separation).

The required square-like spectral filter response in N-WDM is the cumulative transfer function of the multiplexing components. Hence, we need to take into account the response of the multiplexer, typically of Gaussian shape. A typical optical N-WDM implementation would thus separately multiplex the even and odd channels, shape each group to square-like channel response with a 50% spectral duty cycle, and passively combine the two interleaved halves (Fig. 2).

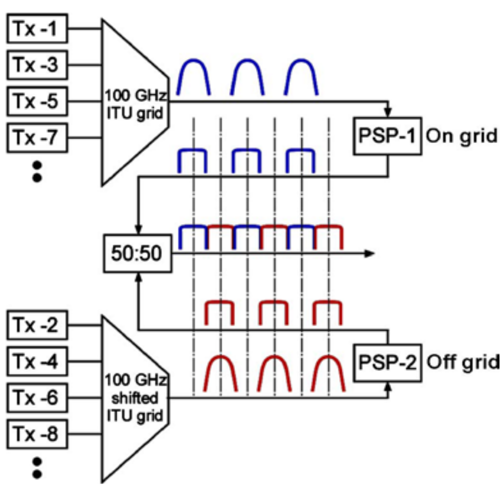

Fig. 2. Proposed method for generating a Nyquist-WDM superchannel: odd square channels (marked in blue) are generated using an on-grid PSP filtering the output of a 100 GHz ITU grid demultiplexer, while even square channels (marked in red) are generated using an off-grid PSP filtering the output of a 100 GHz shifted ITU grid demultiplexer.

The PSP needs to flatten the spectral response of the multiplexer, by imparting excess loss to the central spectral components, such that their magnitude equates the edge spectral components. In our specific example making use of a 100 GHz spaced PSP, two 100 GHz spaced multiplexers are utilized, one for multiplexing the odd channels (*on-grid*) and the other for the even channels (*off-grid*). Each set is then spectrally shaped using a PSP to a square spectrum of 50 GHz bandwidth, and the two interleaving signal components are passively combined. For such scenarios, the colorless property of the PSP is ideally suited, as the PSP imparts the same response to multiple channels simultaneously at high resolution.

The elements of the PSP, consisting of the AWG PLC, an $f = 100$ mm Fourier lens, and the LCoS phase SLM, were assembled on an optical table. A circulator was used to separate the input and output light to the PLC. We used Holoeye PLUTO LCoS SLM that has 1920×1080 pixels of 8 μm pitch, with a system spatial dispersion of $dx/d\lambda = 10$ [mm/nm], which translates to 100 MHz shift in center frequency per SLM column. The entire 100 GHz spectrum spans over 1000 columns. The insertion loss of the PSP is 15 dB, caused mostly by excessive AWG losses (~12.5 dB) and SLM losses (~2.5 dB).

For the N-WDM filtering application, the 100 MHz addressability dictates the precision at which the filter bandwidth can be set, and the 3 GHz resolution sets the roll-off shape (deviation from ideal square-like filter response). This is experimentally shown in Fig. 3, where the filter edge is displaced in increments as fine as 100 MHz. The roll-off shape is always maintained, and determined by the spectral resolution, regardless of the filter bandwidth, with a decrease from −0.5 to −10 dB (equivalent to a 90-10 fall) in 5 GHz bandwidth.

In order to amplitude modulate the dispersed spectral components with a phase-only LCoS SLM, we use the direction orthogonal to the dispersion to locally manipulate the reflected beam. To prescribe amplitude modulation, we apply a phase tilt, on a column-by-column basis, that introduces a coupling loss back into the AWG for each spectral component, subject to the optical resolution constraint.

In order to generate filtering for both on/off grid channels with the same PSP, a flat spectral response is required, as experimentally achieved (dashed-purple line

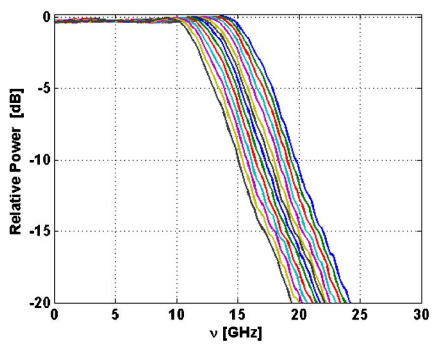

Fig. 3. Experimental results of PSP filter width change, one column at a time. For each position, 10 dB attenuation is reached at less than 5 GHz bandwidth. Although the system has 100 MHz addressability, the filter edge position is shifted here in 400 MHz increments for clarity only.

in Fig. 4). As a first demonstration of the flattening abilities of the PSP, we used an etalon-based tunable spectral filter with a Lorentzian line shape that was placed after an amplified spontaneous emission source. The filter response is plotted in Fig. 4 as a dashed-black line. The PSP was placed afterward, and flattened the spectral response by applying an inverse attenuation function over prescribed bandwidths. In this fashion, we show square-like spectral response for 30, 40, and 50 GHz bandwidths with <0.5 dB ripple [Fig. 4(a)]. As we prescribe larger bandwidths, the overall filter attenuation at the center must be increased [see Fig. 4(b)] in order to achieve flat equalization over the bandwidth target.

The temporal response of the flattened spectrum was characterized by filtering ultrashort pulses (100 fs) emitted from a Spectra Physics Tsunami+Opal mode locked laser ($\lambda = 1.55\ \mu m$, 80 MHz rate). The laser output was fiber coupled and traversed the etalon filter and the PSP, allowing transmission of the single flattened channel only. With the PSP, we applied the same cascaded spectral responses that were measured and shown in Fig. 4(a). The temporal response of 30, 40, and 50 GHz channel bandwidths was measured using a high-speed sampling (HSS) scope, resulting in sinc^2 shaped intensity

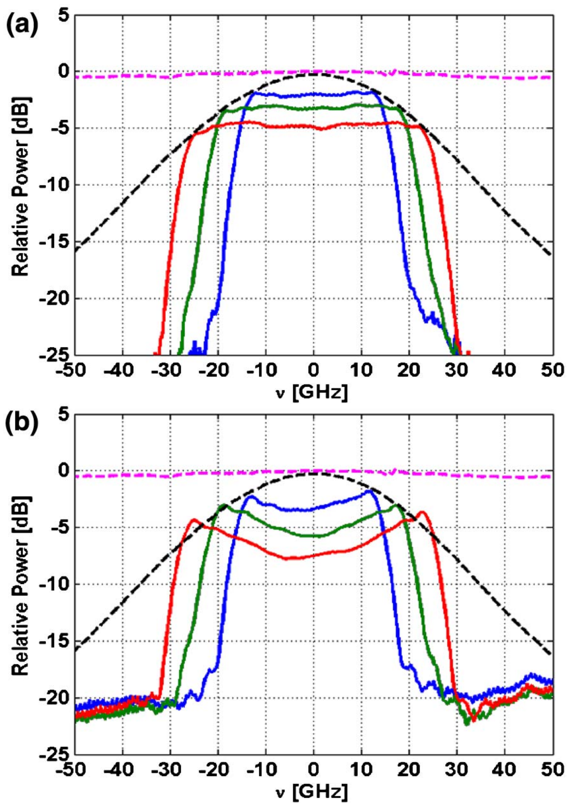

Fig. 4. Experimental results of rectangular spectral filter response, compensating a commercial multiplexing filter (marked with dashed-black line) for three selected bandwidths: 30, 40, and 50 GHz. (a) Cascaded flattened spectrum for three bandwidths. As the bandwidth becomes larger, overall filter attenuation must be increased in order to achieve equalization. (b) Encoded PSP response without the multiplexer [different colors match those of (a)]. The dashed-purple line denotes the PSP response without any spectral shaping, showing a flat response along the entire usable bandwidth.

pulses with widths of 33, 25, and 20 ps, respectively (Fig. 5). A comparison to the expected sinc^2 functions shows an excellent match to the measured results.

Our N-WDM solution is based on the colorless property of the PSP, and would operate simultaneously for all WDM channels spaced at FSR. In order to demonstrate this ability, a combination of flattened 50 GHz on-grid and off-grid channels is needed. Although two different 100 GHz multiplexers are required (on and off grid), it is still desirable to use identical PSP in both channel sets. The PSP AWG is designed with 100 GHz FSR aligned for on-grid operations. When placed in cascade with an on-grid multiplexer, the central 50 GHz are flattened by applying varying tilted phases with the LCoS SLM, and a large constant phase tilt outside the central band for high attenuation [Fig. 6(a)]. For off-grid channel flattening, the outer parts of the FSR are shaped using the varying tilted phase, where the central part is blocked by the large attenuation [Fig 6(b)]. This demonstrates the coherent combining of frequency components separated to two different diffraction orders at the FSR edge. The PSP spectral response is shown in Figs. 6(c) and 6(d), showing the desired 50 GHz inverse correction function for both (on/off grid) channel sets.

In order to demonstrate optical N-WDM channel filtering, we used a Finisar WaveShaper (1000S) to simulate multiplexed Gaussian WDM channel spectra both on-grid [Fig. 6(e)] and off-grid [Fig. 6(f)]. Both multiplexer responses were compensated by the PSP functions introduced in Figs. 6(b) and 6(d), resulting in rectangular spectral shaping having 50% duty cycle [Figs. 6(g) and 6(h)]. The two branches can then be passively combined, resulting in the entire spectrum being occupied with no spectral gaps and <1 dB ripple [Fig 6(i)].

The filtering abilities of the high-resolution PSP that were demonstrated here can be the key for better utilization of the available communication spectrum by better conforming to the N-WDM format. The high-resolution PSP can also support more aggressive time-frequency packing formats that do allow controlled amounts of either channel crosstalk or ISI with excess channel coding

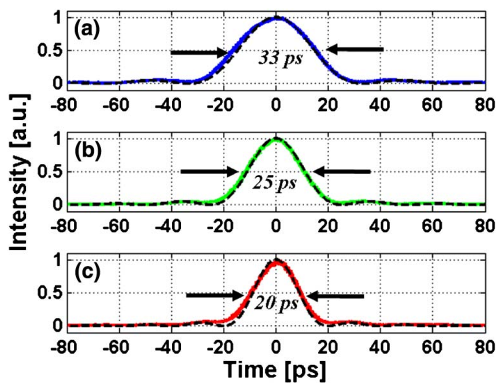

Fig. 5. Time-domain measurements of (a) 30 GHz, (b) 40 GHz, and (c) 50 GHz carved spectra, resulting in 33, 25, and 20 ps width sinc^2 shaped pulse intensities, respectively, measured with a high-speed sampling scope. The measured temporal results are plotted as solid color lines, matching the bandwidth filters of Fig. 4. Expected sinc^2 functions with the desired widths are plotted as dashed black lines, showing an excellent match to the measured results.

for error-free signal recovery [15]. We also demonstrated on/off grid flattening abilities, which enable the use of identical PSP devices for a complete N-WDM system.

The loss contributions of the AWG (~12.5 dB) are caused mostly by fabrication errors and can be overcome by a phase error correction mechanism [16], to allow future application in an actual N-WDM network. Although system losses are worse than in a state-of-the-art waveshaper (typical insertion loss of –5 dB), our PSP resolution of 3 GHz is at least twice as good [11]. We should note that temperature changes of the system result in a spatial shift in the dispersed spectrum. This can be compensated by tracking the LCoS filter spectral position and actively compensating for the thermal shift in the passband position.

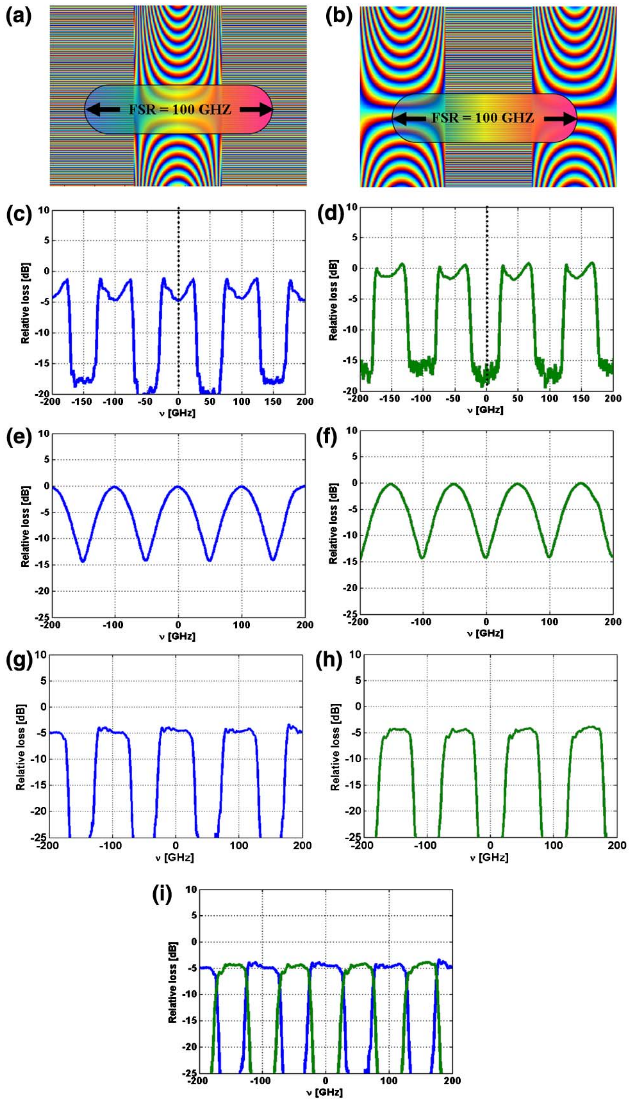

Fig. 6. Experimental demonstration of optical N-WDM filtering. (a) SLM pattern for on-grid channel filtering with varying phase tilts along the central 50 GHz and large constant phase tilt outside, and (b) SLM pattern for the off-grid channel filtering with varying phase tilts along the outer 50 GHz and large constant phase tilt along the center. Resulting (c) on-grid and (d) off-grid PSP spectral response. (e) On-grid and (f) off-grid Gaussian response of multiplexer, simulated with Finisar WaveShaper. Cascaded spectral filtering response for (g) on-grid and (h) off-grid, yielding interlaced rectangular shaped channels with 50% duty cycle. (i) Passively combined on-grid and off-grid components of each branch, resulting in full spectral coverage with <1 dB ripple.

The authors thank the Israel Ministry of Industry and Trade TeraSanta program and EC FP7 ICT FOX-C and OTONES programs for funding.

References

1. G. Bosco, A. Carena, V. Curri, P. Poggiolini, and F. Forghieri, IEEE Photon. Technol. Lett. **22**, 1129 (2010).
2. Y. Ma, Q. Yang, Y. Tang, S. Chen, and W. Shieh, Opt. Express **17**, 9421 (2009).
3. G. Bosco, V. Curri, A. Carena, P. Poggiolini, and F. Forghieri, J. Lightwave Technol. **29**, 53 (2011).
4. X. Zhou, L. Nelson, P. Magill, B. Zhu, and D. Peckham, in *Optical Fiber Communications Conference*, OSA Technical Digest (Optical Society of America, 2011), paper PDPB3.
5. R. Schmogrow, M. Winter, M. Meyer, D. Hillerkuss, S. Wolf, B. Baeuerle, A. Ludwig, B. Nebendahl, S. Ben-Ezra, J. Meyer, M. Dreschmann, M. Huebner, J. Becker, C. Koos, W. Freude, and J. Leuthold, Opt. Express **20**, 317 (2012).
6. D. Hillerkuss, M. Winter, M. Teschke, A. Marculescu, J. Li, G. Sigurdsson, K. Worms, S. Ben Ezra, N. Narkiss, W. Freude, and J. Leuthold, Opt. Express **18**, 9324 (2010).
7. K. Lee, C. T. D. Thai, and J.-K. K. Rhee, Opt. Express **16**, 4023 (2008).
8. Z. Wang, K. S. Kravtsov, Y.-K. Huang, and P. R. Prucnal, Opt. Express **19**, 4501 (2011).
9. A. J. Lowery and L. Du, Opt. Express **19**, 15696 (2011).
10. G. Gavioli, E. Torrengo, G. Bosco, A. Carena, S. Savory, F. Forghieri, and P. Poggiolini, IEEE Photon. Technol. Lett. **22**, 1419 (2010).
11. R. Cigliutti, E. Torrengo, G. Bosco, N. P. Caponio, A. Carena, V. Curri, P. Poggiolini, Y. Yamamoto, T. Sasaki, and F. Forghieri, J. Lightwave Technol. **29**, 2310 (2011).
12. Z. Dong, J. Yu, H. Chien, N. Chi, L. Chen, and G. Chang, Opt. Express **19**, 11100 (2011).
13. M. Nakazawa, T. Hirooka, P. Ruan, and P. Guan, Opt. Express **20**, 1129 (2012).
14. D. Sinefeld and D. M. Marom, IEEE Photon. Technol. Lett. **22**, 510 (2010).
15. N. Sambo, F. Paolucci, F. Cugini, M. Secondini, L. Poti, G. Berrettini, G. Meloni, F. Fresi, G. Bottari, and P. Castoldi, in *Optical Fiber Communications Conference*, OSA Technical Digest (Optical Society of America, 2013), paper OTh1H.5.
16. D. Sinefeld, N. Goldshtein, R. Zektzer, N. Gorbatov, M. Tur, and D. M. Marom, in *Advanced Photonics Congress*, OSA Technical Digest (Optical Society of America, 2012), paper JTu5A.55.

Chapter 3B.

Generation of WDM adaptive-rate pulse bursts by cascading narrow/wideband tunable optical dispersion compensators

David Sinefeld, Yiska Fattal and Dan M. Marom

Published in Optics Letters:

D. Sinefeld, Y. Fattal, and D. M. Marom, "Generation of WDM adaptive-rate pulse bursts by cascading narrow/wideband tunable optical dispersion compensators," Opt. Lett. 37, 4290-4292 (2012).

Generation of WDM adaptive-rate pulse bursts by cascading narrow/wideband tunable optical dispersion compensators

David Sinefeld,* Yiska Fattal, and Dan M. Marom

Applied Physics Department, Hebrew University, Jerusalem 91904, Israel

**Corresponding author: sinefeld@gmail.com*

Received June 11, 2012; revised August 14, 2012; accepted September 11, 2012; posted September 12, 2012 (Doc. ID 170378); published October 11, 2012

We demonstrate passive generation of optical pulse trains with each pulse having distinct center carrier and spectra using tunable group delay (GD) staircase transfer functions. The GD steps result from opposite and equal magnitude GD slopes from narrowband and wideband tunable optical dispersion compensators. We use this technique to split the spectrum of a femtosecond pulse to a pulse burst with precise control of pulse time separation.

OCIS codes: 130.2035, 320.5540.

Chirped pulses are the basis for many signal processing systems, such as photonically assisted analog-to-digital conversion (ADC), enabling rapid sampling of an optical signal with the benefit of color component separation, effectively slowing down the optoelectronic detection speed by the wavelength parallelism factor [1]. Chirped pulses are also useful in converting an ultrafast optical signal by way of parametric wave mixing to a frequency mapped signal, performing temporal imaging and serial-to-parallel conversion [2,3]. Some applications preferably require a discrete colored pulse train such as photonic ADC [4,5], as opposed to a continuous carrier sweep. This can be achieved by a photonic spectral processor (PSP) [6,7], which uses a phase spatial light modulator (SLM), which can be used for applying different phase slopes to different spectral channels. However, adding phase slopes to the spectrum using the PSP approach results in losses which increase with the associated time delay [6], and the use of an active SLM component to generate the desired group delay (GD) function is expensive.

Our proposed method for generating a WDM pulse burst with passive components only is based on realizing a transfer function consisting of a GD staircase, by cascading a continuous chromatic dispersive (CD) element with a narrow free spectral range (FSR) WDM dispersion compensator of opposite GD slope, as shown in Fig. 1 (first reported in [8]). Here we report improved experimental results and introduce measurements of the high-speed temporal response. Continuous (or WB) CD is characterized by fixed GD slope versus wavelength, with the slope defining the CD (in ps/nm units). Finite (or NB) FSR CD has sawtooth GD versus wavelength pattern. Their cascade, when the slopes are equal in magnitude and opposite in sign, create GD stairs where the step height, ΔGD, is given by

$$\Delta\mathrm{GD[ps]} = \mathrm{CD[ps/nm]} \cdot \Delta\lambda\mathrm{[nm]}, \qquad (1)$$

where $\Delta\lambda$ is the FSR. If an ultrashort pulse traverses the staircase transfer function, it will be filtered to a burst of subpulses, each being transform-limited, delayed in time, and of contiguous spectral extent. Furthermore, if both the WB and NB CD are made tunable, then the pulse burst is also rate adaptable, with the rate being the inverse of ΔGD.

In this Letter, we demonstrate the tuning ability of the GD staircase with customized tunable optical dispersion compensator (TODC) processors, and produce for the first time WDM adaptive-rate optical pulse bursts by filtering an incident ultrashort pulse in the telecom-band.

We previously demonstrated a NB TODC, realized by translation of an arrayed waveguide grating (AWG) whose output radiates to free space [Fig. 2(a)] [9]. The AWG defines the FSR, according to the incremental length change of the waveguide arms, FSR $= \lambda/m$, where m is the AWG diffraction order and λ is the wavelength inside the waveguide. The angularly dispersed light at the output facet, $d\theta/d\lambda$, is converted to spatial dispersion with a Fourier lens, and additional phase curvature due to an offset, Δz, between the AWG output from the lens front focal plane is converted to CD according to [9,10]

$$\mathrm{CD} = \frac{2\lambda_0}{c_0}\left(\frac{d\theta}{d\lambda}\right)^2 \Delta z. \qquad (2)$$

Hence, a desired CD is set by translation only, and a periodic GD sawtooth pattern is generated. We applied the same technique toward realization of a WB TODC. WB support was achieved by replacing the AWG with a bulk grating [Fig. 2(b)]. Since the bulk grating's angular dispersion is much smaller, and to eliminate

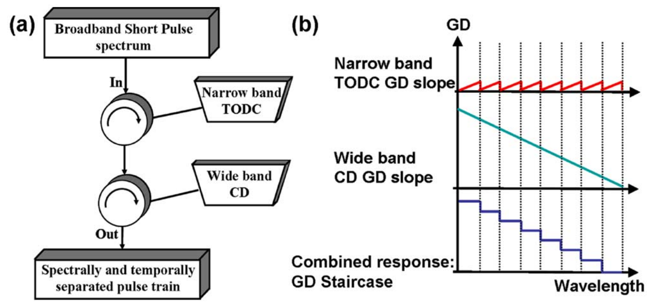

Fig. 1. (Color online) Layout of the tunable GD system: (a) System arrangement. (b) NB TODC and WB TODC GD slopes and the resultant GD staircase.

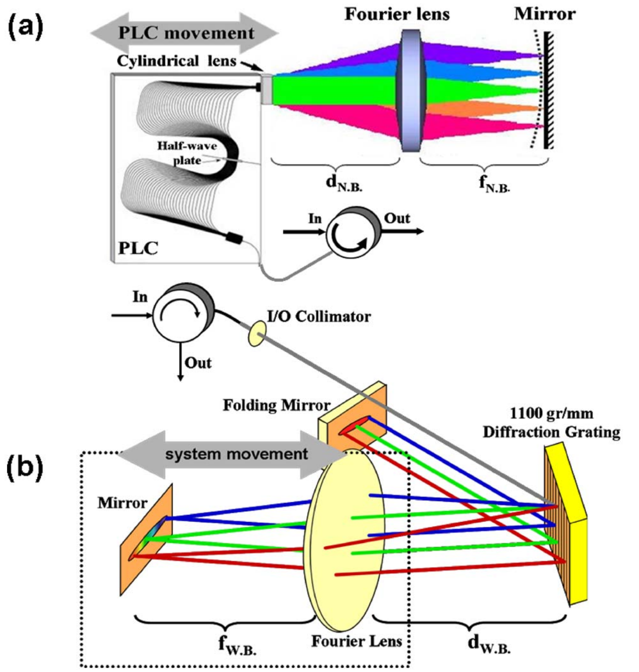

Fig. 2. (Color online) (a) NB TODC based on high resolution dispersion from an AWG. Changing the grating-lens distance, $d_{N.B}$, results in quadratic spectral phase or GD slope. (b) WB TODC of similar nature with a bulk diffraction grating. The system is double-passed to maximize the CD capacity and avoid spectral narrowing.

spatiotemporal coupling effects, the system is double-passed (by reflecting off a folding mirror and experiencing four grating diffraction events). The NB TODC has a 100 GHz (0.81 nm) FSR, yielding $m \cong 1900$, with output waveguides at pitch of $p = 16$ μm, leading to angular dispersion of $d\theta/d\lambda = 120$ mrad/nm. In contrast, the WB TODC with a 1100 gr/mm grating mounted near Littrow has $d\theta/d\lambda = 5.7$ mrad/nm. Due to the CD dependence on angular dispersion squared [Eq. (2)], the WB TODC has to translate 220 times as much for an identical CD setting (including factor 2 due to double-passing WB TODC).

The elements of the NB TODC and the WB TODC were assembled on separate compact optical benches. The tunable WB CD used a Fourier lens with focal length of 500 mm, to accommodate for large grating displacements from the front focal plane. The overall optical length of the setup is approximately 4 m, since the light travels along the system four times. A circulator was used to separate the input and output light to each subsystem. The TODCs were characterized separately and jointly using a LUNA OVA (Optical Vector Analyzer). The insertion loss (IL) of each subsystem is less than 10 dB, thus the overall IL was ~18.5 dB [Fig. 3(d)]. Reduction of IL and system size can be implemented by using more efficient passive elements, such as single-mode fiber (SMF) for the WB CD generation and etalon [11] or sampled fiber bragg grating [12] based TODC for the NB response.

The tuninig ability and accuracy of the system is shown in Figs. 3 and 4. The dispersion of the WB and the NB systems was set to ±18.75 (blue) and ±50 ps/nm (green). The combination of the NB TODC GD slopes [Fig. 3(a)] with the WB TODC slopes [Fig. 3(b)] resulted

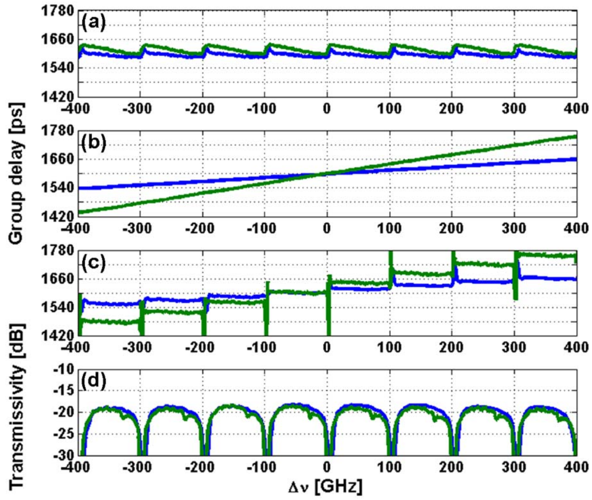

Fig. 3. (Color online) Plots of measured GD with slopes of ±18.75 ps/nm (blue) and ±50 ps/nm (green). (a) NB TODC. (b) WB TODC. (c) The combined TODC with the GD staircase pattern, with step heights of 15 ps (blue) and 40 ps (green). (d) IL of the combined TODC in both cases.

in the desired GD staircase pattern [Fig. 3(c)]. Since the NB FSR is 0.81 nm, the GD staircase step height is ~15 ps (40 ps) for GD slopes of ±18.75 ps/nm (±50 ps/nm), resulting 66.6 GHz (25 GHz) pulse bursts.

The two GD staircase patterns were used to filter ultrashort (100 fs) pulses at $\lambda_0 = 1.55$ μm from a mode-locked laser (MLL). We used Spectra Physics Tsunami + Opal MLL, with a pulse rate of 80 MHz and average power of 300 mW. Each filtered ultrashort pulse generates a finite duration WDM pulse burst. A continuous WDM pulse sampling sequence can be generated by employing a higher repetition rate MLL. The generated pulse bursts were measured with a high-speed optical sampling scope (HS-OSS) (65 GHz), having interpulse spacings of 15 and 40 ps (Fig. 4). The NB TODC has a spectral filtering bandwidth of ~60 GHz, leading to filtered, transform-limited pulses of ~17 ps duration FWHM. For the 25 GHz pulse burst, this corresponds to a pulse burst duty cycle of 0.33. For both pulse bursts, no loss degradation was observed, and the loss was

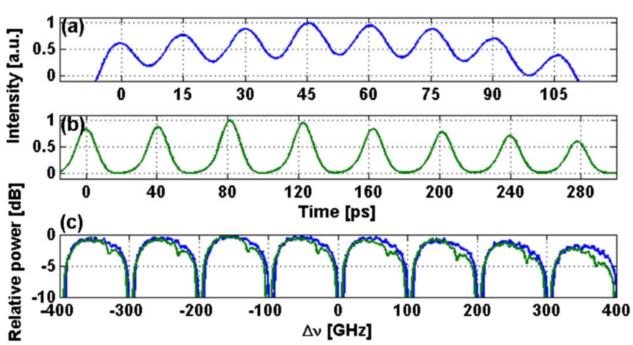

Fig. 4. (Color online) High-speed oscilloscope (HS-OSS) measurements of the WDM pulse bursts that were generated with GD system: (a) 15 ps spaced pulses. (b) 40 ps spaced pulses. (c) OSA measurement of the relative power of the filtered MLL spectrum for both 15 ps (blue) and 40 ps (green) spaced pulses.

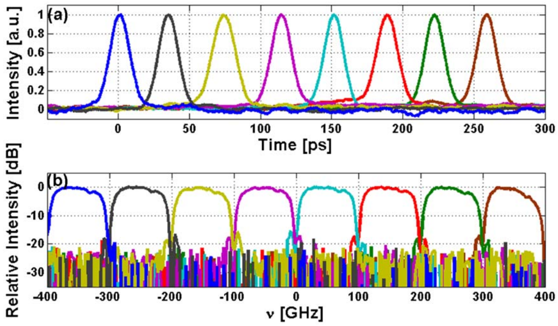

Fig. 5. (Color online) Validation experiment of unique pulse center carrier and spectrum by WDM channel filtering, and subsequent HS-OSS measurements and corresponding OSA measurements, collected and normalized for each filtered pulse separately. (a) Temporal measurements and (b) spectral measurements. The colors in (a) and (b) are matched, showing that each pulse has distinguished spectral content.

relatively uniform along all pulses [Fig. 3(d)]. With a PSP approach [6], where each pulse is independently delayed, there will be delay-dependent losses along the spectrum. To show that the pulse burst is truly wavelength distinguishable, we used a WDM channel filter allowing the transmission of one WDM channel at a time for selecting individual pulses from the pulse burst. While keeping the time frame along the whole measurements, we performed both temporal measurements with the HS-OSS, and spectral measurement using an optical spectrum analyzer (OSA), resulting in a direct correspondence between pulse position and spectrum (Fig. 5).

Since our WB TODC is limited in its dispersion generating range to ~80 ps/nm and in bandwidth to 6.4 nm (or 8 FSR periods), due to the finite grating and lens apertures, we also demonstrated the GD staircase generation concept with a spool of 10 km SMF (Fig. 6). Since the LUNA OVA cannot measure such distances due to its limited coherence length, we used a modulation phase shift method instead, in order to characterize the GD. The SMF spool was measured to have 170 ps/nm GD slope, which was compensated by the NB TODC to give ~136 ps GD difference between adjacent channels [Fig. 6(c)] corresponding to a 7.5 GHz pulse burst with an overall IL of −15 dB. This arrangement was also measured by the HS-OSS [Fig. 6(d)]. The resulting pulse burst contains ~50 pulses having an envelope function following the spectrum of the MLL, with a ~15% duty cycle, and spanning nearly 7 ns.

In summary, we have demonstrated the transfer function of a GD staircase, capable of slicing an ultrashort pulse to a sequence of spectrally nonoverlapping transform-limited pulses using only passive components. The resultant pulse burst rate depends on the applied CD and the FSR of the TODC element, and can be made adaptive when using tunable processors as demonstrated herein. The technique is scalable toward generation of pulse bursts at rates of hundreds of gigahertz, provided the input pulse is sufficiently broadband [13] and as the FSR of the NB TODC is increased to the desired value. The timing accuracy of the technique is determined by higher-order dispersion, i.e., deviation from linearity in the GD slope. This can be ameliorated by dispersion compensation techniques. The resulting pulse burst

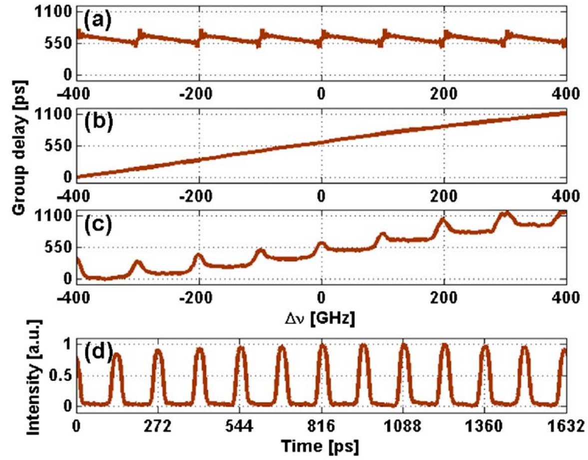

Fig. 6. (Color online) Staircase GD produced by a combination of CD from 10 km SMF and a NB TODC. (a) NB TODC with GD slope of −170 ps/nm. (b) WB TODC with GD slope of 170 ps/nm. (c) The combined setup with the resultant GD staircase pattern, with step height of 136 ps. (d) HS-OSS measurements of the WDM pulse burst.

technique is different from [14], which is not wavelength distinguishable.

The authors would like to thank Civcom for the privilege of using LUNA OVA to carry out GD measurements, U. Levy for loaning of the HS-OSS, and the Ministry of Industry Kamin program for funding.

References

1. Y. Han and B. Jalali, J. Lightwave Technol. **21**, 3085 (2003).
2. M. A. Foster, A. C. Turner, R. Salem, M. Lipson, and A. L. Gaeta, Opt. Express **15**, 12949 (2007).
3. H. C. H. Mulvad, E. Palushani, H. Hu, H. Ji, M. Lillieholm, M. Galili, A. T. Clausen, M. Pu, K. Yvind, J. M. Hvam, P. Jeppesen, and L. K. Oxenløwe, Opt. Express **19**, B825 (2011).
4. A. Yariv and R. G. M. P. Koumans, Electron. Lett. **34**, 2012 (1998).
5. J. Kim, M. J. Park, M. H. Perrott, and F. X. Kärtner, Opt. Express **16**, 16509 (2008).
6. D. Sinefeld, C. R. Doerr, and D. M. Marom, Opt. Express **19**, 14532 (2011).
7. X. Yi, L. Li, T. X. H. Huang, and R. A. Minasian, Opt. Lett. **37**, 608 (2012).
8. D. Sinefeld, Y. Fattal, and D. Marom, in *National Fiber Optic Engineers Conference*, OSA Technical Digest (Optical Society of America, 2012), paper JTh2A.3.
9. D. Sinefeld, S. Ben-Ezra, C. R. Doerr, and D. M. Marom, Opt. Lett. **36**, 1410 (2011).
10. K. Seno, N. Ooba, K. Suzuki, T. Watanabe, K. Watanabe, and S. Mino, IEEE Photon. Technol. Lett. **21**, 1701 (2009).
11. X. Shu, K. Sugden, P. Rhead, J. Mitchell, I. Felmeri, G. Lloyd, K. Byron, Z. Huang, I. Khrushchev, and I. Bennion, IEEE Photon. Technol. Lett. **15**, 1111 (2003).
12. K.-M. Feng, J.-X. Chai, V. Grubsky, D. S. Starodubov, M. I. Hayee, S. Lee, X. Jiang, A. E. Willner, and J. Feinberg, IEEE Photon. Technol. Lett. **11**, 373 (1999).
13. J. M. Dudley, G. Gentry, and S. Coen, Rev. Mod. Phys. **78**, 1135 (2006).
14. D. E. Leaird, S. Shen, A. M. Weiner, A. Sugita, S. Kamei, M. Ishii, and K. Okamoto, IEEE Photon. Technol. Lett. **13**, 221 (2001).

Chapter 3C.

Tunable fiber ring laser with an intracavity high resolution filter employing two-dimensional dispersion and LCoS modulator

David Sinefeld and Dan M. Marom

Published in Optics Letters:

D. Sinefeld and D. M. Marom, "Tunable fiber ring laser with an intracavity high resolution filter employing two-dimensional dispersion and LCoS modulator," Opt. Lett. 37, 1-3 (2012).

Tunable fiber ring laser with an intracavity high resolution filter employing two-dimensional dispersion and LCoS modulator

David Sinefeld* and Dan M. Marom

Applied Physics Department, Hebrew University, Jerusalem 91904, Israel
**Corresponding author: sinefeld@gmail.com*

Received September 15, 2011; revised November 10, 2011; accepted November 10, 2011;
posted November 10, 2011 (Doc. ID 154804); published December 16, 2011

We demonstrate a tunable fiber ring laser employing a two-dimensional dispersion arrangement filter, with the lasing determined by a liquid crystal on silicon (LCoS) spatial light modulator. Lasing wavelengths can be tuned discontinuously across the communication C-band at an addressable resolution of less than 200 MHz. We introduce full characterization of the laser output including phase and amplitude stability and short and long-term bandwidth measurements.

OCIS codes: 060.2330, 060.2320, 140.3510.

Tunable fiber ring lasers have important applications in optical communication systems, fiber sensors, infrared spectroscopy, and optical instrumentation, as they offer easy integration with these all-fiber systems [1–4]. Lasing wavelength tuning is achieved by a filter placed inside the ring cavity, where the tuning mechanism can be based on a Fabry–Perot etalon [5,6], a fiber Bragg grating [7,8], or electro-optic [9], piezo-electric [10], and acousto-optic [11] modulators. A gain element (typically a fiber amplifier) and an output coupler complete the ring cavity (see the inset of Fig. 1). These lasers are favorably characterized by a high side mode suppression ratio (SMSR) and a large tuning range, but their tuning is continuous along the spectrum due to the filter characteristics, which is not acceptable in certain applications such as optical communications. This can be alleviated by extra hardware to prevent laser output during tuning events, impacting cost.

In the last couple of years, tunable fiber lasers based on an intracavity, free-space, adaptive filter employing a spatial light modulator (SLM) and a diffraction grating were introduced [12–13]. This arrangement allows full access to all the spectral components and enables discontinuous lasing wavelength jumps. However, the tuning performances of the reported fiber lasers were limited due to the relatively low resolution and addressability of the filter's diffraction grating and SLM. We recently presented [14] a tunable fiber ring laser employing an extremely high resolution filter utilizing a two-dimensional (2D) dispersion arrangement [15]. With this combination, we have demonstrated a tunable ring laser with a tuning resolution of 200 MHz along 30 nm (the communication C-band). This paper provides further design details and full characterization of our 2D tunable fiber laser.

The layout and concept of the 2D filter arrangement is shown in Fig. 1 and discussed in detail in [15]. Light is angularly dispersed using a 2D optical arrangement from two crossed gratings: a high resolution waveguide grating router (WGR) and a free-space bulk grating. The 2D dispersed light is projected with a Fourier lens onto a liquid crystal on silicon (LCoS), 2D, pixelated, phase-only modulator. The WGR has a free spectral range (FSR) of 100 GHz and a spectral resolution of 3 GHz. The crossed 1200 gr/mm holographic diffraction grating placed after the WGR separates the diffraction orders in the orthogonal direction. The resultant dispersion forms a contiguous series of dispersed 100 GHz channels on the spectral plane (Fig. 2(a)). At this plane, we place the LCoS reflective modulator with 512×512 square pixels of 15 μm pitch (total size of 7.68×7.68 mm^2), capable of prescribing phase delays $\in [0, 2\pi]$. The spatial dispersion in the WGR direction results in 512 columns spanning a 93 GHz wide spectrum. Each column of the modulator addresses a particular center frequency, at 182 MHz shift in center frequency. The spatial dispersion in the bulk grating direction results in an offset of 15 pixels for successive diffraction orders (spaced at 100 GHz). Because of the limited size of our LCoS SLM, only 30 WDM channels spaced at 100 GHz are modulated and reflected back. We set the lasing wavelength by attenuating all wavelengths (by setting a linear phase ramp that reduces the coupling back), except for the particular wavelength that is transmitted, seen as a clear window with no phase tilt applied (see Fig. 2(b)).

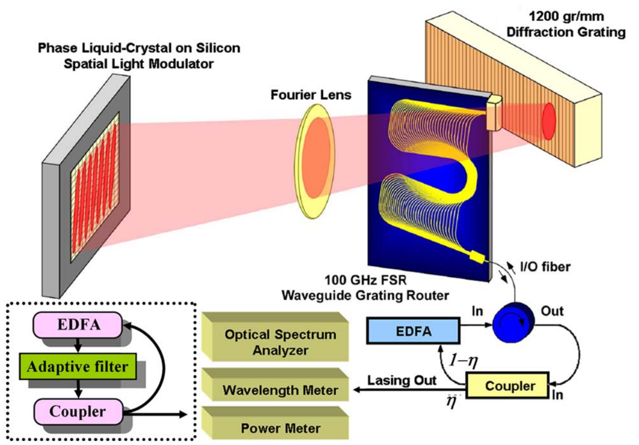

Fig. 1. (Color online) Layout of the ring laser: amplified light goes through crossed gratings (waveguide grating router (WGR) and bulk), which disperse the spectrum across the two-dimensional LCoS array, enabling high resolution access to the spectral components along the communication c-band. Inset: layout of a ring laser based on an adaptive filter and gain module inside the cavity.

0146-9592/12/010001-03$15.00/0

The window spans 18 pixels along the high dispersion axis, matching the optical resolution (setting it smaller only increases the loss). The ring cavity is completed with a circulator (couple in and out of our filter), an erbium doped fiber amplifier (EDFA), and an output coupler. The first lasing experiment used a 90/10 output coupler (10% output) placed after the EDFA, and lasing was observed on an optical spectrum analyzer (OSA). Changing the horizontal position of the window results in jumping from one diffraction order to another, leading to a 100 GHz change in the output wavelength (Fig. 3(a)). Changing the vertical position of the window, along a specific diffraction order, results in fine changes in the output wavelength with a spectral step size of l82 MHz (Fig. 3(b)). We coarsely tune the wavelength by selecting the WGR diffraction order (separated by the bulk grating) and finely tune the wavelength by selecting within the WGR diffraction order. The insertion loss of the 2D filter arrangement is approximately 14 dB (mostly due to coupling from the planar light circuit (PLC)); hence we use an EDFA amplifier with 22 dB gain and 18 dBm saturation power. This leads to a gain saturated output power level of 8 dBm (using the 10% tap, i.e., 10 dB less that the EDFA saturation power), constant along the output spectrum (Fig. 3). The SMSR is greater than 50 dB.

We experimented with different output coupler values and positions, using three available couplers with splitting values of 1/99, 10/90, and 50/50, providing five output coupling values: 1%, 10%, 50%, 90%, and 99%. We also swapped the position of the EDFA and the tap splitter. In each of the above arrangements, we measured both the output power and the SMSR (see Fig. 4). The highest output power was measured with the 50% output tap with the EDFA before the tap splitter, resulting in 15 dBm output power (3 dB less than the EDFA saturation level due to the 50/50 output coupler). For 1% output, we measured output of −2 dBm, e.g., 20 dB less than the saturation level. Those three results imply that the EDFA reached its saturation level. However, when we used an output coupler of 90% and 99%, the losses of the ring cavity were too high, the EDFA was unsaturated, and the laser output power was lower. In the case of EDFA after

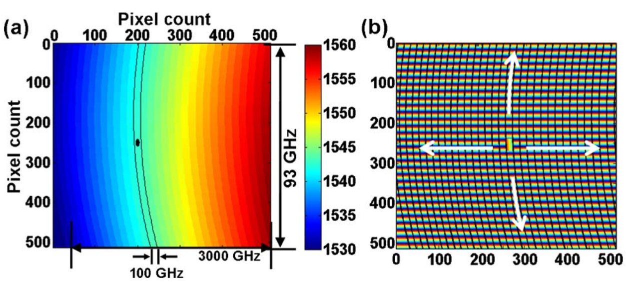

Fig. 2. (Color online) (a) 2D spatial wavelength dispersion on the SLM. The WGR provides high resolution on the narrow FSR. The bulk grating separates the WGR diffraction orders. The black lines mark the borders of a specific WGR diffraction order, while the black ellipse denotes the spot size for a specific wavelength. (b) Exemplary applied LCoS phase, attenuating all spectral components except the lasing line, which appears as an open window. Scanning the lasing window along the white arrows selects the lasing frequency (horizontal translation selects WGR diffraction order; vertical translation selects along the fast axis or within the diffraction order).

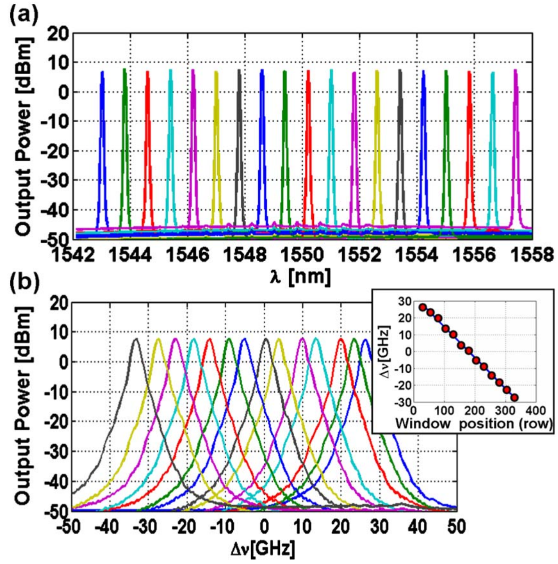

Fig. 3. (Color online) Output of the fiber laser. (a) Laser lines from different diffraction orders of the WGR. (b) Laser lines from different locations of the same WGR diffraction order. Inset: linear fit of the center frequency verses mask opened window position, resulting in a slope of 182 MHz per SLM row. The slight deviation from linearity is caused by the uncertainty in the lasing line position within the 3 GHz spectral window.

the coupler, we have the same curve shape but with much lower output power due to the filter's 14 dB attenuation. The SMSR depends on the EDFA location too, where in the case of EDFA after coupler, better results are obtained (except for the extreme cases of the 1/99 coupler, in which the output power is lower than −20 dBm and the SMSR is therefore lower). The best performance was obtained when the EDFA was placed before a 10% coupler output resulting in 8 dBm output power and an SMSR of 58 dB.

The spectral plots of the laser output, as shown in Fig. 3(b), do not reflect the actual laser line width, but rather reflect the OSA resolution limit. To properly measure the laser line width, we mixed our fiber laser output with that of a reference 100 KHz line width external cavity laser. The reference laser was set to a slightly different wavelength, resulting in an intermediate frequency beating between the two lasers. This was detected with a high speed photodetector connected to a high speed realtime scope (Fig. 5(a)). In adddition, a slow detector was connected directly to the fiber laser to track its output

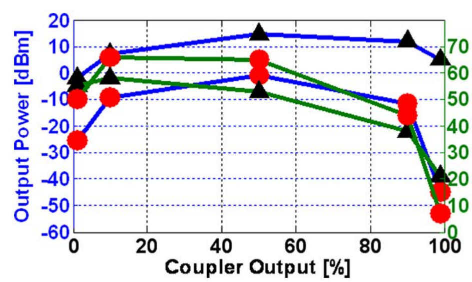

Fig. 4. (Color online) Output power (blue line) and SMSR (green line) of the fiber laser versus output tap value, measured in various combinations: (a) EDFA before the coupler (results marked with black triangles); (b) EDFA after the coupler (results marked with red circles).

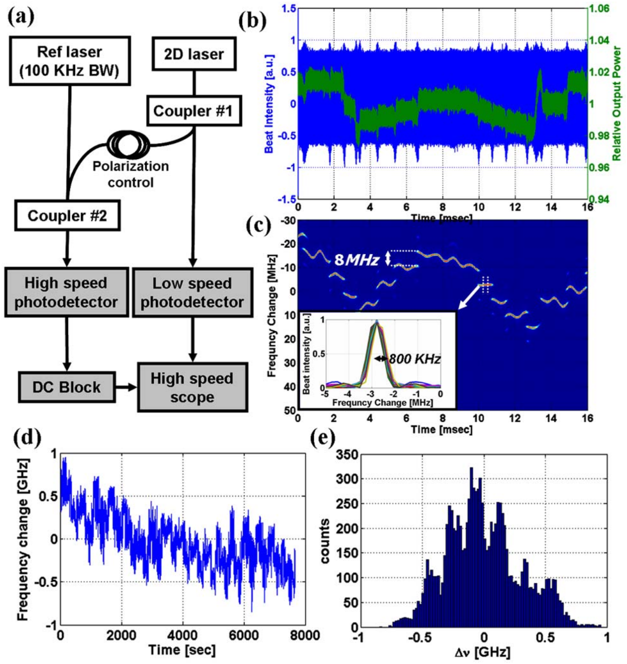

Fig. 5. (Color online) Measuring laser line width. (a) Setup for line width measurement using a high speed detector to measure the beating between a reference laser and the 2D laser, while a slow detector measures the direct output power of the 2D laser. (b) Registered powers of the beat frequency (blue) and the output power (green), with correlation between intensity spikes and mode hops. (c) Spectrogram of the interferometric measurement showing mode hops occurring every 1-3 ms. Frequency hop is approximately 8 MHz. Inset: cross section of the spectrogram showing instantaneous laser line width of 800 KHz. (d) Results of 10 000 measurements of laser relative lasing frequency taken along 8000 seconds. The central frequency changes are due to mode hoping and thermal drift. (e) Histogram of the above 10 000 measurements showing the long-term frequency excursion of the laser output.

power. The detected power results are shown in Fig. 5(b). Changes in the relative frequency between the 2D and the reference laser are shown as "spikes" in the beat intensity, and they correlate with power changes with a transient duration of a few microseconds. A spectrogram of the beat intensity measurement (Fig. 5(c)) shows that every few milliseconds a mode hopping event occurs inside the ring laser, with a lasing frequency hop of approximately 8 MHz. This correlates to a fiber cavity length of 38 meters, which is reasonable due to the EDFA fiber length. A vertical cross section of the spectrogram (shown in the inset of Fig. 5(c)) shows the instantaneous laser line width is approximately 800 KHz. This narrow line width can be utilized in self-homodyne sensing applications. However, the rapid mode hopping likely precludes the laser's use in other coherent reception applications, and in application requiring high intensity stability. A histogram of 10 000 relative frequency measurements taken with an ~1 second interval in an uncontrolled environment gives the long duration lasing wavelength stability bandwidth of 1.3 GHz (Fig. 5(d)–(e)). This bandwidth is smaller than the 3 GHz filter window, since the lasing preferentially occurs close to the filter peak, where losses are minimal. In order to examine the output power stability of the laser, an intensity measurement was performed over 800 seconds

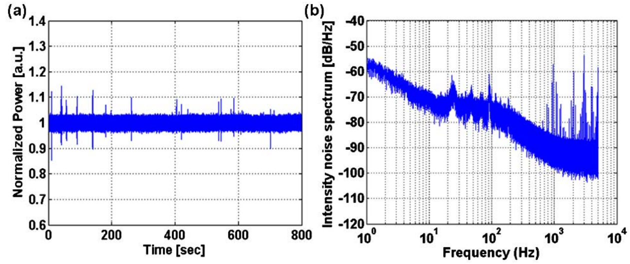

Fig. 6. (Color online) Laser output power measurements: (a) Intensity measurement versus time taken over 800 seconds sampled at 10 KHz. (b) RIN measurement results.

(Fig. 6(a)), resulting in a small change in output power along the measurement. The power spectrum of this measurement, shown in Fig. 6(b), expresses the relative intensity noise (RIN) of the laser output. The spikes shown in the RIN plot around 1 KHz are attributed to the mode hopping rate, which is accompanied by intensity changes every few milliseconds.

In summary, we demonstrated the functionality of a tunable ring laser based on a high resolution, 2D dispersive arrangement and an EDFA gain amplifier. We operated the laser with various coupler ratios and EDFA positions and found a configuration that gave maximal output power of 15 dBm and SMSR greater than 50 dB with a tuning ability of less than 200 MHz along the *C*-band. We have measured the spectral bandwidth of the laser, resulting in a long duration bandwidth of 1.3 GHz and an instantaneous bandwidth of 800 KHz and output power stability of a few percent.

References

1. L. Paraschis, O. Gerstel, and R. Ramaswami, in *Proceedings of Optical Fiber Communication Conference* (Optical Society of America, 2004), Paper MF105.
2. N. J. C. Libatique and R. K. Jain, IEEE Photon. Technol. Lett. **13**, 1283 (2001).
3. K. T. V. Grattan and B. T. Meggitt, *Optical Fiber Sensor Technology* (Chapman & Hall, 1995).
4. H. Y. Ryu, W. K. Lee, H. S. Moon, and H. S. Suh, Opt. Commun. **275**, 379 (2007).
5. N. Park, J. W. Dawson, K. J. Vahala, and C. Miller, Appl. Phys. Lett. **59**, 2369 (1991).
6. S. Yamashita and M. Nishihara, IEEE J. Sel. Top. Quantum Electron. **7**, 41 (2001).
7. Y. W. Song, S. A. Havstad, D. Starodubov, Y. Xie, A. E. Willner, and J. Feinberg, IEEE Photon. Technol. Lett. **13**, 1167 (2001).
8. X. He, X. Fang, C. Liao, D. N. Wang, and J. Sun, Opt. Express **17**, 21773 (2009).
9. C. S. Kim, F. N. Farokhrooz, and J. U. Kang, Opt. Lett. **29**, 1677 (2004).
10. A. P. Luo, Z. C. Luo, and W. C. Xu, Opt. Lett. **34**, 2135 (2009).
11. D. A. Smith, M. W. Maeda, J. J. Johnson, J. S. Patel, M. A. Saifi, and A. Von Lehman, Opt. Lett.**16**, 387 (1991).
12. F. Xiao, K. Alameh, and Y. T. Lee, Opt. Express **17**, 23123 (2009).
13. F. Xiao, K. Alameh, and Y. T. Lee, IEEE Photon. Technol. Lett. **23**, 182 (2011).
14. D. Sinefeld and D. M. Marom, in *Proceedings of the Conference on Lasers and Electro-Optics* (Optical Society of America, 2011), Paper CTuI5.
15. D. Sinefeld, C. R. Doerr, and D. M. Marom, Opt. Express **19**, 14532 (2011).

Chapter 4. Summary and Future Directions

This thesis presented the research of photonic spectral processing for high rate optical signals, with various applications in the field of optical communication. The main idea behind this work is to modify the coarse pulse shaping approach to better resolve a signal's spectral contents and manipulate its amplitude and phase response for controlling and reshaping the signal.. For this purpose a high resolution spectral processor is needed, with the ability to resolve fine spectral features. Such resolution cannot be easily achieved with regular bulk diffraction gratings; instead we employed custom arrayed waveguide gratings (AWG) which are engineered to have extremely high dispersion. Using this approach, we introduced an elegant way for spectrally manipulating high rate communication signals with a phase-only spatial light modulator (SLM) , targeting the application of wavelength division multiplexing (WDM) signals with channel separation of 100 GHz.

We combined the AWG, which was manufactured according to our specifications, together with free space optics and a liquid crystal on silicon SLM in order to construct a controllable device which can apply spectral manipulations for both phase and amplitude with extremely high spectral resolution. This device, which we named a photonic spectral processor (PSP), can serve for signal shaping, retiming and impairment mitigation.

The results presented in this thesis were divided into two groups. The first group addressing the development of three PSP variants. The main developments results are:

- **High resolution (~3GHz), state-of-the-art colorless PSP**. With this device we demonstrated dispersion compensation abilities and sharp filtering for 100 GHz bandwidth. This system is based on the basic combination of an AWG, Fourier optics and SLM, and its colorless property imply that the free spectral range (FSR) of the system is matched to the 100 GHZ spacing of WDM channel plan.

- **Compact passive PSP serving as a tunable optical dispersion compensator (TODC)**. With this simple TODC version which was based solely on a longitudinal movement of an AWG, we managed to compensate for dispersion of 40 Km fiber length for a 42.5 GHz DPSK transmission format.
- **Full c-band, high resolution PSP based on two-dimensional optical dispersion arrangement.** The system combines the AWG with a free space diffraction grating. Using this 2D arrangement, the same high resolution as in the colorless PSP was demonstrated, with the ability to control each WDM channel separately along the whole c-band.

The second group contains articles which demonstrate several applications of spectral processing for communication, analog-to-digital conversion and as a tunable fiber laser device. The main results of those researches are:

- **Colorless PSP for Nyquist-WDM filtering:** The Nyquist-WDM signaling concept allows to place two signals at the density limit, when the channel separation matches the baud rate. Here we create this all-optically, with a sharp shaping filter. We devised a system solution that requires two such filters working separately on the odd and even channels. The rectangle spectral response was measured in the temporal domain using a femtosecond laser resulting in an exact match to the desired *sinc* function, showing that the pulse is indeed transform limited.
- **Wideband and periodic TODC combination for group delay staircase:** The result of combining the two opposite TODC devices is a group delay staircase pattern which serves for WDM pulse stream generation from a mode locked laser femtosecond source. We showed that by using this arrangement we can tune the rate of the WDM pulse stream, with precise control of pulse time separation.
- **High resolution tunable fiber ring laser using the two dimensional PSP:** We placed our tunable filter with a fiber ring laser with an EDFA gain section. We demonstrated maximal output power of 15 dBm and SMSR greater than 50 dB with a spectral tuning ability of less than 200 MHz along the C-band, and introduced full characterization of the laser output including

phase and amplitude stability and short and long-term bandwidth measurements.

In summary, high resolution photonic spectral processing is a core technology which itself can be implemented in optical communication systems for spectral filtering or for signal impairment mitigation. Moreover, as the spectral resolution and bandwidth of such devices increase, they can serve as a key component for several new applications such as very sharp spectral filtering, OFDM signal shaping, photonically assisted ADC and arbitrary waveform generation. Pushing this technology even further, towards sub GHz spectral processing resolution, is therefore a promising lead for establishing this approach as an important method for controlling fast optical signals. Since the optical resolution of the PSP is limited by the dispersive element which controls the spectral performance (resolution and bandwidth) of the system, the key to achieve higher resolution is dependent on the performance of the AWG which is being used. The next generation of spectral processors will therefore be realized with an AWG with larger bandwidth (~200 GHZ) and sub GHz resolution. Fabrication of such an AWG brings on many challenges, since the length difference between adjacent waveguides becomes larger, and the PLC performance is degraded due to fabrication phase errors. These fabrication errors can be overcome by an ultra violet (UV) trimming method which changes the refractive index of each waveguide permanently in order to reach minimal phase errors, in the cost of complicating the PLC production process. In this way, a high resolution PSP could be developed, resulting in an important tool in the field of research of fast optical signals, and as one of the building blocks of the modern long-haul, cutting edge, optical communication systems in the next following decades.

Bibliography

[1] G. P. Agrawal, *Fiber Optic Communication systems* , (John Wiley, 1997).

[2] A. M. Weiner, Ultrafast Optics (Wiley, 2009).

[3] E. P. Ippen and C. V Shank, in *Ultrashort Light Pulses-Picosecond Techniques and Applications*, S. L. Shapiro, ed. (Springer-Verlag, Berlin, 1977), p. 83.

[4] R. Trebino and D. Kane, “Using phase retrieval to measure the intensity and phase of ultrashort pulses: frequency-resolved optical gating,” J. Opt. Soc. Am. A 10, 1101-1111 (1993).

[5] C. Iaconis and I. A. Walmsley, “Spectral phase interferometry for direct electric-field reconstruction of ultrashort pulses,” Opt. Lett. 23, 792 (1998).

[6] C. Schmidt-Langhorst, R. Ludwig, H. Hu, and C. Schubert, "Single-Channel 1-Tb/s Transmission over 480 km DMF for Future Terabit Ethernet Systems," in Proc. OFC, paper OTuN5 (2009).

[7] Y. Ma, Q. Yang, Y. Tang, S. Chen, and W. Shieh, "1-Tb/s single-channel coherent optical OFDM transmission over 600-km SSMF fiber with subwavelength bandwidth access," Opt. Express 17, 9421-9427 (2009).

[8] Y. Huang, D. Qian, F. Yaman, T. Wang, E. Mateo, T. Inoue, Y. Inada, Y. Toyota, T. Ogata, M. Sato, Y. Aono, and T. Tajima, "Real-Time 400G Superchannel Transmission using 100-GbE based 37.5-GHz Spaced Subcarriers with Optical Nyquist Shaping over 3,600-km DMF link," in Proc. OFC, paper NW4E.1 (2013).

[9] I. Morita and W. Peng, “High capacity WDM transmission using terabit super-channels,” in Proc. ECOC, paper Th2.C.3 (2012).

[10] R. Dischler, F. Buchali, A. Klekamp, W. Idler, E. Lach,A. Schippel, M. Schneiders, S. Vorbeck, R. Braun, “Terabit Transmission of High Capacity Multiband OFDM Superchannels on Field Deployed Single Mode Fiber," in Proc. ECOC, Paper Tu3C.6 (2010).

[11] M. Haurylau, G. Chen, H. Chen, J. Zhang, N.A. Nelson, D. H. Albonesi, E. G. Friedman, and P. M. Fauchet, “On-chip optical interconnect roadmap: challenges and critical directions,” IEEE J. Sel. Top. Quantum Electron. 12, 1699-1705 (2006).

[12] A. M. Weiner, D. E. Leaird, J. S. Patel, and J. R. Wullert, "Programmable Femtosecond Pulse Shaping by Use of a Multielement Liquid-Crystal Phase Modulator," Opt. Lett. 15, 326-328 (1990).

[13] D. Meshulach, D. Yelin, Y. Silberberg, ”Adaptive real-time femtosecond pulse shaping,” J. Opt. Soc. Am. B 15, 1615-1619 (1998).

[14] A. M. Weiner, ”Femtosecond pulse shaping using spatial light modulators,” Rev. Sci. Instrum. 71 1929-1960 (2000).

[15] M.A.F. Roelens et al, “Dispersion trimming in a reconfigurable wavelength selective switch,” IEEE J. Lightwave Technol 26, 73-78 (2008).

[16] D.T. Neilson et al, “MEMS-based channelized dispersion compensator with flat passbands,” IEEE J. Lightwave Technol. 22, 101-105 (2004).

[17] D. T. Neilson, et al., “Channel equalization and blocking filter utilizing microelectromechanical mirrors,” IEEE J. Select. Top. Quant. Electron. vol. 10, no. 3, pp. 563- 569, May-June 2004.

[18] S. Sohma, et al., “Flexible Chromatic Dispersion Compensation Over Entire L-Band for Over 40-Gb/s WDM Transparent Networks Using Multichannel Tunable Optical Dispersion Compensator,” IEEE Photon. Technol. Lett. vol. 21, no. 17, pp. 1271-1273, Sept, 2009.

[19] M. Shirasaki, “Chromatic dispersion compensator using virtually imaged phased array,” IEEE Photon. Technol. Lett. vol. 9, no. 12, pp. 1598-1600, Dec 1997.

[20] K. Seno, K. Suzuki, N. Ooba, K. Watanabe, M. Ishii, H. Ono, and S. Mino, "Demonstration of channelized tunable optical dispersion compensator based on arrayed-waveguide grating and liquid crystal on silicon," Opt. Express 18, 18565-18579 (2010)

[21] C. R. Doerr, R. Blum, L. L. Buhl, M. A. Cappuzzo, E. Y. Chen, A. Wong-Foy, L. T. Gomez, and H. Bulthuis, “Colorless tunable optical dispersion compensator based on a silica arrayed-waveguide grating and a polymer thermooptic lens,” IEEE Photon. Technol. Lett. 18(11), 1222-1224 (2006).

[22] D. M. Marom, C. R. Doerr, M. A. Cappuzzo, E. Y. Chen, A. Wong-Foy, L. T. Gomez, and S. Chandrasekhar, “Compact colorless tunable dispersion compensator with 1000-ps/nm tuning range for 40-Gb/s data rates,” J. Lightwave Technol. 24(1), 237–241 (2006).

[23] K. Suzuki, N. Ooba, M. Ishii, K. Seno, T. Shibata, and S. Mino, “40-Wavelength Channelized Tunable Optical Dispersion Compensator with Increased Bandwidth Consisting of Arrayed Waveguide Gratings and Liquid Crystal on Silicon,” in Proc. OFC, paper OThB3 (2009).

[24] K. Seno, N. Ooba, K. Suzuki, T. Watanabe, K. Watanabe, and S. Mino, "Tunable Optical Dispersion Compensator Consisting of Simple Optics With Arrayed Waveguide Grating and Flat Mirror," IEEE Photon. Technol. Lett. 21, 1701-1703 (2009).

[25] M. Smit, C. van Dam, “Phasar-based WDM-devices: principles, design and applications” IEEE J. Sel. Top. Quantum Electron. 2, 236-250 (1996).

[26] H. Takahashi, S. Suzuki, K. Kato, and I. Nishi, “Arrayed-waveguide grating for wavelength division multi/demultiplexer with nanometer resolution,” Electron. Lett. 26, 87-88 (1990).

[27] K. Okamoto, *Foundamentals of optical waveguides* (Elsevier, 2006).

[28] T. Kamalakis, T. Sphicopoulos, and D. Syvridis, “An estimation of performance degradation due to fabrication errors inAWGs,” J. Lightw. Technol., vol. 20, no. 9, pp. 1779–1787, Sep. 2002.

[29] D. A. Zauner, J. Hubner, K. J. Malone, and M. Kristensen, "UV trimming of arrayed-waveguide grating wavelength division demultiplexers," Electron. Lett. 34, 780-781 (1998).

[30] D. Sinefeld, N. Goldshtein, R. Zektzer, N. Gorbatov, M. Tur, and D. M. Marom, "Output Radiating Arrayed Waveguide Grating: Characterization of Phase Errors and UV Trimming," in Proc. Advanced Photonics Congress, paper JTu5A.55 (2012).

[31] J. Dunayevsky, D. Sinefeld, and D. Marom, "Adaptive Spectral Phase and Amplitude Modulation Employing an Optimized MEMS Spatial Light Modulator," in Proc. OFC, paper OM2J.5 (2012).

[32] A. Boskovic, M. Sharma, N. Antoniades, M. Lee “Broadcast and Select OADM nodes Application and Performance Trade-offs”, in Proc. OFC, paper TuX2 (2002).

[33] C. Soutar and K. H. Lu, "Determination of the physical properties of an arbitrary twisted-nematic liquid crystal cell" Opt. Eng. 33 2704–12 (1994).

[34] A. Yariv, and P. Yeh, *Photonics: Optical Electronics in Modern Communications* (Oxford University Press, New York, NY, 2006), 6th ed.

[35] D. Sinefeld and D. M. Marom, "Insertion Loss and Crosstalk Analysis of a Fiber Switch Based on a Pixelized Phase Modulator," J. Lightwave Technol. 29, 69-77 (2011).

[36] X. Wang, B. Wang, P. J. Bos, J. E. Anderson, J. J. Pouch, and F. A. Miranda, “Finite-difference time-domain simulation of a liquid-crystal optical phased array,” J. Opt. Soc. Am. A 22, 346-354, (2005).

[37] K. H. Fan-Chiang, S. T. Wu and S.H. Chen, "Fringing-field effects on high-resolution liquid crystal microdisplays," Display Technology, Journal of, 1, 304-313, (2005).

[38] D. Sinefeld and D. M. Marom, "Spectral processor implemented with hybrid free-space and guided-wave optics and active LCoS modulator," Electrical and Electronics Engineers in Israel IEEE 25th Convention of , 380-383 (2008).

[39] D. Sinefeld, S. Ben-Ezra, and D. M. Marom, "Adaptive Spectral Filtering for Nyquist-WDM Generation with an LCoS-based Photonic Spectral Processor," in Proc. OFC, paper JW2A.30 (2013).

[40] D. Sinefeld and D. M. Marom, “Colorless photonic spectral processor using hybrid guided-wave/free-space optics arrangement and LCoS modulator,” in Proc. OFC, Paper OThB4 (2009).

[41] D. Sinefeld and D. M. Marom, “Hybrid guided-wave/free-space optics photonic spectral processor based on LCoS phase only modulator,” IEEE Photon. Technol. Lett. 22, 510–512 (2010).

[42] J. Leuthold, D. Marom, S. Cabot, J. Jaques, R. Ryf, and C. Giles, "All-optical wavelength conversion using a pulse reformatting optical filter," J. Lightwave Technol. 22(1), 186-192 (2004).

[43] S. Sygletos, R. Bonk, T. Vallaitis, A. Marculescu, P. Vorreau, J. Li, R. Brenot, F. Lelarge, G.-H. Duan, W. Freude, and J. Leuthold, "Filter assisted wavelength conversion with quantum-dot SOAs," J. Lightwave Technol. 28(6), 882–897 (2010).

[44] D. Hillerkuss, M. Winter, M. Teschke, A. Marculescu, J. Li, G. Sigurdsson, K. Worms, S. Ben Ezra, N. Narkiss, W. Freude, and J. Leuthold, "Simple all-optical FFT scheme enabling Tbit/s real-time signal processing," Opt. Express 18, 9324-9340 (2010)

[45] T. K. Chan, J. Karp, R. Jiang, N. Alic, S. Radic, C. F. Marki, J. E. Ford, “1092 channel 2-D array demultiplexer for ultralarge data bandwidth,” J. Lightwave Technol. 25, 719-725, (2007).

[46] V. R. Supradeepa, C. B. Huang, D. E. Leaird, and A. M. Weiner, “Femtosecond pulse shaping in two dimensions: towards higher complexity optical waveforms,” Opt. Express 16(16), 11878–11887 (2008).

[47] D. Sinefeld, C.R. Doerr, and D. M. Marom, “Photonic spectral processor employing two-dimensional WDM channel separation and a phase LCoS modulator,” in Proc. OFC, paper OMP5 (2010).

[48] D. Sinefeld, C.R. Doerr, and D. M. Marom, “A photonic spectral processor employing two-dimensional WDM channel separation and a phase LCoS modulator,” Opt. Express 19, 14532-14541 (2011).

[49] D. Sinefeld and D. M. Marom, "High Resolution Tunable Fiber Laser Employing Two-Dimensional Dispersion and a Phase LCoS Modulator," in Proc. CLEO, paper CTuI5 (2011).

[50] S. Ryu, Y. Horiuchi and K. Mochizuki, “Novel chromatic dispersion measurement method over continuous gigahertz tuning range”, J. Lightwave Technol. 7, pp. 1177-1180, 1989.

[51] T. Niemi, G. Genty and H. Ludvigsen, ”Group-delay measurements using the phase-shift method: improvement on the accuracy,” in Proc. ECOC paper Th.M.1.5 (2001).

[52] R. Fortenberry, W. V. Sorin and P. Hernday, ”Improvement of group delay measurement accuracy using a two-frequency modulation phase-shift method,” IEEE Photon. Technol. Lett. 15, pp. 736-738, 2003.

[53] Y. Palti and D. M. Marom, "Spectral Amplitude and Phase Optical Device Characterization Apparatus," in: The 12th Meeting on Optical Engineering and Science in Israel, OASIS, (2009).

[54] LUNA technologies, Optical Vector Analyzer, User guide, ch.8

[55] D. K. Gifford, B. J. Soller, M. S. Wolfe, and M. E. Froggatt, "Optical vector network analyzer for single-scan measurements of loss, group delay, and polarization mode dispersion," Appl. Opt. 44, 7282-7286 (2005).

[56] B. L. Heffner, “Deterministic, analytically complete measurement of polarization-dependent transmission though optical devices,” IEEE Photon. Technol. Lett. 4, 451–454 (1992).

[57] B. L. Heffner, “Automated measurement of polarization mode dispersion using Jones matrix eigenanalysis,” IEEE Photon. Technol. Lett. 4, 1066–1069 (1992).

[58] R. C. Jones, “A new calculus for the treatment of optical systems VI. Experimental determination of the matrix,” J. Opt. Soc. Am. 37, 110–112 (1947).

[59] D. Sinefeld, D. Shayovitz, O. Golani, and D. M. Marom, "Adaptive Rate and Bandwidth WDM Optical Sampling Pulse Streams with LCoS-based Photonic Spectral Processor," in Proc. OFC, paper OTu3C.2 (2013).

[60] D. Sinefeld, S. Ben-Ezra, C. R. Doerr, and D. M. Marom, "All-channel tunable optical dispersion compensator based on linear translation of a waveguide grating router," Opt. Lett. 36(8), 1410-1412 (2011).

[61] J. W. Goodman, *Introduction to Fourier optics*, 3rd Ed., (Roberts and Company Publishers, 2005).

[62] D. T. Neilson, R. Ryf, F. Pardo, V. A. Aksyuk, M. E. Simon, D. O. Lopez, D. M. Marom, and S. Chandrasekhar, “MEMS-based channelized dispersion compensator with flat passbands,” J. Lightw. Technol. 22, 101–105 (2004).

[63] T. Ono, Y. Yano, K. Fukuchi, T. Ito, H. Yamazaki, M. Yamaguchi, and K. Emura, “Characteristics of optical duobinary signals in terabit/s capacity, high-spectral efficiency WDM systems,” J. Lightwave Technol. 16, 788-797 (1998).

[64] D. Boivin, M. Hanna and J.R. Barry, “Reduced-bandwidth duobinary differential continuous-phase Modulation format for optical communications,” IEEE Photon. Technol. Lett. 17, 1331-1333 (2005).

[65] C. K. Madsen and J. H. Zhao, *Optical filter design and analysis: A signal processing approach* (Wiley-Interscience, 1999).

[66] D. Sinefeld, S. Ben-Ezra, and D. M. Marom, "Nyquist-WDM filter shaping with a high-resolution colorless photonic spectral processor," Opt. Lett. 38, 3268-3271 (2013).

[67] D. Sinefeld, Y. Fattal, and D. M. Marom, "Generation of WDM adaptive-rate pulse bursts by cascading narrow/wideband tunable optical dispersion compensators," Opt. Lett. 37, 4290-4292 (2012).

[68] D. Sinefeld and D. M. Marom, "Tunable fiber ring laser with an intracavity high resolution filter employing two-dimensional dispersion and LCoS modulator," Opt. Lett. 37, 1-3 (2012).

[69] G. Bosco, V. Curri, A. Carena, P. Poggiolini, and F. Forghieri, “On the performance of Nyquist-WDM terabit superchannels based on PMBPSK, PM-QPSK, PM-8QAM or PM-16QAM subcarriers,” J. Lightwave Technol. 29, 53–61 (2011).

[70] Z. Dong, J. Yu, H. Chien, N. Chi, L. Chen, and G. Chang, "Ultra-dense WDM-PON delivering carrier-centralized Nyquist-WDM uplink with digital coherent detection," Opt. Express 19, 11100-11105 (2011).

[71] M. Nakazawa, T. Hirooka, P. Ruan, and P. Guan, “Ultrahigh-speed “orthogonal” TDM transmission with an optical Nyquist pulse train,” Opt. Express 20(2), 1129–1140 (2012).

[72] M. A. Foster, A. C. Turner, R. Salem, M. Lipson, and A. L. Gaeta, "Broad-band continuous-wave parametric wavelength conversion in silicon nanowaveguides," Opt. Express 15, 12949-12958 (2007).

[73] H. C. H. Mulvad, E. Palushani, H. Hu, H. Ji, M. Lillieholm, M. Galili, A. T. Clausen, M. Pu, K. Y., J. M. Hvam, P. Jeppesen, and L. K. Oxenløwe, "Ultra-high-speed optical serial-to-parallel data conversion by time-domain optical Fourier transformation in a silicon nanowire," Opt. Express 19, B825-B835 (2011).

[74] A. Yariv and R. G. M. P Koumans, “Time interleaved optical sampling for ultra-high speed A/D conversion,” Elec. Lett 34, 2012-13 (1998).

[75] J. Kim, M. J. Park, M. H. Perrott, and F. X. Kärtner, “Photonic subsampling analog-to-digital conversion of microwave signals at 40-GHz with higher than 7-ENOB resolution,” Opt. Express 16, 16509–16515 (2008).

[76] G. C. Valley, " Photonic analog-to-digital converters," Opt. Express 15, 1955–1982 (2007).

[77] A. S. Bhushan, F. Coppinger, B. Jalali, S. Wang and H. F. Fetterman, “150 Gsample/s wavelength division sampler with time-stretched output,” Electron. Lett. 34, 474-475 (1998).

[78] A. S. Bhushan, F. Coppinger, S. Yegnanarayanan, and B. Jalali, “Non-dispersive wavelength-division sampling,” Opt. Lett. 24, 738-740 (1999).

[79] J. U. Kang and R. D. Esman, “Demonstration of time interweaved photonic four-channel WDM sampler for hybrid analogue-digital converter,” Electron. Lett. 35, 60-61 (1999).

[80] X. Yi, L. Li, T. X. H. Huang, and R. A. Minasian, "Programmable multiple true-time-delay elements based on a Fourier-domain optical processor," Opt. Lett. 37, 608-610 (2012).

[81] F. Xiao, K. Alameh, and Y. T. Lee, "Tunable multi-wavelength fiber lasers based on an Opto-VLSI processor and optical amplifiers," Opt. Express 17, 23123-23129 (2009).

[82] F. Xiao, K. Alameh and Y. T. Lee, "Tunable Multiwavelength Fiber Ring Lasers Based on an Opto-VLSI Processor," IEEE PTL 23,182-184, (2011).

אופטיקה אדפטיבית ליישומי תקשורת אופטית: פתרונות מרחביים למגוון יישומים ספקטרליים בתחום התקשורת המהירה

חיבור לשם קבלת תואר דוקטור לפילוסופיה

מאת

דוד שינפלד

הוגש לסנט האוניברסיטה העברית בירושלים
אוקטובר / 3102

עבודה זו נעשתה בהדרכתו של:

פרופ' דן מרום

תקציר

במהלך העשורים האחרונים השימוש באותות אופטיים מהירים הופך דומיננטי יותר ויותר, הן במחקר מדעי טהור והן ביישומים הנדסיים. מערכות אלקטרואופטיות מהירות הן ליבת הטכנולוגיה של רשתות תקשורת מודרניות, ומהוות בסיס למספר רב של יישומים בתחום של עיבוד אותות אופטי. יישומים כאלה מבוססים על היכולת לשלוט, לפלטר ולעבד אותות בעלי רוחב סרט גדול. באופן מסורתי, שליטה כזו יכולה להתבצע באמצעות שימוש באלקטרוניקה מהירה. עם זאת, העלייה המתמשכת בקצבים הנדרשים הופכת אפשרות זו ללא מעשית, שכן האותות מהירים מדי לשליטה אפילו עבור המערכות האלקטרוניות המהירות ביותר הקיימות. האלטרנטיבה היא להשתמש במערכת אופטית, בה השליטה באותות נעשית בתחום התדר (הספקטרום). מערכות כאלו נדרשות לבצע מניפולציות על אותות בעלי רוחב סרט גדול וזאת ברזולוציה ספקטרלית גבוהה, והן חיוניות כחלק מרשת תקשורת אופטית שבה הם משמשות לסינון אותות, להשוואה בין עוצמות של ערוצי צבע שונים ולתיקון שגיאות הנגרמות משינויים בערוץ התקשורת.

בעבודה זו מוצגות תוצאות המחקר של משפחת מערכות אופטיות המשלבות אופטיקת מנחי גלים יחד עם אופטיקה מרחבית על מנת להדגים עיבוד ספקטרלי של אותות אופטיים ברזולוציה חסרת תקדים, כאשר אפנון הרכיבים הספקטרליים נעשה באמצעות מאפנן אור מרחבי. היכולת לשלב טכנולוגיות חדשניות הכוללות מעגל אופטי פלנרי הממומש כסריג עקיפה בעל רזולוציה ספקטרלית גבוהה, יחד עם מאפנן פאזה מרחבי אשר הותאם מתעשיית המקרנים לעולם התקשורת האופטית, מאפשרת להפגין יכולת של עיבוד ספקטרלי אופטי ברזולוציה גבוהה. למערכת כזו יש יכולת להתאים ערכי פאזה ואמפליטודה לכל רכיב ספקטרלי ובצורה זו לשלוט בתכונות הזמניות של האות. ניתן לתכנן מערכת כזו כך שתפעל בכל ספקטרום התדרים של תחום התקשורת, במחיר של רזולוציה נמוכה, או לחילופין, לתכנן מערכת כזו ברזולוציה גבוהה מאד, אך שתפעל בתחום צר של תדרים המותאם לרוחב הסרט של ערוץ שידור צבעי בודד. על ידי שימוש במערך אופטי דו ממדי הכולל שילוב של סריג עקיפה יחד עם המעגל האופטי הפלנרי, הצלחנו להציג מעבד ספקטרלי חדש המותאם לכל תחום התקשורת האופטית ברזולוציה גבוהה שלא הוצגה בעבר.

בהתבסס על הישגים אלה מספר מערכות חדשניות פותחו ונחקרו מספר יישומים שלהן. בעבודה זו מוצגות תוצאות המחקר שפורסמו בשישה מאמרים אשר ממחישים את התכנון והיישום של מערכות עיבוד אופטי ספקטרלי המבוססות על שילוב של אופטיקה פלנרית ומאפנן אור מרחבי. המאמרים מחולקים לשתי קבוצות: בקבוצה הראשונה מוצגים שלושה מאמרים המתארים את ההתפתחות של מערכות אלו ממערכת בסיסית המטפלת בערוץ תקשורת צבעי בודד ועד למערכת המשלבת סריגים ואופטיקה פלנרית שמאפשרת שליטה ספקטרלית ברזולוציה גבוהה בכל הספקטרום. הקבוצה השניה מכילה שלושה מאמרים המתארים כמה יישומים של טכנולוגיה זו. היישומים המתוארים במאמרים אלו מדגימים את אפשרויות השימוש במעבד אופטי ספקטרלי, כדוגמת היכולת לסנן אותו ברזולוציה אופטית

גבוהה מאד, יכולת המאפשרת לקבל ביצועים מוגבלי רוחב סרט לפי תיאוריית נייקוויסט. מאמר נוסף עוסק באפשרות לאפנן פאזה עבור רכיבים ספקרליים שונים ולייצר בצורה זו מדרגות פאזה ספקטרליות המשמשות לייצור מערך פולסים צבעי. בנוסף, הודגם לייזר מתכוונן חדש המבוסס על יכולת הכוונון הגבוהה של המעבד הספקטרלי הדו-ממדי. התקנים אלו, המאפשרים שליטה ברזולוציה גבוהה ברכיבים ספקטרליים יכולים לשמש מרכיב חשוב בשליטה ובשיפור של איכות אותות אופטיים מהירים, ופיתוחם חיוני להתקדמות עולם התקשורת האופטית.